

JOURNAL

OF THE SOUTH AFRICAN INSTITUTION OF CIVIL ENGINEERING



Volume 61 Number 2
June 2019

$$F = \frac{1}{\Sigma W \sin \alpha} \sum \left[\frac{c' B + (W - uB) \tan \phi'}{\cos \alpha + (\sin \alpha \tan \phi' / F)} \right]$$

- Evaluation of empirical equations to predict bridge pier scour in a non-cohesive bed under clear-water conditions
- The influence of gradient on saturation flow rate at signalised intersections
- Artificial aeration of stepped spillways by crest piers and flares for the mitigation of cavitation damage
- Understanding public transport needs in Cape Town's informal settlements: a Best-Worst-Scaling approach
- Stormwater runoff quality on an urban highway in South Africa
- The collapsible nature of residual granite soils of the Cape Granite Suite

$\frac{\partial^2 h}{\partial x^2} + k_z \frac{\partial^2 h}{\partial z^2} = 0$
The logo for the South African Institution of Civil Engineers (saice), consisting of the lowercase letters "saice" in a bold, sans-serif font, with a stylized arch or wave shape above the letter "a".

PUBLISHER

South African Institution of Civil Engineering
Block 19, Thornhill Office Park,
Bekker Street, Vorna Valley, Midrand, South Africa
Private Bag X200, Halfway House, 1685, South Africa
Tel +27 11 805 5947, Fax +27 11 805 5971
<http://www.saice.org.za>
civilinfo@saice.org.za

EDITOR-IN-CHIEF

Dr Peter Day
Consultant, Jones & Wagener (Pty) Ltd
Adjunct Professor of Geotechnical
Engineering, University of Stellenbosch
Tel +27 11 519 0200
day@jaws.co.za

JOINT EDITOR-IN-CHIEF

Prof Chris Clayton
University of Southampton
c.clayton@soton.ac.uk

EDITOR

Verelene de Koker
Tel +27 11 805 5947, Cell +27 83 378 3996
verelene@saice.org.za

JOURNAL EDITORIAL PANEL

Prof Y Ballim – University of the Witwatersrand
Prof W Burdzik – University of Pretoria
Prof CRI Clayton – University of Southampton
Dr P Day – Jones & Wagener (Pty) Ltd (chairman)
Prof J du Plessis – University of Stellenbosch
Prof GC Fanourakis – University of Johannesburg
Prof M Gohner – University of the Witwatersrand
Prof PJ Gräbe – University of Pretoria
Dr C Herold – Umfula Wempiro Consulting
Prof G Heymann – University of Pretoria
Prof A Ilemobade – University of the Witwatersrand
Prof SW Jacobsz – University of Pretoria
Prof EP Kearsley – University of Pretoria
Prof C Roth – University of Pretoria
Prof W Steyn – University of Pretoria
Mr M van Dijk – University of Pretoria
Prof C Venter – University of Pretoria
Prof A Visser – University of Pretoria
Dr E Vorster – Aurecon South Africa (Pty) Ltd
Prof J Wiium – University of Stellenbosch
Prof A Zingoni – University of Cape Town
Prof M Zuideest – University of Cape Town

PEER REVIEWING

The *Journal of the South African Institution of Civil Engineering* is a peer-reviewed journal
that is distributed internationally

DESIGN AND REPRODUCTION

Marketing Support Services, Ashlea Gardens, Pretoria

PRINTING

Fishwicks, Pretoria

Papers for consideration should be submitted
online at: <http://journal.saice.org.za>

The South African Institution of Civil Engineering accepts no responsibility for any statement made or opinion expressed in this publication. Consequently, nobody connected with the publication of this journal, in particular the proprietor, the publisher and the editors, will be liable for any loss or damage sustained by any reader as a result of his or her action upon any statement or opinion published in this journal.



CONTENTS

2 Evaluation of empirical equations to predict bridge pier scour in a non-cohesive bed under clear-water conditions

J K Vonkeman, G R Basson

DOI: 10.17159/2309-8775/2019/v61n2a1

21 The influence of gradient on saturation flow rate at signalised intersections

M M Bruwer, C J Bester, E S Viljoen

DOI: 10.17159/2309-8775/2019/v61n2a2

28 Artificial aeration of stepped spillways by crest piers and flares for the mitigation of cavitation damage

J Koen, D E Bosman, G R Basson

DOI: 10.17159/2309-8775/2019/v61n2a3

39 Understanding public transport needs in Cape Town's informal settlements: a Best-Worst-Scaling approach

M Teffo, A Earl, M H P Zuideest

DOI: 10.17159/2309-8775/2019/v61n2a4

51 Stormwater runoff quality on an urban highway in South Africa

A Robertson, N Armitage, M H P Zuideest

DOI: 10.17159/2309-8775/2019/v61n2a5

57 The collapsible nature of residual granite soils of the Cape Granite Suite

N Fouché, S Y Asante

DOI: 10.17159/2309-8775/2019/v61n2a6



JEANINE K VONKEMAN, who is an Associate Member of SAICE, is a postgraduate student in Hydraulic Engineering at Stellenbosch University. She completed her BEng (*cum laude*) in Civil Engineering at the University of Pretoria in 2014 and is currently working towards a PhD on a numerical model for bridge pier scour, which was upgraded from her MEng degree.

Contact details:

PhD Civil Engineering Student

Stellenbosch University

Private Bag X1

Matieland 7602

South Africa

T: +27 83 286 8760

E: jkvonkeman@gmail.com / jvonkeman@sun.ac.za



PROF GERRIT R BASSON Pr Eng, who is a Member of SAICE, is a professor in Hydraulic Engineering in the Civil Engineering Department at Stellenbosch University. He obtained a PhD from Stellenbosch University in 1996 and has more than 30 years' experience mainly in the fields of river hydraulics, fluvial morphology and the design of large hydraulic structures. He has worked on projects in 21 countries.

Contact details:

Professor in Hydraulic Engineering

Department of Civil Engineering

Stellenbosch University

Private Bag X1

Matieland 7602

South Africa

T: +27 21 808 4355

E: grbasson@sun.ac.za

Evaluation of empirical equations to predict bridge pier scour in a non-cohesive bed under clear-water conditions

J K Vonkeman, G R Basson

Pier scour has been cited as the main mechanism responsible for the failure of bridges spanning rivers. Despite extensive research since the 1950s, there is no universally agreed upon procedure to accurately predict the equilibrium scour depth. Experimental data was generated by 48 tests with four flows and three pier shapes to evaluate the capability of 30 empirical equations to predict the local scour depth. Fine sand and crushed peach pips were used to address the scaling challenges of the equations by means of an equivalent movability number. The equations yielded a wide range of mostly unreliable results, particularly for the non-cylindrical pier shapes. Nevertheless, the HEC-18 models are recommended, in conjunction with Shen *et al* (1969), and Ali and Karim (2002), because they rely on the pier Reynolds number, a parameter which is significant in the vortex formation. Prediction models taking the horseshoe vortex into consideration could offer better scour depth predictions. Field data was analysed to improve the HEC-18 equation with new factors for pier shape and armouring for different confidence intervals. The armouring factor is based on the particle Reynolds number as opposed to the widely adopted critical velocity, and achieves considerably less scatter about the line of equality despite under-predictions for the cylindrical piers. Alternatively, a diagram comparable to the Modified Liu Diagram has the potential to predict bridge pier scour even though the pier structure parameters are omitted. Further research and improved prediction models should be considered, particularly advanced numerical models which are becoming increasingly feasible.

BACKGROUND

The placement of a bridge pier in a hydraulic environment changes the flow field, yielding it susceptible to local scour whereby the surrounding sediment is washed away by swiftly moving water. As a result, the bridge foundation may be undermined and the structural stability compromised. In fact, local scour at piers has been cited as the main mechanism responsible for the collapse of bridges founded in alluvial beds (Deshmukh & Raikar 2014). Huber (1991) and Sumer (2007) estimate that 60% of all structural bridge failures can be attributed to scouring and not to overloading. Extensive research has been conducted on the prediction of bridge pier scour depth since the 1950s, and yet there is no universally agreed upon procedure to accurately predict the equilibrium scour depth (Rooseboom 2013).

Most scour equations traditionally used in bridge designs have been developed on the basis of experimentation, dimensional

analyses and simplified theoretical models. The equations have been derived by assuming dominant parameters, reducing them to simplified relationships and then calibrating them by means of a coefficient from laboratory and field data.

The comparison of different empirical equations has been the topic of many studies. Johnson (1995) used field data to evaluate the accuracy of seven pier scour equations. Landers and Mueller (1996) analysed five selected equations with field data. Gaudio *et al* (2010) tested six formulae by using original field data and synthetic data produced by the Monte Carlo technique. In more recent studies, Toth (2015) evaluated ten different equations. One of the most comprehensive studies is that of Sheppard *et al* (2014) who evaluated 23 equations for under-prediction using compiled laboratory and field databases. The equations were then combined to produce the Sheppard & Melville Model. Similarly, Mueller (1996) and Mueller

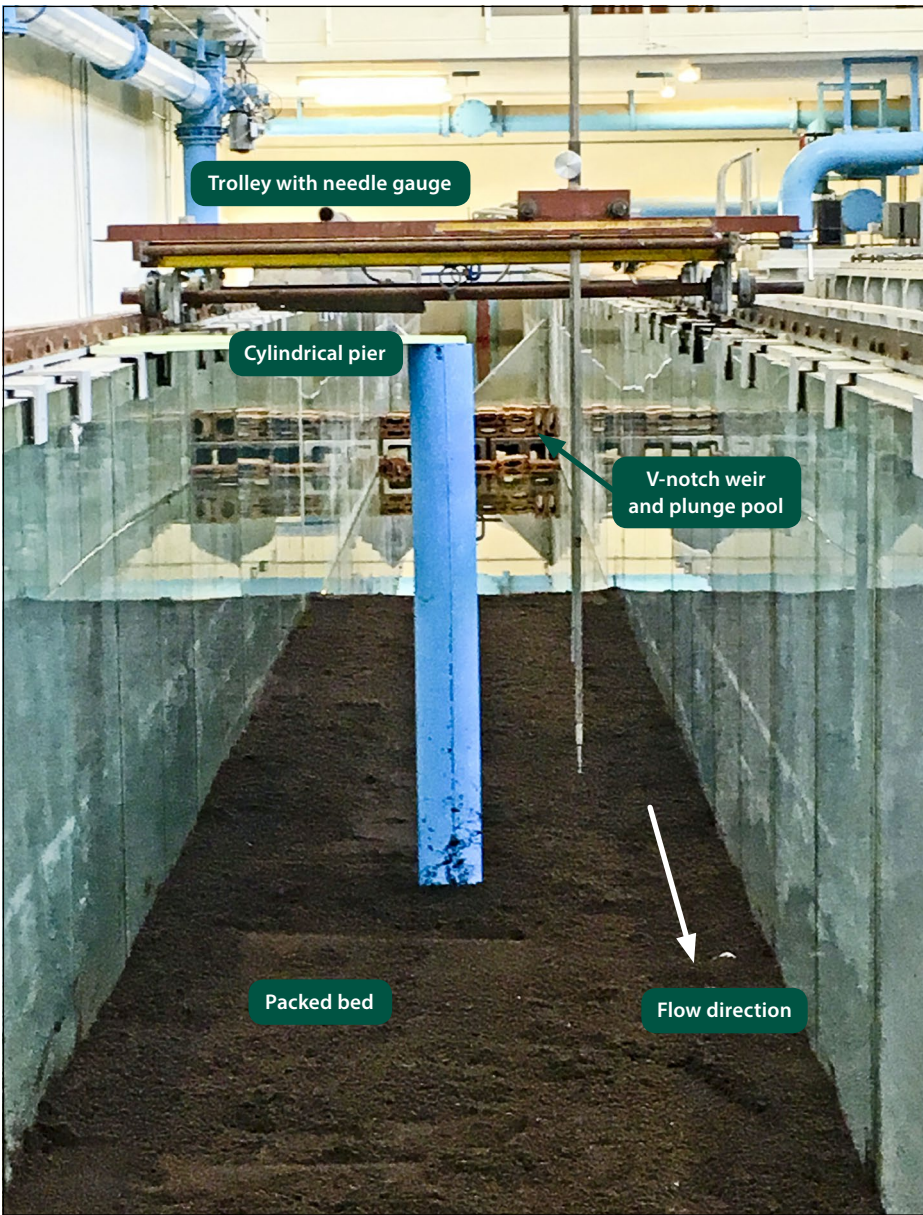


Figure 1 Photo of the laboratory flume setup with cylindrical pier and sediment bed

and Wagner (2005) evaluated 22 and 26 equations respectively, and improved the HEC-18 method. The comparative studies are based on statistical analyses using, amongst others, percentage error, residuals, standard deviation, bias or rankings. Without exception, the authors all concluded that the various empirical equations produce significantly different predictions from the field and that further research is required. Furthermore, the following conclusions were also recurring:

- The equations produce results that are not only different from the field or laboratory, but are in weak agreement with one another. The equations are not universal and only yield good results under conditions similar to those from which they were derived.
- Most of the formulae overestimate observed scour depths and may perform better in conservative designs. However,

this leads to uneconomical designs of unnecessarily expensive foundations or countermeasures. On the other hand, some of the formulae are not fit for pier design due to under-predictions, for example Froelich (1988).

- Generally, it appears that the HEC-18 formulae by the US Federal Highway Administration (FHWA) are favoured for results that most closely resemble the field and rarely under-predict scour depth. It is also known as the CSU (Colorado State University) equation with modifications in the form of coefficients for the effect of the bed material. The Shen *et al* (1969) model, one of the equations upon which the HEC-18 formula was based, relies on the pier Reynolds number and also performed well in the literature study.
- Further research and improved models are recommended (Arneson *et al* 2012).

The intention of this study was to simulate bridge pier scour in a laboratory and to gain an understanding of the scouring process. The data generated by the physical modelling was then applied to evaluate different methods for predicting the equilibrium scour depth. The objective was to demonstrate the shortcomings of thirty of the better-known empirical equations and to emphasise the need for improved prediction methods to pave the way for future research on numerical modelling. A summary of the different methods is presented in the Appendix to this paper. Finally, field data was analysed to generate a new equation based on the particle Reynolds number as opposed to the widely adopted critical velocity.

EXPERIMENTAL WORK

Experimental work was conducted at the Civil Engineering Hydraulics Laboratory, Stellenbosch University, in a rectangular flume with a 40 m length, 1 m width and 1.24 m depth. A sediment bed was packed in the flume around a scaled pier model, and water was released to emulate channel flow and local scouring. The tests were performed for subcritical flow under clear-water conditions (Froude number $Fr < 0.26$ and critical velocity ratio $v/v_c < 1$) and for a constant water depth $y = 0.2$ m which was manually controlled with a sluice gate at the downstream end of the flume. A V-notch weir controlled the inflow and a plunge pool with tubes aligned the flow to ensure that uniform, fully developed flow would reach the pier after a 9 m entrance length. Figure 1 shows a photograph of the experimental setup.

A total of 48 different tests were conducted whereby a combination of four different flows, three pier shapes and two sediment materials was used. The three different pier shapes included a cylindrical pier, a round-nosed pier and a sharp-nosed pier, as indicated in Figure 2. The pier models were designed based on a model-to-prototype scale of 1:15 with a diameter (or width) D of 110 mm and a length L/D ratio of 7. The different inflows that were tested had approach velocities of 0.28, 0.31, 0.34 and 0.37 m/s for the fine sand material, while those for the crushed peach pits were 0.14, 0.17, 0.20 and 0.23 m/s.

The submerged scour pattern that formed in the vicinity of the scaled pier model was manually surveyed and the flow pattern was visualised by Acoustic Doppler

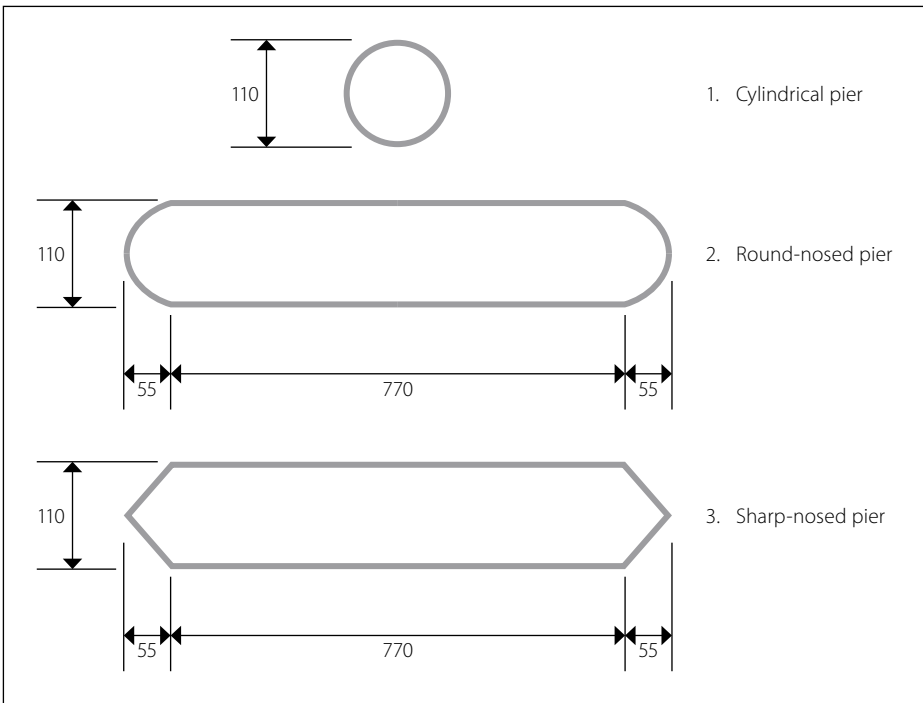


Figure 2 The different pier shapes with dimensions

Velocimetry (ADV) measurements. Furthermore, the flow field was measured for the flume setup without sediment, i.e. a fixed bed to simulate rigid plane-bed flow. Ten percent of the experiments were duplicated three times to ensure repeatability of the results, and showed a maximum deviation of 9%.

Model-to-prototype scaling

Empirical equations are formulated specifically for full-scale field applications with sediment, such as sand with a relative density of 2.6. Consequently, equations developed from physical models are faced with scaling challenges whereby they overestimate the actual scour field depths (Lee & Sturm 2009). Sediment transport problems are normally modelled by applying Froude similarity, and the median grain size is scaled according to the Shields' criterion (Heller 2011). This may result in a very small model sediment size that exhibits cohesive inter-particle forces not present in sand bed rivers (Lee & Sturm 2009). According to FHWA (Arenson *et al* 2012), "it is not possible to scale the bed material size". Heller (2011) recommends that a sediment with a smaller density and larger grain diameter should be employed to incorporate the non-scalable effects of the hydraulic forces in the settling velocity and density. Thus, crushed peach pips, albeit a biomaterial, were used to more accurately replicate alluvial sediment in the field.

The material properties measured for the two sediments, presented in Table 1, were

the median particle size d , maximum theoretical relative density MTRD or s , angle of repose ϕ , settling velocity w and critical velocity v_c . Both sediment beds may be classified as uniformly graded based on the particle size distributions $\sigma_g = (d_{84}/d_{16})^{0.5} < 2$. These values were obtained from standard sieve analyses, rice density tests, fixed funnel tests and settling column tests.

Rooseboom *et al* (1983) argue that particle size poorly represents the transportability of sediment and instead recommend the use of settling velocity. The Modified Liu Diagram in Figure 3 (based on Rooseboom *et al* 1983) was generated to obtain an identical movability number, and thereby scale the density and particle sizes for the peach pips to that of a representative in-situ alluvial sediment (refer to Table 1). The movability number (or stream power) and the particle Reynolds number are defined in Equations 1 and 2 respectively.

$$\frac{v^*}{w} = \frac{\sqrt{gy_1 S_f}}{w} \quad (1)$$

$$Re_p = \frac{\sqrt{gy_1 S_f} d}{v} \quad (2)$$

where S_f is the energy slope, g is the gravitational acceleration and v is the kinematic viscosity. Equation 3 was used to relate the particle density and size with settling velocity. Several different approximations for the coefficient exist, but a value of 1.1 is recommended C_D for the scaling of rough sediment particles > 1 mm, while Stoke's Law should be applied for particles < 0.1 mm (Van Rijn 1987) and Zanke (1977) to particles < 1 mm.

Table 1 Sediment characteristics measured for the fine sand and crushed peach pips

| Properties | d_5 (mm) | σ_g | MTRD | ϕ_{sat} | ϕ_{dry} | w_s (m/s) | v_c (m/s) | Scaled d (mm) | Scaled MTRD |
|------------|------------|------------|------|--------------|--------------|-------------|-------------|-----------------|-------------|
| Fine sand | 0.214 | 1.36 | 2.63 | 45° | 28° | 0.036 | 0.375 | 3.21 | 2.63 |
| Peach pips | 0.740 | 1.57 | 1.28 | 44° | 32° | 0.032 | 0.225 | 1.87 | 2.63 |

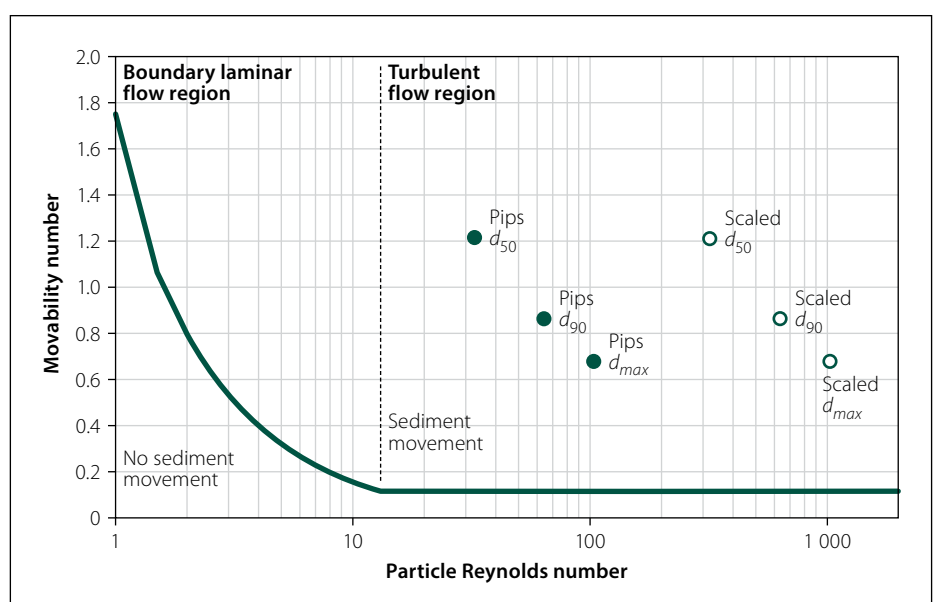


Figure 3 Modified Liu Diagram to scale peach pips

Table 2 Critical flow velocities (m/s) determined by empirical equations

| Equation | Hancu (1971) | Neill (1973) | Gao <i>et al</i> (1993) | Richardson & Davis (1995) | Melville (1997) | Sheppard <i>et al</i> (2014) | Equation 4 |
|------------|--------------|--------------|-------------------------|---------------------------|-----------------|------------------------------|------------|
| Fine sand | 0.276 | 0.314 | 0.284 | 0.283 | 0.276 | 0.242 | 0.328 |
| Peach pips | 0.166 | 0.374 | 0.170 | 0.428 | 0.360 | 0.302 | 0.204 |

$$w = \begin{cases} \frac{C_D \sqrt{(\rho_s/\rho - 1)gd}}{18\nu}, & d > 1 \text{ mm} \\ \frac{10\nu/d(\sqrt{1 + 0.01d^3} - 1)}{18\nu}, & d < 0.1 \text{ mm} \\ 10\nu/d(\sqrt{1 + 0.01d^3} - 1), & 0.1 < d < 1 \text{ mm} \end{cases} \quad (3)$$

where ρ_s and ρ is the density of the sediment and fluid respectively.

Incipient motion

Most of the empirical equations for bridge pier scour rely on incipient motion described empirically by critical velocity. The threshold of movement can also be described in terms of shear stress, settling velocity and stream power. Numerous equations exist to define the critical velocity, and ambiguities exist whereby some of the equations for bridge pier scour fail to reference an appropriate equation to determine the critical velocity (Breusers *et al* 1977; Jain 1981; Sheppard & Miller 2006). The threshold of sediment movement is clearly an important parameter in scour calculations, and yet literature neglects to address that different equations for critical velocity could yield different scour depth predictions. Therefore, critical velocities determined experimentally (see Table 1) were used in the analysis (unless specified otherwise) to ensure that the relative velocity ratio ν/ν_c was maintained for both model and prototype scales.

The scaling challenge is further demonstrated by the empirical equations which over-predict the critical velocity for the peach pip particles (as shown in Table 2), because they do not account for density, unlike Gao *et al* (1993), Hancu (1971) and Equation 4. It is derived from the Shields diagram that assumes the shear stress limit for incipient motion for $Re > 400$ is $\tau_c = 0.056(\rho_s - \rho)gd$ (Graf 1971). The Hancu (1971) model for scour depth relies on a critical velocity that is also derived from the Shields diagram and proves to be one of the more accurate scour equations in the subsequent section.

$$\nu_c = 1.9 \sqrt{gd(s - 1)} \left(\frac{R}{d} \right)^{1/6} \quad (4)$$

where R is the hydraulic radius. The equations used in Table 2 are given in the Appendix.

Time to reach equilibrium

Local scour is a time-dependent process whereby equilibrium is progressively achieved as the scour hole grows and the bed shear stresses near the bed gradually fall below the critical shear stress (Roulund *et al* 2005). Melville and Chiew (1999) believe that the equilibrium depth takes several days or months to develop, while Breusers *et al* (1977) claim that the time to reach equilibrium depth may be infinite. However, flood peaks often do not last long enough to develop an equilibrium scour depth and it is impractical to run an experiment for several days. Owing to the divided notion in literature on the time required to reach equilibrium scour, additional tests were performed to establish a suitable time scale for each test to achieve equilibrium scour.

Figure 4 shows that no significant change was observed in the scour hole depth d_s for both sediment beds after two hours, as was the case for Melville (1975), Roulund *et al* (2005) and Mohammed *et al* (2016). Evidently scour development is rapid in the beginning; 50–80% of the equilibrium scour depth develops within 10% of the time required for equilibrium (Melville & Chiew 1999). Therefore, it was assumed that the equilibrium condition is reached when the increase in scour depth does not exceed 5% of the pier diameter.

The empirical equation proposed by Guo (2014) for a time-dependent scour depth was assessed by curve-fitting it to Figure 4. The equation gave an equilibrium scour depth for the peach pips after seven hours as 1.25 times larger than that observed after three hours in the laboratory. The curve-fitting also indicated that the equilibrium scour depth for the fine sand was achieved after 40 minutes. Of the thirty scour equations considered in the study, the only models that attempt to account for time is that of Melville and Coleman (2000), and Ali and Karim (2002) which employ exponential functions.

The scour process

The complex junction flow associated with bridge pier scour results in the formation of separated flow, lee-wake and horseshoe vortices, as illustrated by the photographs in Figure 5. The horseshoe vortex is the main mechanism responsible for scouring. A down-flow in front of the pier is driven by the strong pressure gradient and the vertical velocity component which rolls up when it comes into contact with the bed. The resulting circulation, flow separation and shear layer scour the hole, comparable to an impinging jet digging up the sediment material. The ends of the system are swept downstream and the sediment is deposited

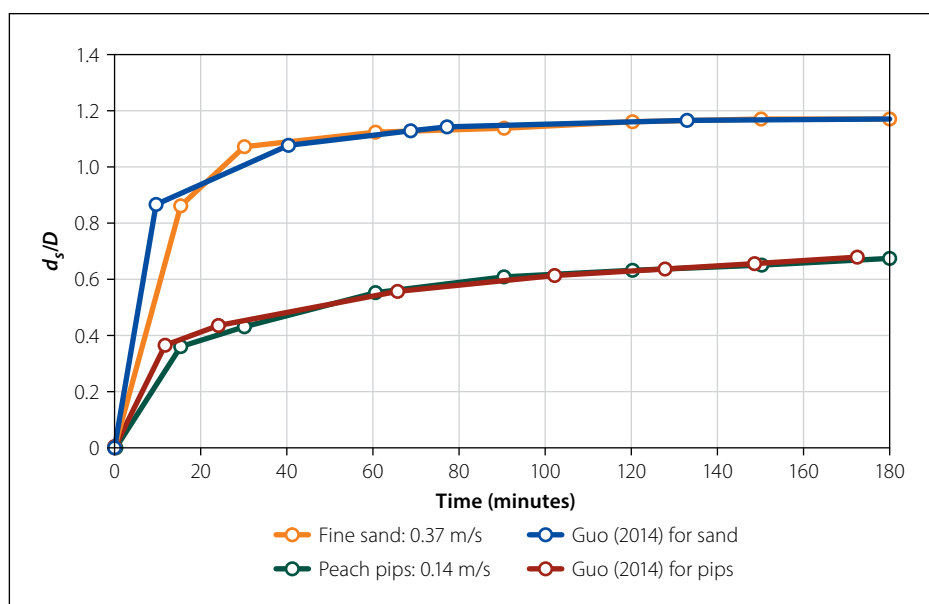


Figure 4 Development of relative scour depth with time in the laboratory

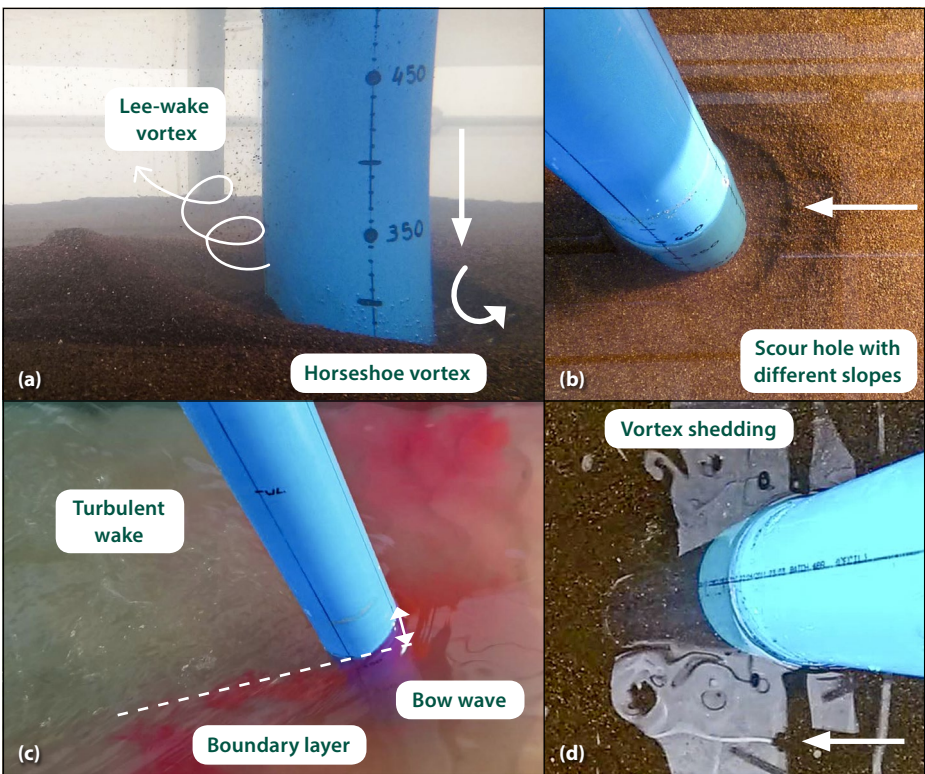


Figure 5 Photographs of the flow pattern elements associated with bridge pier scouring

Table 3 Maximum bridge pier scour depth and extent from experimental work (m)

| | | Cylindrical pier | | | Round-nosed pier | | | Sharp-nosed pier | | |
|------------|-------------|------------------|-------|-------|------------------|-------|-------|------------------|-------|-------|
| | v (m/s) | d_s | l_s | w_s | d_s | l_s | w_s | d_s | l_s | w_s |
| Fine sand | 0.28 | 0.099 | 0.15 | 0.20 | 0.056 | 0.16 | 0.19 | 0.060 | 0.17 | 0.22 |
| | 0.31 | 0.111 | 0.19 | 0.24 | 0.080 | 0.18 | 0.22 | 0.065 | 0.18 | 0.25 |
| | 0.34 | 0.114 | 0.19 | 0.24 | 0.094 | 0.23 | 0.24 | 0.084 | 0.20 | 0.25 |
| | 0.37 | 0.121 | 0.25 | 0.26 | 0.102 | 0.25 | 0.25 | 0.090 | 0.20 | 0.27 |
| Peach pips | 0.14 | 0.063 | 0.13 | 0.13 | 0.037 | 0.12 | 0.13 | 0.009 | 0.06 | 0.01 |
| | 0.17 | 0.116 | 0.21 | 0.22 | 0.077 | 0.17 | 0.18 | 0.050 | 0.13 | 0.14 |
| | 0.20 | 0.127 | 0.24 | 0.28 | 0.095 | 0.23 | 0.25 | 0.072 | 0.15 | 0.20 |
| | 0.23 | 0.135 | 0.24 | 0.30 | 0.111 | 0.25 | 0.28 | 0.106 | 0.17 | 0.24 |

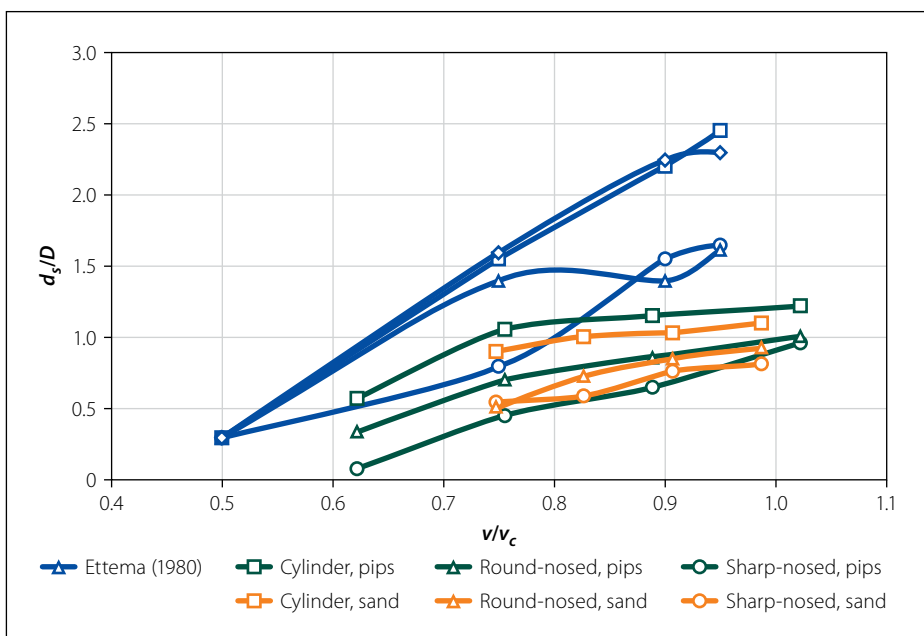


Figure 6 The effect of relative velocity on relative scour depth from experimental work

in the low-pressure zone behind the pier to form the characteristic horseshoe shape.

A bow wave is formed at the free surface in front of the pier caused by an upward flow circulating in a direction opposite to that of the horseshoe vortex. The bow wave has the ability to counteract and weaken the horseshoe vortex only in shallow flow depths.

The slope of the scour hole can be divided into different regions, as demonstrated by Figure 5(b). The primary area is driven by the vortex and bed shear stress, while the secondary area is driven by the slope stability or shear slides with a slope angle approximating that of the saturated angle of repose.

The lee-wake vortex forms behind the pier. As the flow reaches the pier, the velocity decreases abruptly and the flow is deflected away from the pier. The flow accelerates where the streamlines converge and a boundary layer is formed, as observed by the coloured dye wands in Figure 5(c). The lee-wake vortices are caused by the rotation of the boundary layer over the surface of the pier. Unstable shear layers form at the pier surface near the bed, which roll up and detach from either side of the pier at the boundary layer. At low Reynolds numbers $< 3.5 \times 10^6$, unstable vortices are shed from alternating sides of the pier and are swept downstream (Breusers *et al* 1977). Figure 5(d) shows the lee-wake vortex for a Reynolds number of 80×10^3 , a pier Reynolds number of 15×10^3 and a typical Strouhal number of 0.2.

Results for experimental work

Table 3 summarises the unscaled scour depth d_s , length l_s and width w_s results from the experimental work. The maximum scour depth was measured at the upstream nose of the pier where the horseshoe vortex circulates. Generally, the length is $0.47d_s$ and the width is $0.4d_s$.

The local scour process is affected by several different yet interrelated parameters of which the relative velocity, relative sediment size, relative flow depth and time to reach equilibrium scour have been identified as the most significant (Williams 2014). The effect of the approach velocity, pier shape and sediment type on equilibrium scour depth could briefly be examined, but flow depth and pier width were fixed in the experimental work.

Figure 6 illustrates that the relative scour depth increases almost linearly with the relative velocity, in accordance with

Ettema (1980). No local scour pattern was observed below a relative velocity condition of 0.5 in accordance with research such as those by Hancu (1971), Breusers *et al* (1977), Sheppard and Miller (2006), and Sheppard *et al* (2014).

Similarly, the relative scour depth increases with an increasing pier Reynolds number, as shown in Figure 7. The pier Reynolds number $Re_D = vD/\nu$ describes the turbulence induced by the pier and not by the channel. It is easily the chief parameter affecting the strength of the horseshoe vortex (Roulund *et al* 2005), and yet it has rarely been described relative to scour depth, even though the horseshoe vortex is directly responsible for causing scour. The pier Reynolds number should be considered a more significant scour parameter, because it describes the combined effect of the pier size and approach velocity on the vortex strength.

From Figure 7 it is evident that the sand required a larger Reynolds number (or velocity) to scour the same sized hole as that for the peach pips. The two sediment materials have a different median particle size, as well as density, and are thus best compared when both parameters are considered. The crushed peach pips are the more easily erodible material, because they have a lower settling velocity and a lower critical velocity.

On the other hand, similarly sized scour holes are formed for the same relative velocity or flow intensity for both materials in Figure 6. This is in accordance with Lee and Strum (2009) who suggest that a similar scour depth should be obtained for the scaled D/d of 882 for the peach pips and 514 for the sand.

With reference to the figures above, a cylindrical pier yields the largest scour hole,

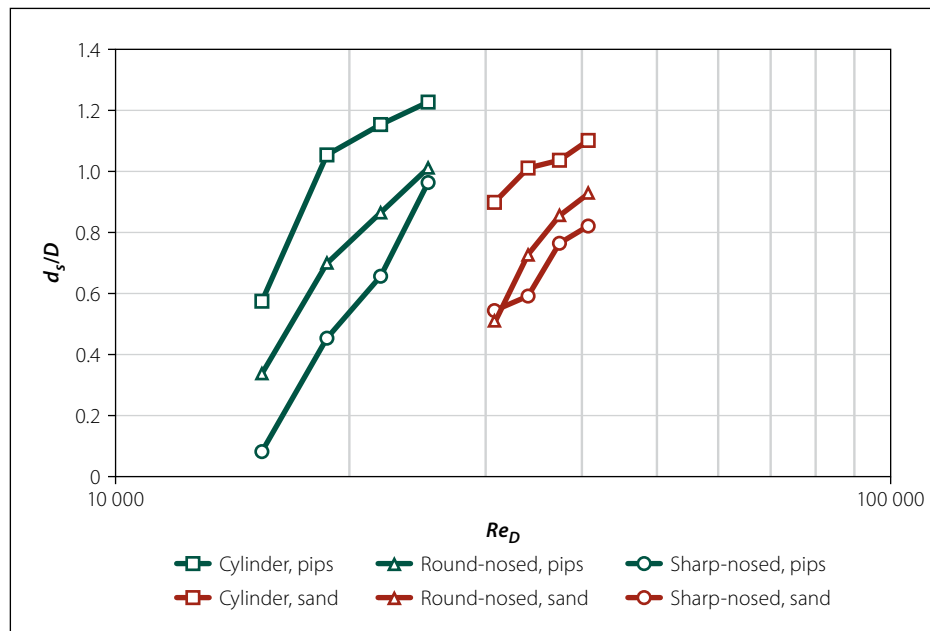


Figure 7 The effect of the pier Reynolds number on the relative scour depth

while the sharp-nosed pier yields the least amount of scouring because practically no vorticity is generated at the nose of the streamlined pier (Tseng *et al* 2000). The round-nosed pier causes less scouring than the cylindrical pier due to its increased relative pier length L/D . Only half of the empirical equations evaluated in this study account for pier shape by incorporating different constants as a shape factor K_s . However, the effect of the pier shape on scouring cannot simply be described by a single dimensionless shape factor, as demonstrated by Figure 8, because different gradients exist for the near linear relationships. The curves for different K_s values in Figure 8 were generated by applying K_s to the curve of the cylindrical pier. It is difficult to mathematically describe the effect of pier shape, but numerical modelling has the ability to overcome this shortcoming.

EVALUATION OF EMPIRICAL EQUATIONS

Thirty empirical equations traditionally employed to predict bridge pier scour were evaluated against the results from the laboratory for a full-scale prototype. The equations were found to yield a wide range of varying and mostly unreliable results for the same case, even under controlled laboratory conditions.

From Figure 9 it is evident that a wide range of scour depths were produced by the equations for each test or boxplot. The scour depth was predominantly over-predicted, as the design equations intend to be conservative when they fail to be accurate. Nevertheless, the empirical equations still predict scour depths varying within a range of 3 m from one another for the same test.

Because empirical equations are generally developed from a standard experimental

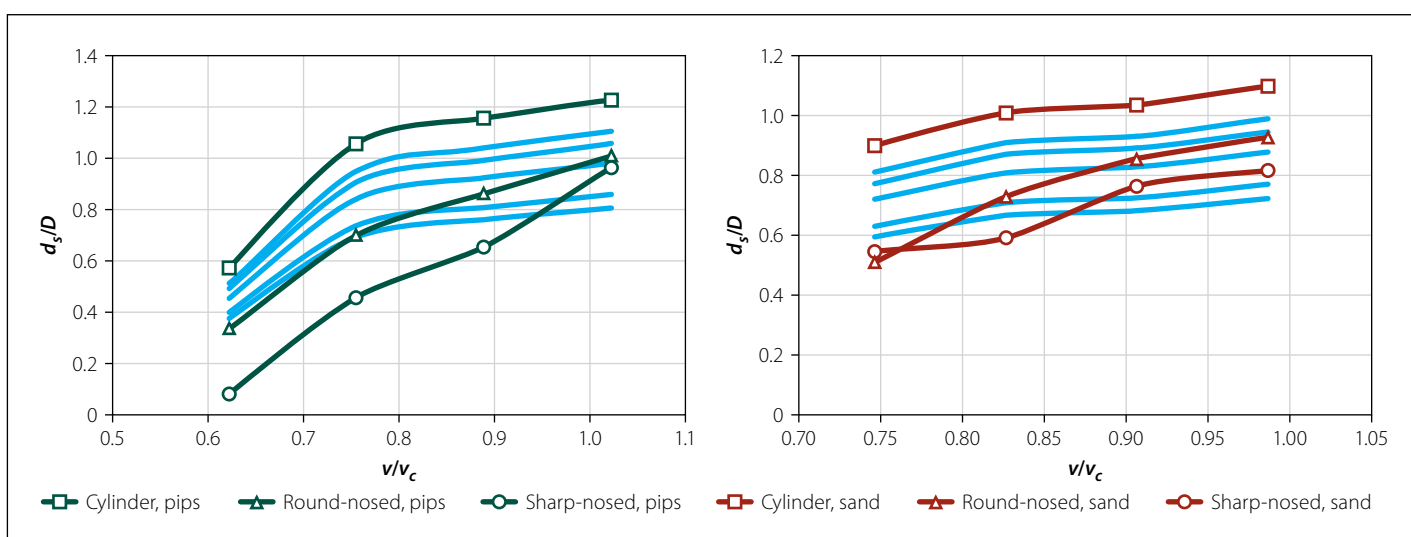


Figure 8 Evaluation of shape factors for the prediction of maximum scour depth

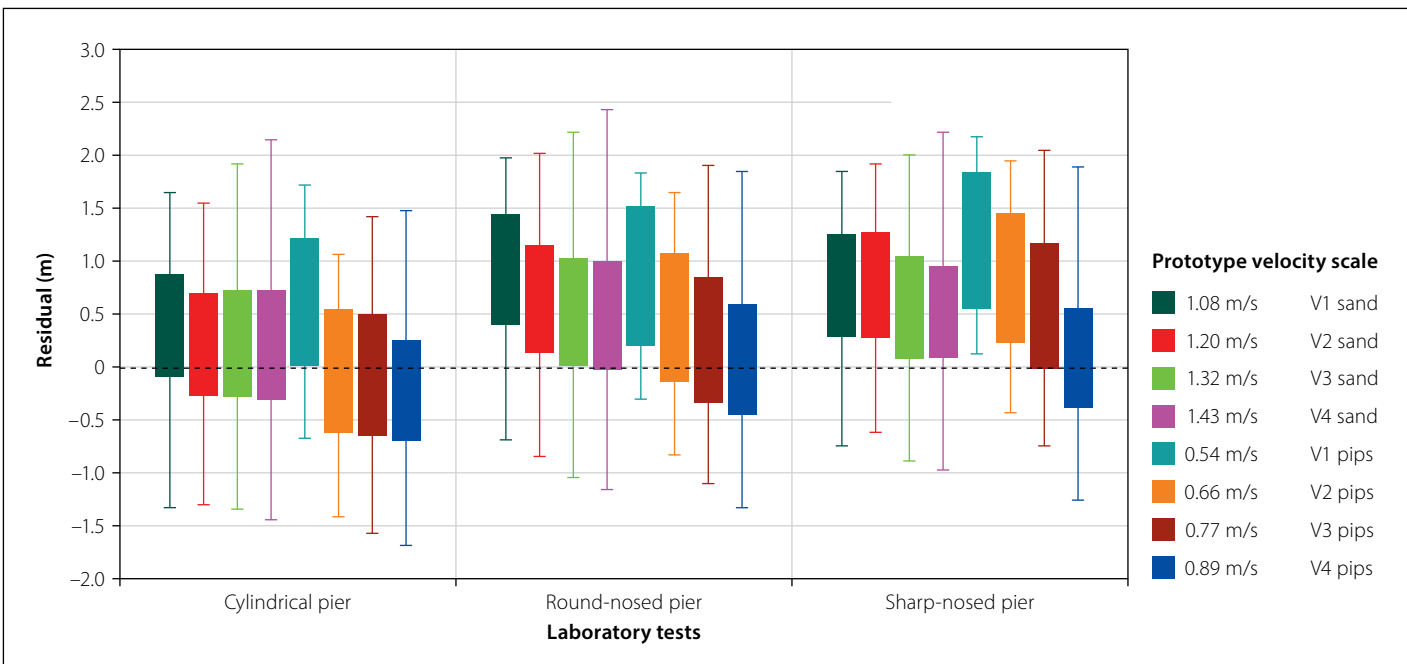


Figure 9 Boxplot showing the distribution of scour depth residuals for the different lab tests

setup with a cylindrical pier in a uniformly graded bed, the most accurate scour depths were predicted for the tests with the cylindrical pier, in addition to those with the crushed peach pips. It can be deduced that the scaling of the peach pips is a better representative of in-situ sediment behaviour than that of the fine sand. Furthermore, increased velocities yield larger scour depths and the equations yield less conservative predictions.

Similarly, the boxplots in Figure 10 compare the statistical spread for each empirical equation, which can be evaluated in conjunction with the more detailed relative scour depth dataset in Figure 11. The percentage error is given by $(d_s^{\text{observed}} - d_s^{\text{calculated}}) / d_s^{\text{observed}} \times 100$.

It is evident from Figure 10 that the equations are in weak agreement with one another and generally overestimate the observed scour depths with a mean error of 78%. The most accurate methods are those of Hancu (1971), and Melville and Kandasamy (1998a), while the safest equations for bridge pier design would be those of Blench (1969), Shen *et al* (1969) and Ali and Karim (2002), followed by the FDOT and HEC-18 equations.

In agreement with the literature study, the HEC-18 and Shen *et al* (1969) equations resembled the observed scour better. In addition, the Shen *et al* (1969) and Ali and Karim (2002) models presumably performed better because they rely on the pier Reynolds number, a parameter which has recently been identified as significant in the vortex formation by numerical model

studies (Roulund *et al* 2005). The implication of this is that models taking the vortex formation into consideration could offer better scour depth predictions.

The simple Blench (1969), and Melville and Kandasamy (1998a) equations, as well as the other old models of Breusers (1965), and Laursen and Toch (1956), were more accurate despite not incorporating the approach velocity or particle size. The equations predict the same scour depth for all the tests (only Melville and Kandasamy, and Laursen and Toch are differentiated by a shape factor) and are therefore considered less applicable. Breusers is the simplest expression which assumes that the maximum bridge pier scour can be estimated at 1.4 times the pier size. Pier size is the most predominant parameter appearing in all the formulae except in the Chitale (1962) model. Subsequently, Chitale also performed deceptively well because only one pier width was tested. Instead, the Chitale and the HEC-18 formulae depend on the Froude number, which can describe the sediment bed forms and their mode of transport (Graf 1971). HEC-18 and most of the other models are also based on the relative flow depth, which can possibly describe the thickness of the boundary layer (Roulund *et al* 2005).

On the other hand, Coleman (1971) and Gao *et al* (1993), also known as the simplified Chinese equation, are not fit for pier design due to under-predictions. In accordance with preceding studies, Froelich (1988) also underestimated scour depth, and as a result the overly conservative

Froelich Design equation came about, which adds the pier width to the predicted scour depth as a precautionary measure. The scour depth was also underestimated by Molinas (2004), particularly for particle sizes < 2 mm as explained by Mueller and Wagner (2005).

Kothiyari, Garde and Ranga (1992) demonstrated the most significant spread of errors. It is the only identified scour model that takes sediment density into consideration and overestimates scour depth, presumably due to the challenges posed by physical model scales.

Generally, formulae developed in affiliation with Melville overestimated the scour depth more than others. These formulae, as well as the HEC-18 equations, calculate the scour depth with a simplified approach using dimensionless correction factors to account for time, channel geometry, sediment size, grade, pier shape, flow alignment, armouring, flow intensity or flow depth. The simplified approach illustrates the effect of each parameter on the scour depth, but by doing so neglects to acknowledge that the parameters are interrelated.

Furthermore, it is difficult to mathematically describe the effect of pier shape on the horseshoe vortex, and subsequently the scour depth, with simply a constant shape factor. Half of the empirical equations evaluated in this study employ different shape factors, and thus the scour depths for the round-nosed and sharp-nosed were largely overestimated, as indicated in Figure 9. Figure 10 also shows boxplots for the empirical equations

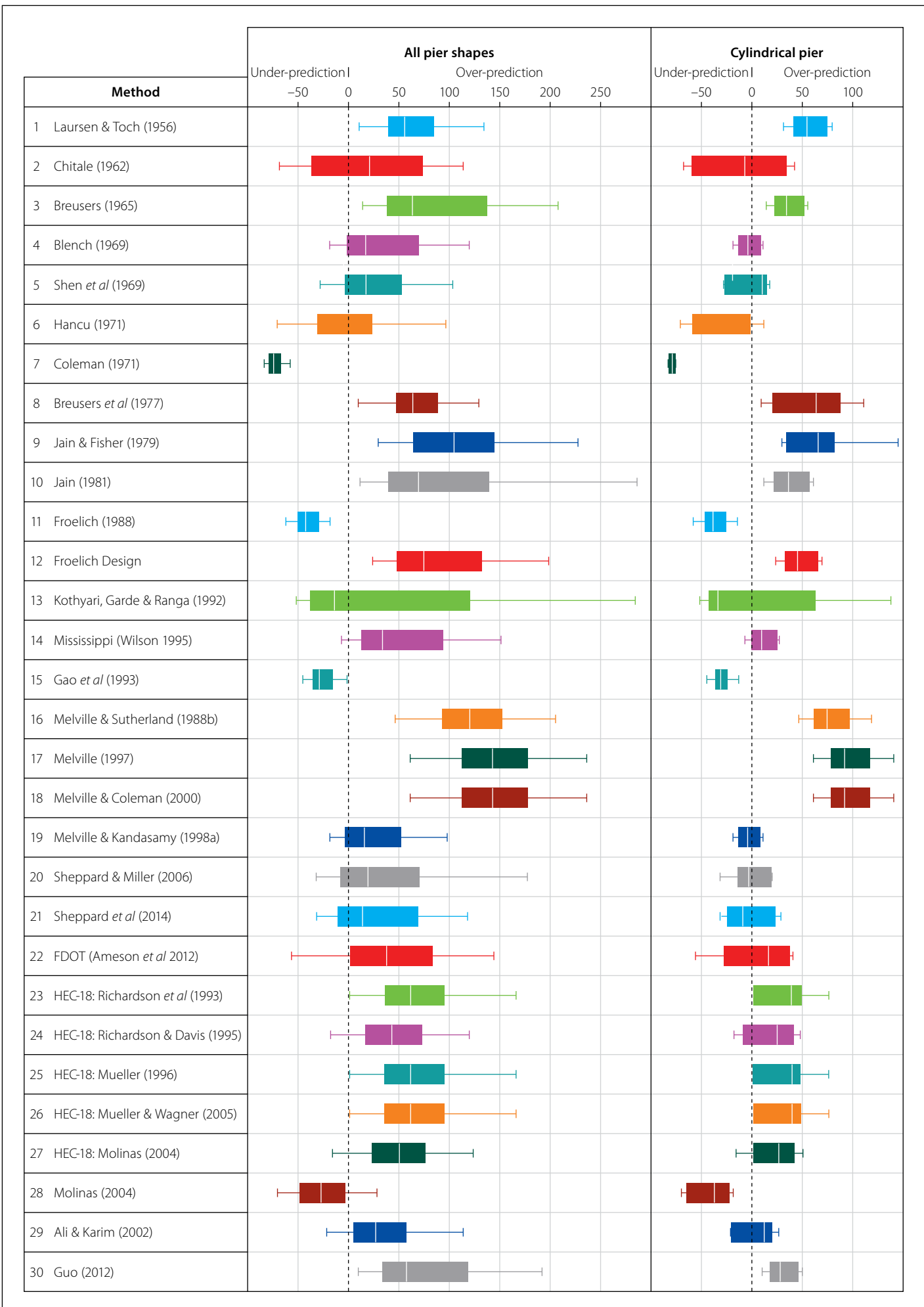


Figure 10 Boxplot showing the distribution of scour depth as a percentage error for the different empirical equations from the experimental work

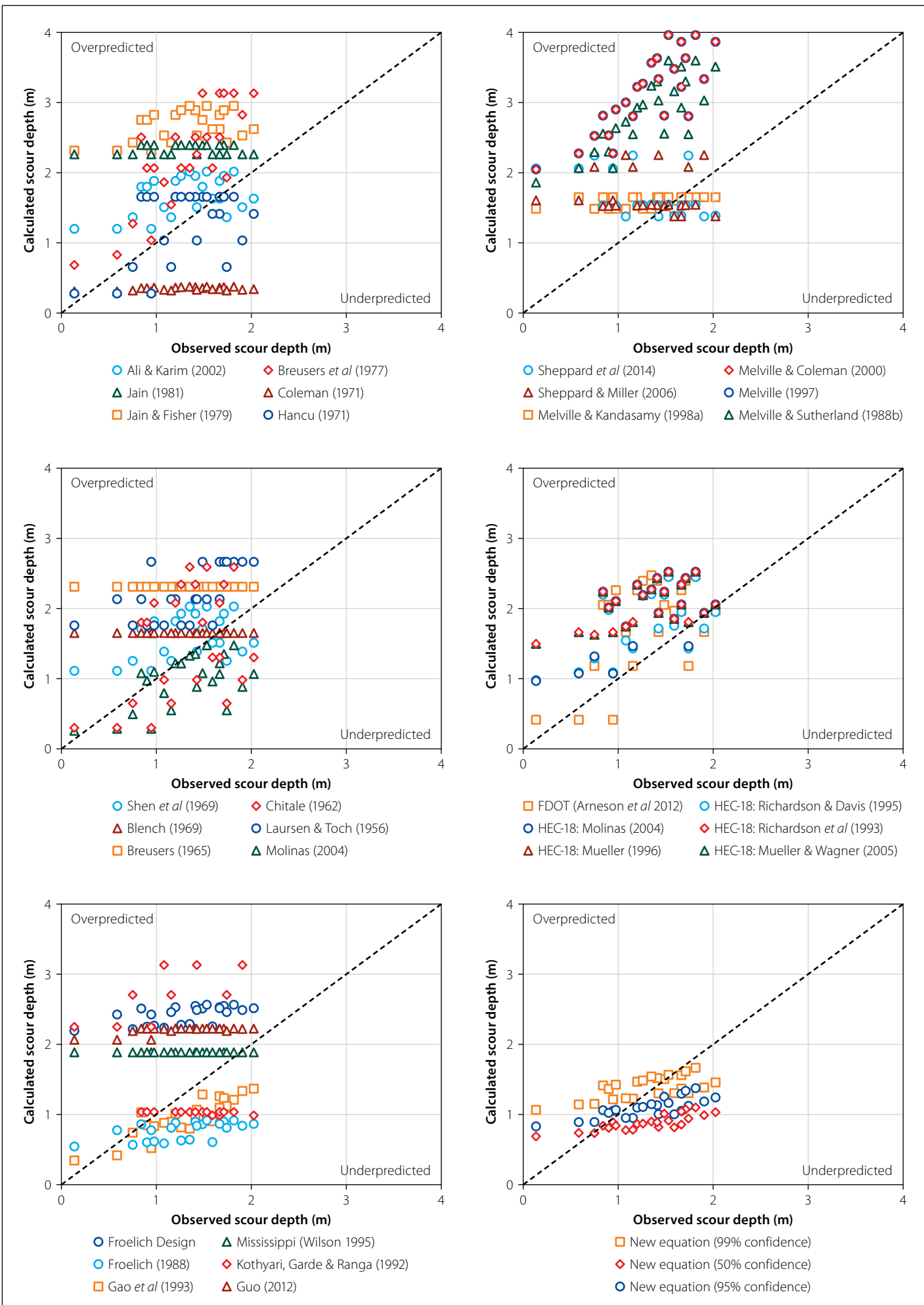


Figure 11 Comparison of relative scour depths observed from the experimental work and calculated by the different empirical equations

applied only to the cylindrical piers. The scour depths are better predicted, but they still have a mean error of 50%. The HEC-18 equations consistently performed the best, with the least under-estimations, while the other equations were inclined to over-predict less.

Five different HEC-18s have been developed with each new FHWA manual revision by improving the factor for armouring K_a . With the exception of Mueller and Wagner (2005), the factor K_a is determined by a dimensionless excess velocity intensity based on the critical velocity formulation by Gao *et al* (1993). The most recent FHWA manual discards the CSU's HEC-18 approach for the Florida DOT (Arneson *et al* 2012) based on Sheppard and Miller (2006), and Sheppard *et al* (2014) for wide piers with a new critical velocity calculation. While this method has a mean error percentage closer to zero, it also has a larger range of residuals (or higher SSR) with more under-predictions.

A new equation based on field data

Because the HEC-18 equations are generally favoured for performing better than the other empirical equations, it was attempted to further improve them by developing new dimensionless factors for armouring and pier shape. HEC-18 equations focus on the flow-structure interaction, but are limited in terms of the flow-sediment interaction (Guo 2012).

Extensive field data from the Bridge Scour Data Management System (BSDMS) (documented by Mueller and Wagner 2005) was used to perform the regression analysis. The 493 pier scour measurements were reduced to 207 measurements to satisfy the criteria for aligned flow, limited debris effects, non-cohesive sediment and upstream measurements at single piers. The measurements were also filtered to ensure the scour depths were captured within a ± 0.3 m accuracy.

A new approach to bridge pier scouring was adopted whereby the unreliable critical velocity was discarded for another parameter, the particle Reynolds number Rep , to evaluate the erodibility of the riverbed. Other parameters were also considered, such as the movability number based on settling velocity, unit stream power and the rate of energy dissipation, but Rep correlated best with the relative scour depth from the field data, as shown in Figure 12 ($R^2 = 0.84$, P -value = 10^{-11} , Significance F = 10^{-61}). The correlation is

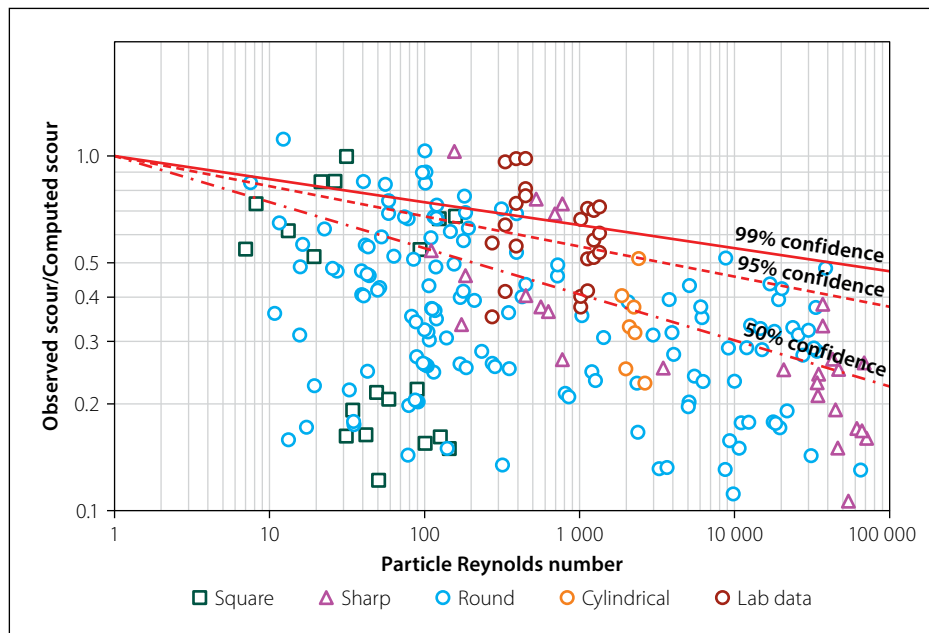


Figure 12 Relationship between the idealised factors K_a and Rep

given for the 50%, 95% and 99% confidence intervals that were determined statistically.

Representative particle sizes other than the mean d_{50} were also considered in an attempt to account for the grading of the sediment bed, but the best correlation was noted for $d = d_{50}$. The particle Reynolds number has the additional benefit that it is based on the channel shape and bed form roughness. However, limited information was captured by the field data, and the energy slope S_f was determined from Chézy by assuming the hydraulic radius $R = y$ flow depth for wide channels. Bed shear stress is also based on the slope and shape of a channel, but these parameters have not been used by the models in this study to describe their effect on scour depth. Note that despite the criterion for accuracy, the field data still displays a broad scatter of data for the observed scour, even at one given site or pier where the structure and sediment parameters are fixed, that the

captured flow parameters v and y alone cannot explain.

A new approach to the pier shape factor was also adopted by accounting for the relative pier lengths L/D and by employing an empirical equation whereby the effect of the pier shape on the scour depth is amplified by greater velocities, or equivalently, greater pier Reynolds numbers associated with the horseshoe vortex. Figure 13 shows that an increased shape factor correlates with the increased scour depths observed for a particle Reynolds number between 100 and 1 000.

The standard HEC-18 equation with the new proposed factors for armouring and pier shape are presented. The standard factors should be used for the bed condition with clear-water scouring $K_b = 1.1$ and for alignment $K_\theta = (\cos\theta + L/D\sin\theta)^{0.65}$. The a and b coefficients in Table 4 were determined for different confidence intervals, for while a good design equation

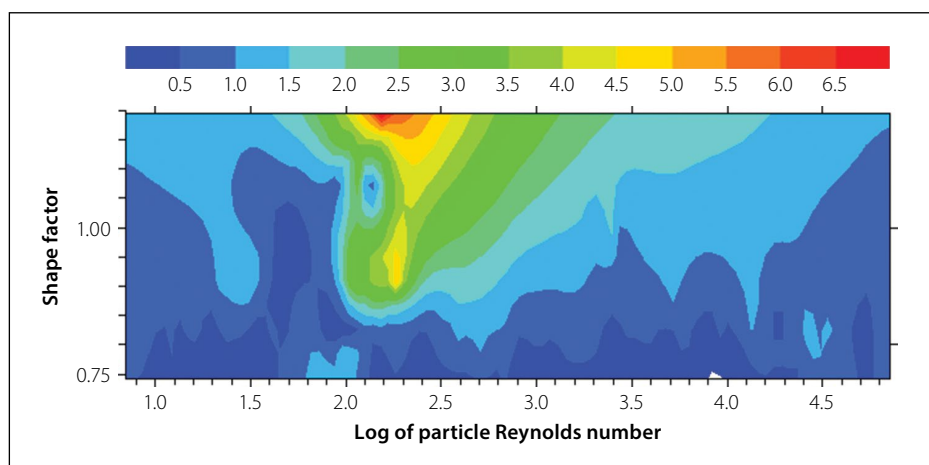


Figure 13 Contour plot for the observed bridge pier scour depth (m) relative to K_s and Rep

with a higher confidence interval may guarantee fewer under-predictions, an empirical equation with a lower confidence interval may yield more accurate predictions. Adopting a new approach with confidence intervals can quantify the trade-off between accuracy and unsafe under-predictions, offering flexibility to the bridge designer.

$$d_s = 2DK_s K_\theta K_a (y_1/D)^{0.35} Fr^{0.43} \quad (5)$$

$$K_a = \left(\frac{\sqrt{g} y_1 S_f}{v} d \right)^a \quad (6)$$

$$K_s = \begin{cases} [1.1 + 1.6E - 8(Re_D)](L/D)^b, & \text{for square-nosed piers} \\ [0.9 + 3.6E - 8(Re_D)](L/D)^b, & \text{for sharp-nosed piers} \\ (L/D)^b, & \text{for round-nosed piers} \\ 1, & \text{for cylindrical piers} \end{cases} \quad (7)$$

Table 4 New equation parameters proposed for different confidence intervals

| Confidence interval | a | b |
|---------------------|--------|-------|
| 99% | -0.065 | -0.03 |
| 95% | -0.095 | -0.08 |
| 50% | -0.130 | -0.09 |

As an alternative to the new proposed empirical equations, the contour plot in Figure 14, based on the Modified Liu Diagram, is capable of predicting bridge pier scour. Despite the fact that the particle Reynolds number and movability number account for all the flow and sediment parameters except for the pier structure, the observed pier scour depth in Figure 14 (not relative scour depth d_s/D) is comparable to the Modified Liu Diagram for incipient motion in Figure 3. Sediment movement is observed for $Rep > 13$ and a movability number > 0.2 in the turbulent flow region (Rooseboom *et al* 1983). The scour depth dramatically increases for a smaller particle Reynolds number between 100 and 1 000, and for a larger movability number above 3. For comparison, the scour depth calculated by the new equations 5, 6 and 7 (99% confidence) produces a smoother contour plot similar to the one observed from the field data, but with deeper scour holes in the far corner of the turbulent movement region. This new diagram relating Rep , v^*/w and d_s has the potential to accurately predict bridge pier scour should it be supplemented and validated

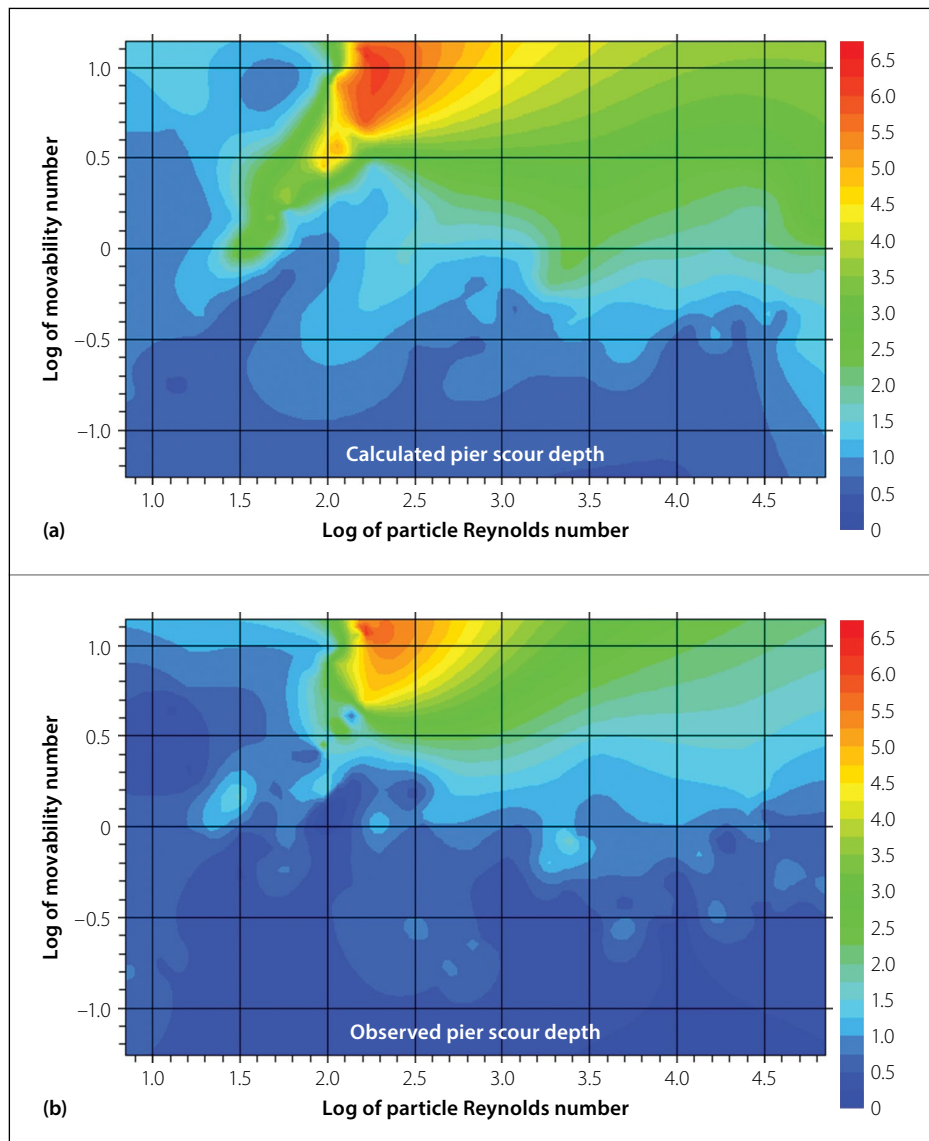


Figure 14 Modified Liu Diagram for bridge pier scour depth (m)

by additional scour data, and should the assumptions for energy slope, channel shape and settling velocity be supported.

The sum of squared residuals, as defined below, was compared against the thirty other empirical equations, for field and lab data, in Figure 15. The equations are ranked according to the least overall error and least under-predictions without any weighting. The new proposed equation ranks the highest, followed by HEC-18 Mueller (1996), Shen *et al* (1969) and Mueller and Wagner (2005) (based on v_c , ReD and d/D respectively).

$$SSR = \sum (d_s^{computed} - d_s^{observed})^2 \quad (8)$$

The new equation (99% confidence) ranked the highest with the least total SSR 186;3 and least under-predictions 1;1 for the field data and lab data combined, followed by the new equation with the 95% and 50% confidence intervals for the combined data. It also had the least total SSR 3 and the

second least under-predictions of SSR 1 for the lab data. The new equation (50% confidence) yielded the least total SSR 71 followed by 94 for the new equation (95% confidence) for just the field data (ranking 11th and 15th in under-predictions). For the lab data, the new equation (95% confidence) ranked second and third, and the new equation (50% confidence) ranked fourth and sixth in the least total SSR and under-predictions respectively.

If the ± 0.3 m accuracy of the pier scour measurements is considered, the SSR for the field data is 12 and for the lab data is 0. The new equation (95% confidence) is therefore also adequately reliable as a design equation (with an SSR for under-predictions of 10 less than the 12 representing the accuracy of the data).

The new proposed equation performs comparably better to the field data than to the lab data. The new equations have achieved considerably less scatter about the line of equality, despite under-predictions

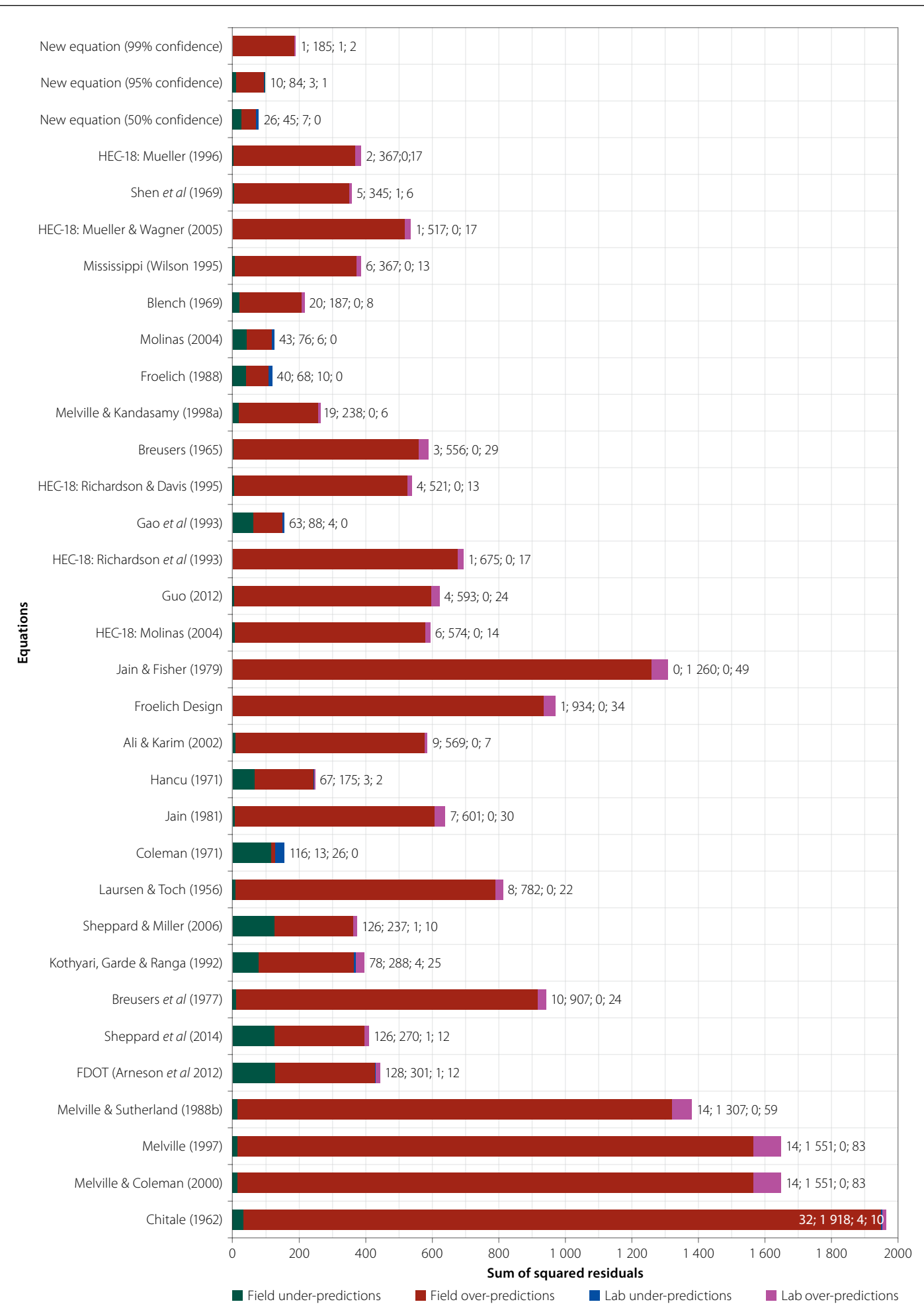


Figure 15 Comparison of the sum of squared residuals for the different equations for lab data and field data

for the cylindrical piers. The new equation (50% confidence) would not be fit for pier design due to under-predictions, but the new equation (99% confidence) is the most accurate method that has a compact boxplot range of error and a mean error percentage closest to but greater than zero (10%) and a minimum of only -28% (acceptable compared to the lab error of 9%).

TRANSITION TOWARDS NUMERICAL MODELLING

Evidently, the scouring process at the riverbed interface is complex and affected by numerous interrelated parameters (Rooseboom 2013). Various attempts have been made to address the complexity by assuming dominant variables and reducing them to simplified relationships to describe scour. However, it is difficult to generalise the scour process, because there are so many interrelated variables that may conceal the influence of one another on scouring. Furthermore, simplifying assumptions are required to quantify the three-dimensional flow patterns, complicated vortex and turbulence structures. These limit the extent to which a mathematical analysis can be made to model scour (Tseng *et al* 2000; Guo 2012). When faced with such uncertainty in bridge design, hydraulic engineers are compelled to pursue costly, labour-intensive and time-consuming physical model studies, which have their own flow visualisation and scaling challenges (Xiong *et al* 2014).

Most sediment studies are still based on empirical formulae derived and calibrated by means of a coefficient from small-scale laboratory experiments, and occasionally field data, despite the availability of sophisticated computers. More weight should be attached to relationships that are fundamentally sound and based on first principles, such as the conservation of mass and momentum, which computer software is capable of solving (Olsen & Malaen 1993). A recently studied alternative is the use of three-dimensional numerical models to better predict equilibrium scour depth.

Numerical solutions by Computation Fluid Dynamics (CFD) are becoming increasingly popular to compute fluid flow as technology advances and the cost of computational time decreases. Hydrodynamic models coupled with sediment transport algorithms have the ability to predict not only scour depth, but also scour geometry (such as l_s and w_s from Table 3). Furthermore, they are not limited in terms

of scale restrictions (Sawadogo 2015) and allow parametric studies of conditions that are otherwise impossible or difficult to investigate in the laboratory (Sumer 2007).

However, numerical models are not without limitations – for example, computer constraints in terms of memory capacity and processors, as well as the computational effort (Sawadogo 2015). The accuracy of the solution relies on the underlying assumptions of governing sediment transport equations and the model's ability to resolve the vortices (Abbasnia & Ghiassi 2011). Although extensive research has been conducted for more than six decades, comparatively little research has been presented on numerical modelling of bridge pier scour (Baykal *et al* 2015). Most of these numerical models focus on resolving the flow and horseshoe vortex, particularly for a flat rigid bed, and not on modelling scour.

Olsen and Melaen (1993), and in a follow-up study Olsen and Kjellesvig (1998) were the first to attempt simulating bridge pier scour with a numerical model by employing convection-diffusion and bed load equations. The results compared fine with empirical formulae, but the simulation took nine weeks to solve 80×10^3 cells, and the horseshoe vortex was not resolved. In more recent studies, Khosronejad *et al* (2012) and Xiong *et al* (2014) developed numerical models, but these also significantly under-predicted the scour pattern at the pier nose because the horseshoe vortex was not properly resolved. Roulund *et al* (2005), and in a follow-up study Baykal *et al* (2015), have shown the most promising results whereby the upstream scour depth agrees well with their experimental work, but a discrepancy of up to 30% was observed for the scour pattern downstream of the pier.

Finally, it may be interesting to note that, unlike the other models, the equation for bridge pier scour by Ali and Karim (2002) was developed from a numerical model for the associated complex flow field.

CONCLUSIONS AND RECOMMENDATIONS

Traditional methods for estimating the maximum scour depth near bridge piers rely on simplistic formulae, each with its own assumptions and limitations, which often yield unreliable results. Thirty of these empirical equations were evaluated for their ability to predict bridge pier scour, and their shortcomings were thereby demonstrated.

In accordance with previous studies, it was confirmed that the equations are in weak agreement with one another. They produce a wide range of errors relative to one another (in the order of 95%), because the equations are not universal and only yield good results under conditions similar to those from which they were derived.

Because the empirical equations are generally developed from a standard experimental setup with a cylindrical pier in a uniformly graded bed, the most accurate scour depths were predicted for the tests with the cylindrical pier. Only half of the empirical equations evaluated in this study account for other pier shapes by incorporating a constant shape factor. However, the effect of the pier shape on scouring cannot simply be described by a single dimensionless shape factor or constant.

Furthermore, the scour holes were better predicted for the tests with crushed peach pits than those with a fine sand bed. It can be deduced that the scaling of the peach pits by the mobility number is a better representative of in-situ sediment behaviour, and that the non-scalable effects of the hydraulic forces in the settling velocity and density can be overcome by using a sediment with a smaller density and larger particle size (Heller 2011).

The scour depth was predominantly over-predicted by the equations while those of Coleman (1971), Froelich (1988) and Gao *et al* (1993) are not fit for pier design due to recurrent under-predictions. While the over-prediction of the observed scour may cause one to query the equilibrium time, two hours have been the basis for the derivation of several equations and are justified by Melville (1975), Roulund *et al* (2005), Mohammed *et al* (2016) and Guo (2014).

Most of the empirical equations for bridge pier scour are reliant on the selection of an appropriate critical velocity. Hancu (1971) proves to be the most accurate scour prediction model for the lab data, presumably because it relies on a critical velocity that is derived from Shields and the sediment density.

No single equation is conclusively the best, but the HEC-18 models appeared to consistently perform better in safely predicting the observed lab and field scour depths for all pier shapes, in agreement with Mueller and Wagner (2005), Gaudio *et al* (2010) and Toth (2015). Generally, the HEC-18 model is favoured by the US FHWA engineers for field results that are least likely to be under-predicted (Arneson *et al* 2012). In

addition, the equations of Shen *et al* (1969), and Ali and Karim (2002) are recommended for conceptual design, because they rely on the pier Reynolds number, a parameter which has been identified as significant in the horseshoe vortex and subsequent scour hole formation. Prediction models taking the vortex formation into consideration could offer better scour depth predictions.

Finally, field data was analysed to improve the standard HEC-18 equation with new factors for armouring and pier shape. The pier shape accounts for L/D and uses a linear equation whereby the effect of the pier shape on the scour depth is amplified by greater pier Reynolds numbers. The new armouring factor is based on the particle Reynolds number as opposed to the widely adopted critical velocity, and achieves considerably less scatter about the line of equality despite under-predictions for the cylindrical piers. A new approach with confidence intervals was adopted to quantify the trade-off between accuracy and under-predictions, offering flexibility to the bridge designer.

The new equation (99% confidence) ranked the highest with the least total SSR and least under-prediction for the scour depths from the field data and lab data combined, followed by HEC-18 Mueller (1996), Shen *et al* (1969), and Mueller and Wagner (2005). If the accuracy of the field pier scour measurements is considered, the new equation (95% confidence) is also adequately reliable as a design equation, while the new equation (50% confidence) would not be fit for bridge design due to under-predictions of the equilibrium bridge pier scour depth. The new proposed equation performs comparably better to the field data than to the lab data. However, it still has the lowest mean error percentage to the other methods of 10%, which is acceptable compared to the lab error of 9%.

As an alternative to the new proposed empirical equations, the diagram in Figure 14 relating Rep , v^*/w and ds is comparable to the Modified Liu Diagram for incipient motion and has the potential to predict bridge pier scour, even though the pier structure parameters are omitted.

The simplicity of conservative empirical equations may be appealing; nonetheless, overestimating the anticipated scour depth leads to uneconomical designs with unnecessarily expensive foundations and countermeasures. Further research and improved prediction models should be considered, particularly advanced CFD numerical models which are becoming increasingly feasible. In short, numerical modelling should be the primary subject of future studies. Numerical models have led to an improved understanding of the flow mechanisms and scour process, which could ultimately lead to improved scour equations derived from first principles and not empirically.

ACKNOWLEDGEMENT

The financial assistance of the National Research Foundation (NRF) towards this research is hereby acknowledged with gratitude. The opinions expressed, and conclusions arrived at, are those of the authors and should not be attributed to the NRF.

APPENDIX

List of empirical equations

d_s = Bridge pier scour depth

ρ = Fluid density

ρ_s = Sediment density

ν = Kinematic viscosity

t = Time

D = Pier diameter or width

L = Pier length

d = Median sediment size

σ_g = Particle size distribution

s = Specific gravity

v_1 = Approach flow velocity

y_1 = Approach flow depth

g = Gravitational acceleration

v_c = Sediment critical velocity

Fr = Froude number

α = Angle of flow in radians

B = Channel width

K_s = Shape factor

| | | |
|---|------------------------------|---|
| 1 | Laursen & Toch (1956) | $d_s = 1.35D^{0.7}y_1^{0.3}K_s$ Square $K_s = 1.1$; Circular $K_s = 1$; Round $K_s = 0.8$; Sharp $K_s = 0.66$ |
| 2 | Chitale (1962) | $d_s = y_1(6.65Fr - 0.51 - 5.49Fr^2)$ |
| 3 | Breusers (1965) | $d_s = 1.4D$ |
| 4 | Blench (1969) | $d_s = 1.8y_1^{0.75}D^{0.25} - y_1$ |
| 5 | Shen <i>et al</i> (1969) | $d_s = 0.00023(v_1D/v)^{0.619}$ |
| 6 | Hancu (1971) | $d_s = 2.42D\left(\frac{2v_1}{v_c} - 1\right)\left(\frac{v_1}{gD}\right)^{1/3}$ for $0.5 < \frac{v_1}{v_c} < 1$ $v_c = 1.2\sqrt{gd}(s-1)(y_1/d)^{0.2}$ |
| 7 | Coleman (1971) | $\frac{v_1}{\sqrt{2gd}} = 0.6\left(\frac{v_1}{D}\right)^{0.9}$ |
| 8 | Breusers <i>et al</i> (1977) | $d_s = D\left(\frac{2v_1}{v_c} - 1\right)\left[2 \tan h\left(\frac{y_1}{D}\right)\right]K_s K_\theta$ for $0.5 < \frac{v_1}{v_c} < 1$ Square $K_s = 1.1$; Circular $K_s = 1$; Round $K_s = 0.8$; Sharp $K_s = 0.66$ Assume v_c from Neill's formulation (1973) |

| | | |
|-----|---|---|
| | | $d_{s1} = 2D(Fr_1 - Fr_c)^{0.25} \left(\frac{y_1}{D}\right)^{0.5}$ for $(Fr - Fr_c) > 0.2$ $d_{s2} = 1.85DFr_1^{0.25} \left(\frac{y_1}{D}\right)^{0.5}$ for $(Fr - Fr_c) < 0$ $d_s = \max(d_{s1}, d_{s2})$ for $0 < (Fr - Fr_c) < 0.2$ $Fr_c = \frac{\nu_c}{\sqrt{gy_1}}$ Assume ν_c from Neill's formulation (1973) |
| 9 | Jain & Fisher (1979) | |
| 10 | Jain (1981) | $d_s = 1.84y_1Fr_c^{0.25} \left(\frac{D}{y_1}\right)^{0.7}$ Assume ν_c from Neill's formulation (1973) |
| 11a | Froelich (1988) | $d_s = 0.32K_s D^{0.62} y_1^{0.47} Fr^{0.22} d^{-0.09}$ Square $K_s = 1.3$; Circular $K_s = 1$; Round $K_s = 1$; Sharp $K_s = 0.7$ |
| 11b | Froelich Design | $d_s = 0.32K_s D^{0.62} y_1^{0.47} Fr^{0.22} d^{-0.09} + D$ |
| 12 | Kothiyari, Garde & Ranga (1992) | $d_s = \left(\frac{D}{d}\right)^{-0.25} \left(\frac{y_1}{D}\right)^{0.16} \left(\frac{\nu_1^2 - \nu_c^2}{(s-1)gd}\right)^{0.4}$ for $\frac{\nu_1}{\nu_c} < 1$ $\nu_c^2 = 1.2[(s-1)gd] \left(\frac{D}{d}\right)^{-0.11} \left(\frac{y_1}{d}\right)^{0.16}$ |
| 13 | Mississippi (Wilson 1995) | $d_s = 0.9D^{0.6} y_1^{0.4}$ |
| 14 | Simplified Chinese Gao <i>et al</i> (1993) | $d_s = 0.46K_s D^{0.6} y_1^{0.15} d^{-0.07} \left(\frac{\nu_1 - \nu_i}{\nu_c - \nu_i}\right)^\eta$ $\eta = \left(\frac{\nu_c}{\nu_1}\right)^{9.35+2.23\log(d)}$ $\nu_c = \left(\frac{y_1}{d}\right)^{0.14} \left[17.6(s-1)d + 6.05E^{-7} \left(\frac{10 + 0.3048y_1}{(0.3048d)^{0.72}}\right) \right]^{0.5}$ $\nu_i = 0.645\nu_c \left(\frac{d}{D}\right)^{0.053}$ Square $K_s = 1.1$; Circular $K_s = 1$; Round $K_s = 0.8$; Sharp $K_s = 0.66$ |
| 15 | Melville & Sutherland (1988b) | $d_s = K_\theta K_\sigma K_s K_{y1} (2.4K_l) K_d$ Gradation factor $K\sigma = 1$ |
| | Alignment factor | $K_\theta = \left(\cos\theta + \frac{L}{D\sin\theta}\right)^{0.65}$ |
| | General shape factor | Square $K_s = 1.1$; Circular $K_s = 1$; Round $K_s = 1$; Sharp $K_s = 0.9$ |
| | Flow intensity factor | $K_1 = \frac{\nu_1 - (\nu_a - \nu_c)}{\nu_c}$ for $\frac{\nu_1 - (\nu_a - \nu_c)}{\nu_c} < 1$ $K_I = 1$ for $\frac{\nu_1 - (\nu_a - \nu_c)}{\nu_c} \geq 1$ $u_c^* = 0.0115 + 0.0125d^{1.4}$ for $0.1 \text{ mm} < d < 1 \text{ mm}$ $u_c^* = 0.0305d^{0.5} + 0.0065d^{-1}$ for $1 \text{ mm} < d < 100 \text{ mm}$ Median armour size $d_a = \frac{d_{max}}{1.8}$ for $\nu_a = 0.8\nu_{ca}$ $\nu_{ca} = 5.75u_{ca}^* \left[\log \left(5.53 \frac{y_1}{d_a} \right) \right]$ $\nu_c = 5.75u_c^* \left[\log \left(5.53 \frac{y_1}{d} \right) \right]$ |

| | | |
|----|------------------------------|--|
| | Sediment factor | $K_d = 0.57 \log \left(2.24 \frac{D}{d} \right)$ for $\frac{D}{d} \leq 25$ $K_d = 1$ for $\frac{D}{d} > 25$ |
| | Depth size factor | $K_{y1} = D$ for $\frac{y_1}{D} > 2.6$ $K_{y1} = 0.78D \left(\frac{y_1}{D} \right)^{0.255}$ for $\frac{y_1}{D} < 2.6$ |
| 16 | Melville (1997) | $d_s = K_\theta K_G K_s K_y K_I K_a$ Channel geometry $K_G = 1$ for a bridge pier |
| | Revised depth size factor | $K_y = 2.4D$ for $\frac{D}{y_1} < 0.7$ $K_y = 2\sqrt{y_1 D}$ for $0.7 < \frac{D}{y_1} < 5$ $K_y = 4.5y_1$ for $\frac{D}{y_1} > 5$ |
| 17 | Melville & Coleman (2000) | $d_s = K_\theta K_G K_s K_y K_I K_d K_t$ Time factor $K_t = \exp \left[-0.07 \frac{v_c}{v_1} \left \ln \left(\frac{t}{t_e} \right) \right ^{1.5} \right]$ for $\frac{v_1}{v_c} < 1$ where t_e = total time to reach equilibrium profile |
| 18 | Melville & Kandasamy (1998a) | $d_s = K_s K_y^n D^{1-n}$ $K = 5, n = 1$ for $0.04 \geq \frac{y_1}{D}$ $K = 1, n = 0.5$ for $0.04 < \frac{y_1}{D} < 1$ $K = 1, n = 0$ for $\frac{y_1}{D} \geq 1$ |
| 19 | Sheppard & Miller (2006) | $d_s = 2.5Df_1f_2f_3$ for $0.47 < \frac{v_1}{v_c} < 1$ $f_1 = \tanh \left[\left(\frac{y_1}{D} \right)^{0.4} \right]$ $f_2 = \left\{ 1 - 1.75 \left[\ln \left(\frac{v_1}{v_c} \right) \right]^2 \right\}$ Assume v_c from Neill's formulation (1973) $f_1 = \frac{\frac{D}{d}}{0.4 \left(\frac{D}{d} \right)^{1.2} + 10.6 \left(\frac{D}{d} \right)^{-0.13}}$ |
| 20 | Sheppard <i>et al</i> (2014) | $d_s = 2.5Df_1f_2f_3K_1D$ for $0.4 \leq \frac{v_1}{v_c} < 1.0$ $f_1 = \tanh \left[\left(\frac{y_1}{K_1 D} \right)^{0.4} \right]$ $f_2 = \left\{ 1 - 1.2 \left[\ln \left(\frac{v_1}{v_c} \right) \right]^2 \right\}$ $f_3 = \left[\frac{K_1 D}{d} \right] \left[0.4 \left(\frac{K_1 D}{d} \right)^{1.2} + 10.6 \left(\frac{K_1 D}{d} \right)^{-0.13} \right]^{-1}$ $K_1 = 1$ for cylindrical piers $K_1 = 0.86 + 0.97 \left(\alpha - \frac{\pi}{4} \right)^4$ for rectangular piers |

| | | |
|-----|---|--|
| | Sheppard <i>et al</i> (2014) (continued) | $u_c^* = \left\{ 16.2d \left[\frac{9.09 \times 10^{-6}}{d} - d \left(38.76 + 9.6 \ln(d) \right) - 0.005 \right] \right\}^{1/2}$ $Re = \frac{u_c^* d}{v} \text{ for } 5 \leq Re \leq 70$ $\nu_c = 2.5u_c^* d \ln \left\{ 73.5 \frac{y_1}{d} \left[Re \left(2.85 - 0.58 \ln(Re) + 0.002 Re \right) + \frac{111}{Re} - 6 \right]^{-1} \right\} \text{ for } Re > 70$ $\nu_c = 2.5u_c^* \ln \left(\frac{2.21y_1}{d} \right) \text{ for } Re < 70$ |
| 21 | FDOT (Arneson <i>et al</i> 2012) | $d_s = 2.5f_1 f_2 f_3 K_1 D \text{ for } 0.4 < \frac{y_1}{\nu_c} \leq 1.0$ $\nu_c = 2.5u_c^* \log \left(5.53 \frac{y_1}{d} \right)$ $u_c^* = 0.0377 + 0.041d^{1.4} \text{ for } 0.1 \text{ mm} < d < 1 \text{ mm}$ $u_c^* = 0.1d^{0.5} - \frac{0.0213}{d} \text{ for } 1 \text{ mm} < d < 100 \text{ mm}$ |
| 22 | HEC-18 or CSU equations | $d_s = 2.5DK_s K_\theta K_b K_a \left(\frac{y_1}{D} \right)^{0.35} Fr^{0.43}$ <p>Bed condition factor $K_b = 1.1$ for clear-water scouring</p> |
| 22a | Richardson <i>et al</i> (1993) | Armouring factor $K_a = 1$ |
| 22b | Richardson & Davis (1995) | $K_a = [1 - 0.89(1 - V_R)^2]^{0.5}$ <p>Dimensionless excess velocity intensity</p> $V_R = \frac{\nu_1 - \nu_i}{\nu_{c90} - \nu_i}$ $\nu_i = 0.645\nu_c \left(\frac{d}{D} \right)^{0.053}$ $\nu_{c90} = 6.19y_1^{1/6} d_{90}^{1/3} \text{ where } d_{90} = d\sigma_g^{1.282}$ |
| 22c | Mueller (1996) | $K_a = 0.4V_R^{0.15}$ $V_R = \frac{\nu_1 - \nu_i}{\nu_c - \nu_{i95}}$ $\nu_i = 0.645\nu_c \left(\frac{d}{D} \right)^{0.053}$ $\nu_{i95} = 0.645 \nu_{c95} \left(\frac{d_{95}}{D} \right)^{0.053} \text{ where } d_{95} = d\sigma_g^{1.645}$ |
| | Critical velocity (Neill 1973) | $\nu_c = \theta_s^{0.5} 31.08 y_1^{1/6} d^{1/3} \text{ using Shields parameter}$ $\theta_s = 0.0019d^{-0.384} \text{ if } d < 0.0009 \text{ m}$ $\theta_s = 0.0942d^{0.175} \text{ if } 0.0009 \text{ m} < d < 0.020 \text{ m}$ $\theta_s = 0.047 \text{ if } d > 0.020 \text{ m}$ |
| 22d | Mueller & Wagner (2005) | $K_a = 0.35 \left(\frac{D}{d} \right)^{0.19}$ |
| 22e | Molinias (2004) | $K_a = 1.25 + 3 \sqrt{\frac{d_{cfm}}{d}} V_R^{0.6} \ln(V_R + 0.5)$ $V_R = \frac{\nu_1 - \nu_i}{\nu_{cm} - \nu_i}$ $\nu_i = 2.65y_1^{1/6} d_{35}^{1/3}$ $\nu_{cm} = 6.625y_1^{1/6} d_{cfm}^{1/3}$ $d_{cfm} = \frac{d_{85} + 2d_{90} + 2d_{95} + d_{99}}{6}$ |

| | | |
|----|--------------------|--|
| 23 | Molinas (2004) | $d_s = 0.99K_t K_s K_\theta K_b K_a V_R^{0.55} D^{0.66} y^{0.17}$ Scour initiation $K_i = \left(1 - \frac{v_i}{v_1}\right)^{0.45}$ $Ka = 1.25 + 3 \sqrt{\frac{d_{cfm}}{d}} V_R^{0.6} \ln(V_R + 0.5)$ |
| 24 | Ali & Karim (2002) | $d_s = \frac{K_1 D_*^{1.2} y_1}{\left(\frac{v_1 D}{v}\right)} \left[1 - \text{Exp} \left(-5.32 E^{-4} \frac{v_1 t}{y_1} \right) \right]$ $K1 = 0.1 \sqrt{(s-1)gd^{3/2}} D_*^{-0.3}$ $D_* = [(s-1)gv^{-2}]^{1/3}$ |
| 25 | Guo (2012) | $ds = \sqrt{Dy} \tanh \left(\frac{H^2}{3.75\sigma_g} \right)$ where $\sigma_g = \sqrt{\frac{d_{84}}{d_{16}}}$ Densiometric particle Froude number $H = \frac{v_1}{\sqrt{(s-1)gd}}$ |

REFERENCES

- Abbasnia, A H & Ghiassi, R 2011. Improvements on bed-shear stress formulation for pier scour computation. *International Journal for Numerical Methods in Fluids*, 67, 383–402.
- Ali, K H M & Karim, O A 2002. Simulation of flow around piers. *Journal of Hydraulic Research*, 40(2): 161–174.
- Arneson, L A, Zevenbergen, L W, Lagasse, P F & Clopper, P E 2012. *Evaluating scour at bridges*. Report FHWA-HIF-12-003. Washington, DC: US Department of Transportation, Federal Highway Administration.
- Baykal, C, Sumer, B M, Fuhrman, D R, Jacobsen, N G & Fredsøe, J 2015. Numerical investigation of flow and scour around a vertical circular cylindrical pier. *Philosophical Transactions of the Royal Society A*, 373(2033).
- Blench, T 1969. *Mobile-bed fluviology*. Edmonton, Canada: University of Alberta Press.
- Breusers, H N C 1965. Scour around drilling platforms. *Bulletin of Hydraulic Research*, 19: 276.
- Breusers, H N C, Nicollet, G & Shen, H W 1977. Local scour around cylindrical pier. *Journal of Hydraulic Research*, 15(3): 211–252.
- Chitale, S V 1962. Scour at bridge crossings. *Transactions of the American Society of Civil Engineers*, 127(1): 191–196.
- Coleman, N L 1971. Analyzing laboratory measurements of scour at cylindrical piers in sand beds. *Proceedings*, 14th Congress of the International Association for Hydraulic Research (IAHR), 29 August – 3 September, Paris, Vol 3, pp 307–313.
- Deshmukh, A R & Raikar, R V 2014. A clear-water scour around a circular bridge pier under steady flow for different opening ratios. *International Journal of Research in Engineering and Technology*, 3(1): 158–162.
- Ettema, R 1980. *Scour at bridge piers*. Auckland, New Zealand: University of Auckland, Department of Civil Engineering.
- Froelich, D C 1988. Analysis of onsite measurements of scour at piers. *Proceedings*, ASCE National Conference on Hydraulic Engineering, 8–10 August, Colorado Springs, CO, pp 534–539.
- Gao, D, Posada, G L & Nordin, C F 1993. *Pier scour equations used in the People's Republic of China*. Report FHWA-SA-93-076. Washington, DC: US Department of Transportation, Federal Highway Administration.
- Gaudio, R, Grimaldi, C, Tafarojnoruz, A & Calomino, F 2010. Comparison of formula for the prediction of scour depth at piers. *Proceedings*, 1st International Association for Hydraulic Research (IAHR) Congress, 4–6 May, Edinburgh.
- Graf, W H 1971. *Hydraulics of Sediment Transport*. (Series in Water Resources and Environmental Engineering). New York: McGraw-Hill.
- Guo, J 2012. Pier scour in clear water for sediment mixtures. *Journal of Hydraulic Research*, 50(1): 18–27.
- Guo, J 2014. Semi-analytical model for temporal clear water scour at prototype piers. *Journal of Hydraulic Research*, 52(3): 366–374.
- Hancu, S 1971. On the estimation of local scour in the bridge piers zone. *Proceedings*, 14th International Association for Hydraulic Research (IAHR) Congress, 20–22 November, Delft, Netherlands, Vol 3, pp 299–313.
- Heller, V 2011. Scale effects in physical hydraulic engineering models. *Journal of Hydraulic Research*, 49(3): 293–306.
- Huber, F 1991. Update: Bridge scour. *ASCE Civil Engineering*, 61(9): 62–63.
- Jain, S C & Fischer, E E 1979. *Scour around circular piers at high Froude numbers*. Report FHWA-RD-79-104. Washington, DC: US Department of Transportation, Federal Highway Administration.
- Jain, S C 1981. Maximum clear-water scour around circular piers. *ASCE Journal of the Hydraulics Division*, 107(HY5): 611–626.
- Johnson, P A 1995. Comparison of pier-scour equations using field data. *ASCE Journal of Hydraulic Engineering*, 121(8): 626–629.
- Khosronejad, A, Kang, S & Sotiropoulos, F 2012. Experimental and computational investigation of local scour around bridge piers. *Advances in Water Resources*, 37: 73–85.
- Kothiyari, U C, Garde, R C J & Ranga Raju, K G 1992. Temporal variation of scour around circular bridge piers. *ASCE Journal of Hydraulic Engineering*, 118(8): 1091–1106.
- Landers, M N & Mueller, D S 1996. Evaluation of selected pier-scour equations using field data. *Transportation Research Record*, 1523: 186–195.
- Laursen, E M & Toch, A 1956. *Scour around bridge piers and abutments*. Bulletin No. 4, Ames, IA: Iowa Highway Research Board.
- Lee, S O & Strum, T W 2009. Effect of sediment size scaling on physical modelling of bridge pier scour. *ASCE Journal of Hydraulic Engineering*, 135(10): 793–802.
- Melville, B W 1975. *Local scour at bridge site*. Report No. 117. Auckland, New Zealand: University of Auckland, School of Engineering.
- Melville, B W & Chiew, Y M 1999. Time scale for local scour at bridge piers. *ASCE Journal of Hydraulic Engineering*, 125(1): 59–65.
- Melville, B W & Coleman, S E 2000. *Bridge scour*. Highlands Ranch, CO: Water Resources Publications.
- Melville, B W & Kandasamy, J K 1998a. Maximum local scour depth at bridge piers and abutments. *ASCE Journal of Hydraulic Research*, 26(2): 183–198.
- Melville, B W & Sutherland, A J 1988b. Design methods for local scour at bridge piers. *ASCE Journal of Hydraulic Engineering*, 114(10): 1210–1226.

- Melville, B W 1997. Pier and abutment scour: Integrated approach. *ASCE Journal of Hydraulic Engineering*, 123(2): 125–136.
- Mohammed, Y A, Abdel-Aal, G M, Nasr-Allah, T H & Shawky, A A 2016. Experimental and theoretical investigations of scour at bridge abutment. *Journal of King Saud University – Engineering Sciences*, 28(1): 32–40.
- Molinas, A 2004. *Bridge scour in nonuniform sediment mixtures and in cohesive materials*. Report FHWA-RD-03-083. Washington, DC: US Department of Transportation, Federal Highway Administration.
- Mueller, D S & Wagner, C R 2005. *Field observations and evaluations of streambed scour at bridges*. Report FHWA-RD-03-052. Washington, DC: US Department of Transportation, Federal Highway Administration.
- Mueller, D S 1996. *Local scour at bridge piers in nonuniform sediment under dynamic conditions*. PhD thesis. Fort Collins, CO: Colorado State University.
- Neill, C R 1973. *Guide to bridge hydraulics*. Toronto, Canada: University of Toronto Press.
- Olsen, N R B & Kjellesvig, H M 1998. Three-dimensional numerical flow modelling for estimation of maximum local scour depth. *Journal of Hydraulic Resources*, 36(4): 579–590.
- Olsen, N R B & Melaaen, M C 1993. Three-dimensional calculation of scour around cylindrical piers. *ASCE Journal of Hydraulic Engineering*, 119(9): 1048–1054.
- Richardson, E V & Davies, S R 1995. *Evaluating scour at bridges*, 3rd ed. Report FHWA-IP-90-017. Washington, DC: US Department of Transportation, Federal Highway Administration.
- Richardson, E V, Harrison, L J, Richardson, J R & Davis, S R 1993. *Evaluating scour at bridges*, 2nd ed. Report FHWA-IP-90-017. Washington, DC: US Department of Transportation, Federal Highway Administration.
- Rooseboom, A 2013. *Drainage Manual*, 6th ed. Chapter 8. Pretoria: SANRAL.
- Rooseboom, A, Basson, M S, Loots, C H, Wiggett, J H & Bosman, J 1983. *National Transport Commission Road Drainage Manual*, 2nd ed. Pretoria: Director-General: Transport, Chief Directorate: National Roads.
- Roulund, A, Sumer, B M, Fredsøe, J & Michelsen, J 2005. Numerical and experimental investigation of flow and scour around a circular pile. *Journal of Fluid Mechanics*, 524: 351–401.
- Sawadogo, O 2015. *Coupled fully three-dimensional mathematical modelling of sediment deposition and erosion in reservoirs*. PhD thesis. Stellenbosch University, Department of Water Engineering.
- Shen, H W, Schneider, V R & Karaki, S 1969. Local scour around bridge piers. *ASCE Journal of the Hydraulics Division*, 95(6): 1919–1940.
- Sheppard, D M & Miller, W 2006. Live-bed local pier scour experiments. *Journal of Hydraulic Engineering*, 132(7): 635–642.
- Sheppard, D M, Melville, B & Demir, H 2014. Evaluation of existing equations for local scour at bridge piers. *Journal of Hydraulic Engineering*, 140(1): 14–23.
- Sumer, B M 2007. Mathematical modelling of scour: A review. *Journal of Hydraulic Research*, 45(6): 723–735.
- Toth, E 2015. Asymmetric error functions for reducing the underestimation of local scour around bridge piers. *Journal of Hydraulic Engineering*, 141(7): 04015011.
- Tseng, M H, Yen, C L & Song, C C S 2000. Computation of three-dimensional flow around square and circular piers. *International Journal for Numerical Methods in Fluids*, 34: 207–227.
- Van Rijn, L C 1987. *Mathematical modelling of morphological processes in the case of suspended sediment transport*. PhD thesis. Delft University of Technology, Netherlands.
- Williams, P D 2014. *Scale effects on design estimation of scour depths at piers*. PhD thesis. Stellenbosch University, Department of Civil Engineering.
- Wilson, K V 1995. *Scour at selected bridge sites in Mississippi*. Water-Resources Investigations Report 94-4241. Reston, VA: US Geological Survey.
- Xiong, W, Cai, C S, Kong, B & Kong, X 2014. CFD simulations and analyses for bridge scour development using a dynamic mesh updating technique. *Journal of Computing in Civil Engineering*, 30(1): 1–11.
- Zanke, U 1977. Berechnung der Sinkgeschwindigkeiten von Sedimenten. [Calculation of the sinking velocity of sediments.] *Mitteilungen des Franzius-Instituts für Wasserbau*, 46(243): 231–245.

The influence of gradient on saturation flow rate at signalised intersections

M M Bruwer, C J Bester, E S Viljoen

Saturation flow rate is the maximum hourly traffic volume per lane that can be accommodated through an intersection, and is used in the design and analysis of signalised intersections and traffic signal plans. The most widely applied method to estimate saturation flow rate is provided by the Highway Capacity Manual (HCM), which proposes default values obtained from USA empirical data for application in saturation flow rate calculations. This study considers the applicability of the HCM proposed base saturation flow rates, and particularly the adjustment factors for gradient on saturation flow in the South African context. The data for this research was collected by author ES Viljoen for use in her dissertation conducted in the final year of the BEng degree at Stellenbosch University.

The influence of approach lane gradient on saturation flow rate was investigated for application in the South African environment. The results of this research indicate that the HCM underestimates the influence of approach gradient on saturation flow rate, a similar finding to other international research. The standard use of a base saturation flow rate of 1 900 passenger cars per hour per lane for South African conditions was also commented on. HCM methods do not take into account the influence of speed limit on saturation flow rate, which has been shown to significantly affect saturation flow rate in numerous research projects, and is also commented on in this paper for zones with a 60 km/h and 80 km/h speed limit.

INTRODUCTION

Saturation flow rate is the maximum flow of vehicles per hour that could traverse a single approach lane of a signalised intersection if the approach were allocated green time for a full hour. Saturation flow rate is a critical value in the design and capacity analysis of signalised intersections and the determination of traffic signal phasing plans. It is important that the saturation flow rate used in the design and Level of Service (LOS) analysis of a signalised intersection is representative of actual flow rates, as this value can have a significant impact on the number of vehicles that can be accommodated at an intersection, and therefore the appropriate design of the intersection itself.

A number of factors influence the saturation flow rate of an intersection approach lane, including the location of the intersection, the vehicle composition of the traffic stream and the presence of parking or public transport facilities near the intersection. Geometric elements that are important for saturation flow rate estimation include number of lanes, lane width, accommodation of

turning movements and the gradient of the approach.

The Highway Capacity Manual (TRB 2010, referred to further as HCM2010), describes a method to calculate saturation flow rate that is applied by traffic engineers worldwide, including in South Africa. The HCM2010 method is also used in the majority of traffic simulation packages, including SIDRA, PTV Vistro and Aimsun (Akcelik and Associates (Pty) Ltd 2016; PTV Group 2016; Transport Simulation Systems 2015). The universally applicable equation recommended by HCM2010 to estimate saturation flow rate is accompanied by proposed default values obtained from empirical analysis conducted in the United States of America, detailing typical USA traffic conditions. The applicability of the HCM2010 default values to estimate saturation flow rate for South African traffic conditions is considered in this paper, particularly regarding the impact of approach gradient on saturation flow rates for arterial roads. Base saturation flow rates, as well as the impact of speed limit on base saturation flow, are also commented on.



MEGAN BRUWER, who is an Associate Member of SAICE, joined the Civil Engineering Department of Stellenbosch University as a lecturer in Transportation Engineering in 2015. Megan obtained a BEng in Civil Engineering in 2008 and an MEng in Transportation in 2010. Prior to returning to academics, Megan worked as a consultant engineer primarily involved in public transport systems and road-based traffic engineering. Her research interests include traffic flow theory and the application of ITS to improve data collection for transport planning and traffic management. She is currently completing a PhD in this field.

Contact details:

Department of Civil Engineering
Stellenbosch University
Private Bag X1, Matieland 7602, South Africa
T: +27 21 808 4080
E: mbruwer@sun.ac.za



PROF CHRISTO BESTER Pr Eng, who is a Fellow of SAICE, graduated with a BEng and MEng from Stellenbosch University, and a DEng from the University of Pretoria. After about 20 years with Consulting Engineers and the CSIR he joined Stellenbosch University in 1994 where he lectured and supervised post-graduate students in Transportation and Traffic Engineering until the end of 2017 when he finally retired.

Contact details:
Department of Civil Engineering
Stellenbosch University
Private Bag X1, Matieland 7602, South Africa
T: +27 21 808 4377
E: cjb4@sun.ac.za



ELIZABETH VILJOEN, Candidate Civil Engineer and Associate Member of SAICE, graduated from the Stellenbosch University in 2015 with a BEng degree in Civil Engineering. Her final-year project focused on traffic engineering and defining the influence of the road gradient at an intersection on saturated flow. In February 2016 she joined Aurecon South Africa and is currently based in their Paarl Office focusing on Land Infrastructure. She has designed projects in the field of municipal services and commercial developments, including bulk municipal infrastructure design, stormwater management and construction monitoring.

Contact details:
Aurecon Group South Africa
264 Main Street, Paarl 7646, South Africa
T: +27 21 860 2213
E: elzaan.viljoen@aurecongroup.com

Keywords: saturation flow, gradient, traffic signal

SATURATION FLOW RATE

Traffic flow at signalised intersections

The headway between vehicles passing through a signalised intersection during the green phase decreases until a typical minimum headway, or saturation headway, is reached (Bester & Meyers 2007). This minimum headway is inversely representative of the saturation flow rate. The first headway, i.e. the time interval between the traffic light changing to green and the rear wheels of the first vehicle passing the stop line, is generally longer than subsequent headways between vehicles due to start-up lost time. The driver at the head of the queue must observe the signal changing to green and then accelerate from standstill, and so passes the stop line with some delay after the signal had changed to green. The second driver in the queue has the opportunity to observe and react to the change in traffic signal during the start-up time of the first driver, and so the headway between the second and first vehicle is shorter. This is repeated by subsequent vehicles until headways reduce to a typical minimum headway, which is observed to remain virtually constant until the queue has dissipated.

The minimum headway, or saturation headway, is usually achieved by the time that the fourth to sixth vehicle in the queue has passed the stop line (Garber & Hoel 2015). If a near constant headway is observed after the N th vehicle, Equation 1 can be used to calculate the saturation flow rate (S) in vehicles per hour per lane from observed data; where n is the total number of vehicles queued, t_N is the time in seconds from the start of the green light to when the rear wheel of the N th vehicle passes the stop line, and t_n is the time until the rear wheel of the last queued vehicle passes the stop line in seconds:

$$K_a = \frac{3\,600 \times (n - N)}{t_N - t_n} \text{ (veh/h/ln)} \quad (1)$$

Use of saturation flow rate

Saturation flow rate is a key variable used to calculate the capacity of an approach at a signalised intersection, and is therefore a principal requirement for the correct design of signalised intersections. The capacity c of lane group i is a function of the saturation flow rate (S_i) of the lane group and the proportion of green time g_i allocated to that lane group and cycle

length C , as described by Equation 2 (Garber & Hoel 2015).

$$c_i = S_i \left(\frac{g_i}{C} \right) \quad (2)$$

Optimal cycle length can be determined according to the Webster Method, which uses the ratio of the actual or anticipated lane group traffic volume to saturation flow rate. This ratio is then also used to allocate green time to the various signal phases (Garber & Hoel 2015). Similarly, the HCM2010 uses the ratio of traffic volume to saturation flow rate to determine cycle length and green time allocation (TRB 2010).

HCM2010 method for saturation flow rate estimation

As saturation flow rate is used to design new signalised intersections, the majority of saturation flow rates used by traffic engineers must be estimated, rather than empirically determined using Equation 1. The HCM2010 method to estimate saturation flow is generally accepted and used for this purpose. The HCM2010 adjusts a selected base saturation flow rate according to conditions of traffic and intersection design. Base saturation flow rate is assumed to be the flow that could be accommodated at the approach of an intersection under ideal or base conditions, listed below (TRB 2010):

- Traffic lanes of at least 3.6 m width
- No heavy vehicles in traffic stream (only passenger vehicles)
- Flat gradient at approaches
- No parking or bus stops near the intersection
- No pedestrian crossing activity
- No vehicular turning movements (base saturation flow for straight-through movement).

The base saturation rate is proposed to be 1 900 passenger cars per hour per lane (pc/h/ln) in large metropolitan areas with more than 250 000 population, and 1 750 pc/h/ln in other areas.

The base saturation flow rate is adjusted using a number of factors that take into account departure from the base conditions. Eleven factors in total are proposed for consideration by the HCM2010, including factors to adjust for lane width, heavy vehicle proportion, approach grade, parking and bus stops, the area in which the intersection is located, lane utilisation (for multiple movement type lanes) and

adjustments for the impact of pedestrians and cyclists on turning movements (TRB 2010). Base saturation flow rates are expressed in terms of passenger cars per hour per lane (pc/h/ln). Once the percentage of heavy vehicles is accounted for, saturation flow is expressed as vehicles per hour per lane (veh/h/ln).

South African studies of saturation flow rate

Very little research regarding empirical surveys of saturation flow rate in South Africa is available (Bester & Meyers 2007). This is problematic, as it requires traffic engineers in South Africa to apply the HCM2010 base saturation flow rates based on default USA values and adjustment factors without knowledge of their applicability to local conditions.

The study conducted by Bester and Meyers (2007) reported on observed saturation flow rate at ten intersections in Stellenbosch. A multiple regression analysis was performed to determine the cumulative influence of gradient, number of lanes and speed limit on saturation flow rate. The study determined that each variable had a statistically significant influence on saturation flow rate. Increase in speed limit and number of through lanes were shown to increase saturation flow rate, while an increase in positive approach gradient reduced saturation flow rate (Bester & Meyers 2007).

The 2007 Bester and Meyers study reported a base saturation flow rate higher than that described in the HCM2010. This was specifically based on observations in the Stellenbosch area. They concluded that South African drivers are possibly more aggressive, maintaining shorter following distances (Bester & Meyers 2007). They recommend a base saturation flow rate of 2 246 pc/h/ln for a speed limit of 80 km/h and 2 076 pc/h/ln for a speed limit of 60 km/h. Another 1994 study done in South Africa, conducted for the Department of Transport, reported a base saturation flow rate of 1 928 pc/h/ln (Allers & Stander 1994), which is similar to the HCM2010 suggested value.

The Bester and Meyers (2007) study considered the influence of speed limit and number of through lanes on saturation flow rate. The HCM2010 method does not account for these factors. However, other international studies have indicated these factors to have a significant influence on saturation flow rate. A study conducted by

the Texas Transportation Institute in 2005 determined a base saturation flow rate of 1 905 pc/h/ln (similar to the HCM2010), and found that this rate decreased by 9 pc/h/ln per 1 mph (5.6 pc/h/ln per 1 km/h) decrease in speed limit, and increased by 130 pc/h/ln when the number of through lanes are increased from one lane to two (Bester & Meyers 2007). The 2007 Bester and Meyers study found that speed limit and number of lanes have a similar, albeit greater, effect on saturation flow rate. The saturation flow rate increases with 8.5 pc/h/ln per 1 km/h increase in speed limit, and increases with 288 pc/h/ln when two through lanes are available instead of one.

The influence of gradient

The factor used by the HCM2010 to adjust the base saturation flow rate for the gradient of the approach (f_g) is determined by Equation 3, where P_g is the gradient of the approach in percentage. An uphill gradient is annotated to be positive, and a downhill gradient is negative. Equation 3 is applicable to gradients ranging from -6% to +10% (TRB 2010).

$$f_g = 1 - \frac{P_g}{200} \quad (3)$$

The gradient adjustment factor results in a decrease in saturation flow rate for positive, uphill gradients, and an increase in saturation flow rate for downhill approaches. Essentially, a 1% gradient will result in a 0.5% change in flow rate (10 pc/h/ln from base saturation flow rate of 1 900 pc/h/ln).

The 2007 South African study determined the influence of gradient on saturation flow to be nearly three times more than predicted by the HCM2010 approach when applied to a base saturation flow rate of 1 900 pc/h/ln (Bester & Meyers 2007). Their suggested adjustment factor for gradient is provided in Equation 4, which results in an adjustment of 1.4% change in flow rate for a 1% change in gradient.

$$f_g = 1 - \frac{P_g}{71} \quad (4)$$

Research conducted in 2009 that considered a number of international studies on saturation flow rate, found that the majority of studies indicated a greater influence of gradient on saturation flow rate than indicated by the HCM (Iqbal 2009).

A 1982 study conducted in Kentucky, USA, considered the influence of positive

and negative gradients on saturation flow separately. This study determined that positive gradients (uphill) have less influence on saturation flow rates than negative (downhill) gradients (Agent & Crabtree 1982). The equations for the gradient adjustment factors determined from this study are presented below. Equation 5 indicates the factor for downhill gradients (P_g is negative) and Equation 6 for uphill gradients (P_g is positive). When the equations are written in the same form as the HCM2010 gradient adjustment factors, it is clear that the Agent and Crabtree (1982) factor for positive gradients is the same as suggested by HCM2010 for all gradients (Equation 6), while the negative gradient adjustment factor will have a greater impact on saturation flow rate.

$$f_g = 1 - 1.1 \frac{P_g}{100} = 1 - \frac{P_g}{90.9} \quad (5)$$

$$f_g = 1 - 0.5 \frac{P_g}{100} = 1 - \frac{P_g}{200} \quad (6)$$

From previously conducted South African and international research, it appears that the HCM2010 method underestimates the influence of gradient on saturation flow rate.

DATA COLLECTION

Study area

A headway study was done at 12 approaches of six intersections in Stellenbosch, South Africa, during September 2015. All intersections were located along the same route, the R44, an arterial road heading south from Stellenbosch. Only approaches of the R44 were analysed; minor road approaches were not considered. Intersections with similar properties were selected, and as many factors as possible that influence saturation

flow rate were excluded, or were ensured to remain constant to isolate the influence of gradient.

All the study intersections are located outside of the CBD area of Stellenbosch in suburban or peri-urban zones. The lane width along the route remained consistent at an average of 3.6 m. Only phases with no heavy vehicles present in the queue were observed, and phases were not observed if pedestrians or cyclists were present. None of the intersections had parking or bus stops in the immediate vicinity. Finally, only lanes with exclusive through movements and two through lanes per approach were analysed. The only characteristic from the HCM2010 method that varied appreciably along the route was approach gradient.

The speed limit varied from 60 km/h at two intersections closest to Stellenbosch, to 80 km/h at the remaining four intersections. Because speed limit influence is not considered in the HCM, the influence of speed on base saturation flow rate was also not isolated in this study. Comment is, however, made later in this paper on the apparent effect of speed limit on base saturation flow.

Gradient measurement

The gradient of the intersection approaches was measured using a dumpy level. The level difference was measured over a 20 m distance from the stop line of the approach, and the gradient in percentage was calculated as the change in height over the change in distance. Table 1 indicates the gradient observed at the various approaches.

Vehicle headway analysis

Traffic streams at the intersection approaches along the R44 were recorded with a GoPro Camera. The study was conducted during peak hours to ensure that adequate vehicles were queued to allow

Table 1 Approach gradients

| Intersections along R44 | Speed limit (km/h) | Southbound approach | Northbound approach |
|-------------------------|--------------------|---------------------|---------------------|
| Annandale Rd | 80 | + 4.15% | - 4.15% |
| Webersvallei Rd | 80 | + 4.95 % | - 4.95 % |
| Tegno Rd | 80 | - 3.73 % | + 3.73 % |
| Blaauklippen Rd | 80 | - 1.13 % | + 1.13 % |
| Van Reede Rd | 60 | - 0.55 % | - 2.68 % |
| Safraan Rd | 60 | + 0.15 % | - 0.15 % |

saturation headway to be reached, while downstream congestion was monitored to exclude influence. Adobe Photoshop Element was used to analyse the footage. This software package has a split-second function and can play back footage at a slower speed, so that the exact time stamp (to the nearest 0.01 seconds) at which the back wheel of a vehicle crosses the stop line can be observed with no human error incurred from stopwatch timing. Any phases with heavy vehicles or pedestrian and cyclist activity were excluded from the study. It was also necessary to ignore some phases where downstream congestion prevented vehicles driving freely through the intersection.

Figure 1 indicates the progression of vehicle headways for illustration purposes as the queue of vehicles dispersed from two opposing approach lanes of a single intersection (R44 and Tegno Road intersection). The first vehicle in the queue had a relatively long headway from the time that the traffic signal turned green until the back wheels of that vehicle passed the stop line. The headways between subsequent vehicles then reduced systematically, as anticipated.

Figure 1 presents the headways of vehicles at both the southbound and northbound approaches of the intersection of Tegno Road and the R44, which has a downhill and uphill gradient of 3.73% respectively. Also indicated are trend lines demonstrating the tendency of the headways to reduce as the queue disperses. The trend lines indicate that the headways reach a relatively constant value from the sixth departure from the queue. Saturation headway was consistently

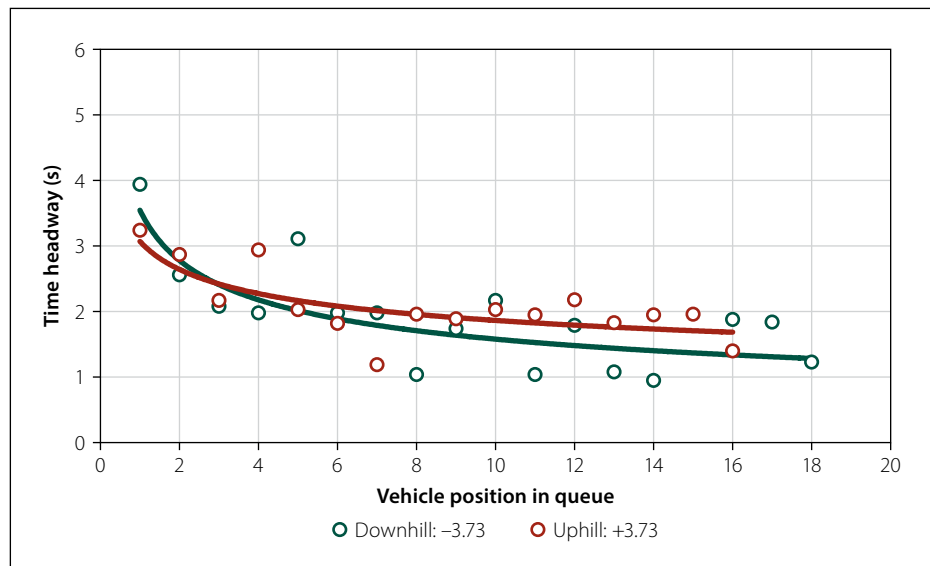


Figure 1 Progression of vehicle headway at the intersection of the R44 and Tegno Road

found to be longer on the uphill approach than on the downhill approach at the same intersection.

SATURATION FLOW RATE RESULTS

Saturation headway results

The results of the headway and saturation flow analysis of six intersections in Stellenbosch are presented in Table 2. Saturation flow rate is indicated in terms of passenger cars per hour per lane, because no heavy vehicles were present in analysed queues.

Four queues were analysed per intersection approach, and the average saturation flow rate and standard deviation of saturation flow rates were determined. In

each case, the vehicle number at which saturation flow was reached (when headways became constant) was evaluated and saturation flow calculated according to Equation 1. The saturation flow was calculated only using vehicles that were in the initial stationary queue. As soon as a gap was measured that was longer than double the gap during saturation flow, the queue was considered spent, and no further headways were included in the analysis. As queue length varied per cycle, the number of headways considered to calculate saturation flow varied in each case. No standard deviation is provided for the northbound approach of Van Reede Street, as only one valid saturation flow rate value was obtained due to downstream congestion.

The average saturation headways between vehicles are less than 2 seconds

Table 2 Saturation flow rate analysis results

| Intersection | Speed limit (km/h) | Direction | Gradient (%) | Headway (seconds) | Saturation flow (pc/h/ln) | Standard deviation |
|----------------------|--------------------|------------|--------------|-------------------|---------------------------|--------------------|
| Annandale Rd/R44 | 80 | Northbound | -4.15 | 1.51 | 2 386 | 41.91 |
| | | Southbound | 4.15 | 2.04 | 1 766 | 66.50 |
| Webersvallei Rd/R44 | 80 | Northbound | -4.95 | 1.57 | 2 300 | 141.28 |
| | | Southbound | 4.95 | 1.94 | 1 859 | 67.73 |
| Tegno Rd/R44 | 80 | Northbound | 3.73 | 1.97 | 1 825 | 115.96 |
| | | Southbound | -3.73 | 1.56 | 2 302 | 137.39 |
| Blaauwklippen Rd/R44 | 80 | Northbound | 1.13 | 1.85 | 1 945 | 17.56 |
| | | Southbound | -1.13 | 1.66 | 2 170 | 79.65 |
| Van Reede Rd/R44 | 60 | Northbound | -2.68 | 1.78 | 2 021 | N/A |
| | | Southbound | 0.55 | 1.89 | 1 900 | 93.07 |
| Safraan Rd/R44 | 60 | Northbound | -0.15 | 1.95 | 1 850 | 90.36 |
| | | Southbound | 0.15 | 1.94 | 1 854 | 53.82 |

per vehicle on all approaches, except the southbound approach of the intersection of the R44 with Annandale Road. This intersection represents the minimum and maximum saturation flows that were observed – 1 766 pc/h/ln and 2 386 pc/h/ln respectively. The saturation flows measured at the intersection of the R44 with Safran Road are essentially equal for the two approaches (1 850 pc/h/ln), which are relatively level.

The influence of gradient on saturation flow rate

It is obvious from the results indicated in Table 2 that gradient has a significant effect on saturation flow rate, with a clear difference in the saturation flow rates on the northbound and southbound approaches of intersections with steep gradients. The highest flow rate is always observed on downhill approaches.

Figure 2 indicates saturation flow rate as a function of gradient resulting from the 2015 acquired Stellenbosch data. Also indicated are HCM2010 saturation flows at different gradients for large cities and other areas. As gradient increases positively, saturation flow rate is observed to decrease, indicated by the linear regression line. The R^2 value of the regression curve indicates that the relationship between gradient and saturation flow rate can be relatively well described, with 75% of variation accounted for. The equation of the regression line indicates an intercept of 2 000 pc/h/ln. This is representative of base saturation flow rate at a gradient of 0% with all other influencing factors constant. It would therefore appear that this study corroborates the findings of Bester and Meyers (2007), that saturation flow in South Africa is higher than is suggested by the HCM (1 900 pc/h/ln in large metropolitan areas with more than 250 000 population, or 1 750 pc/h/ln in other areas) (Transportation Research Board 2010).

From the regression equation presented in Figure 2, the adjustment factor of gradient on saturation flow rate, according to the form of the adjustment factors presented by the HCM2010, is described by Equation 7, as applied to a base saturation flow of 1 900 pc/h/ln. The effect of gradient in this study is six times greater than proposed by the HCM2010, and also higher than the influence determined by the 2007 South African study. The adjustment factor presented by Equation 7 results in a 3% decrease in saturation flow rate for a 1%

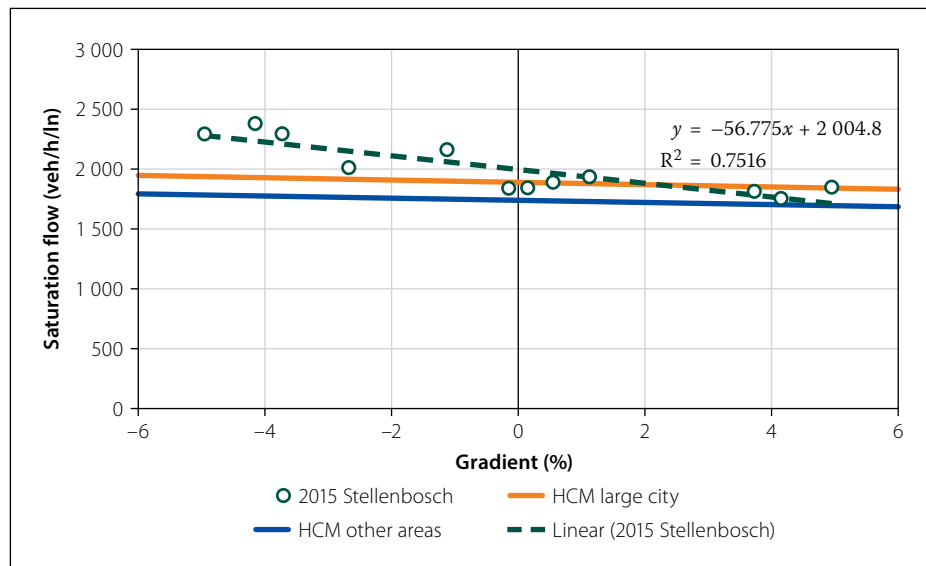


Figure 2 Influence of gradient on saturation flow rate

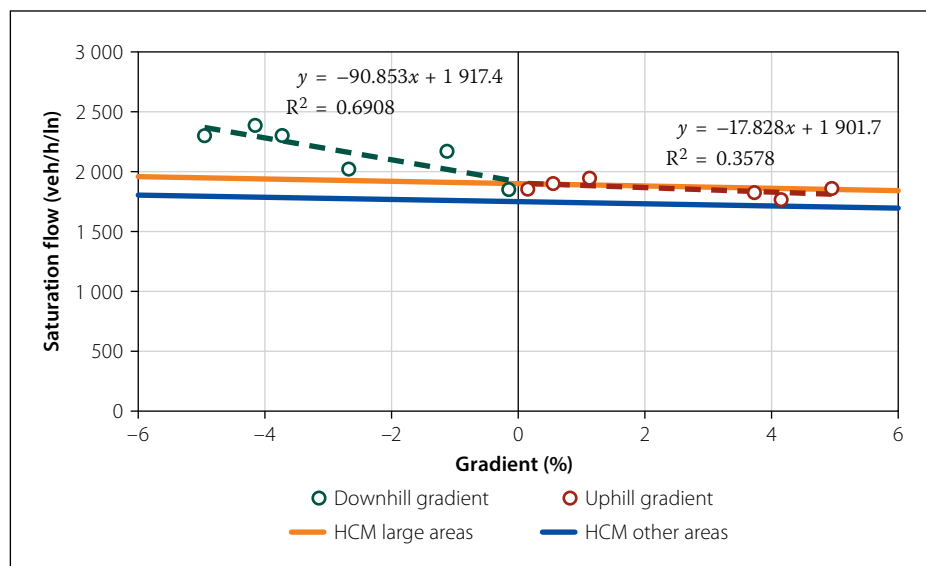


Figure 3 Influence of positive and negative gradient on saturation flow

increase in gradient, similar to the international findings of Iqbal (2009).

$$f_g = 1 - \frac{P_g}{33.5} \quad (7)$$

The influence of positive and negative gradients was then separately considered to determine if uphill and downhill slopes influence saturation flow rate differently. Figure 3 indicates a separate linear regression analysis conducted for positive and negative gradients respectively. From this figure it is evident that negative gradients have a greater influence on saturation flow rate than positive gradients according to the steepness of the regression lines, similar to the findings of the 1982 Kentucky study (Agent & Crabtree 1982).

The intercept of both regression curves, representative of the base saturation flow rate, is close to 1 900 pc/h/ln. For

negative gradients, the saturation flow rate was increased by nearly 5% for every 1% increase in approach steepness, while at positive gradients, a 1% increase in steepness results in only a 1% reduction in flow rate. The R^2 values for these regression analyses are, however, substantially lower than were obtained for the single regression analysis (Figure 2), indicating that the smaller sample for uphill and downhill gradients results in larger variation and less confidence in the outcome.

The influence of speed limit on saturation flow rate

The Highway Capacity Manual does not take speed limit into account when determining saturation flow rate. However, previous research (Bester & Meyers 2007) indicated that speed limit influences saturation flow rate. Higher speed limits tend to increase saturation flow rate and vice versa.

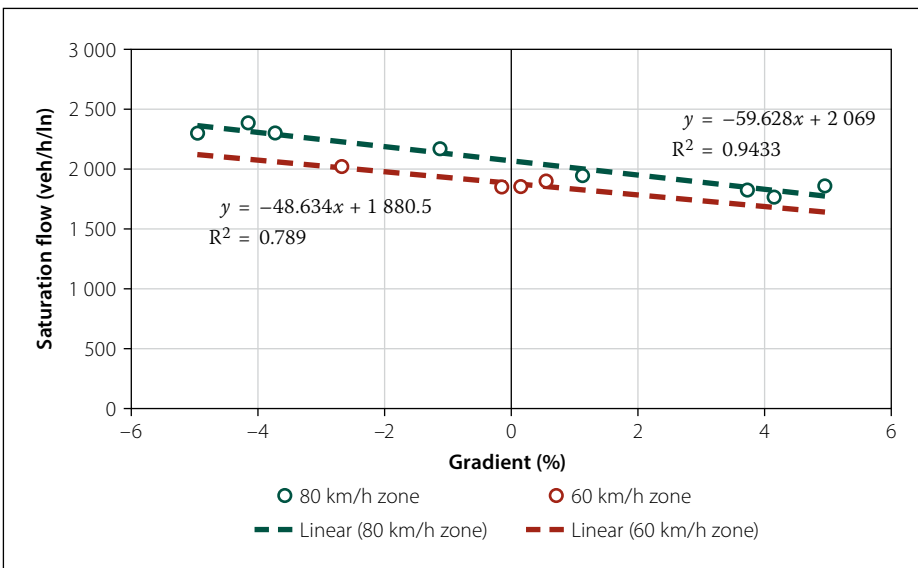


Figure 4 Influence of speed limit on saturation flow rate

In Figure 4 the data sets representing 80 km/h and 60 km/h speed limit zones were analysed separately. A linear regression analysis conducted for each set of data indicates that the influence of gradient on saturation flow rate (indicated by the gradient of the regression line) stays relatively constant at different speed limits. Similar to the model that did not separate speed limit zones (Equation 7), the regression analysis for both 60 km/h and 80 km/h zones represented in Figure 4 results in approximately a 3% decrease in saturation flow rate per 1% increase in gradient.

It must be noted that the sample of four approach lanes in the 60 km/h range is inadequate for a statistical analysis to provide reliable conclusions as to the base saturation flow rate of intersection approaches at this speed limit. Further, analysis of the influence of gradient at a 60 km/h speed limit from the data

presented in this research is also not statistically reliable, due to the narrow range of gradients, most of which are close to 0% gradient. The analysis of speed limit influence was not the primary objective of this research (which was to determine the accuracy of USA-based data to describe the influence of gradient on saturation flow in South Africa); however, it is considered relevant to comment on the influence of speed limit, considering previous research.

While the influence of gradient on saturation flow rate stays relatively constant at different speed limits, the base saturation flow rate, indicated by the intercept of the regression lines, appears to be influenced. In the 60 km/h zone, base saturation flow is 1 880 pc/h/ln, but 2 070 pc/h/ln in 80 km/h zones (190 pc/h/ln difference). This difference in base saturation flow is very similar to the findings of the 2007 South African study, which estimated an increase

of 8.5 pc/h/ln per 1 km/h increase in speed limit (Bester & Meyers 2007), or 170 pc/h/ln for a 20 km/h increase in speed limit.

It is, however, important to note that this research determined significantly lower base saturation flows than the Bester and Meyers (2007) study (suggested base saturation flow rates of 2 076 pc/h/ln for a speed limit of 60 km/h and 2 246 pc/h/ln for a speed limit of 80 km/h). The sample size for intersection approaches with 80 km/h speed limit is limited in the Bester and Meyers (2007) study, with only three approaches considered, only one of which displayed a saturation flow of greater than 2 076 pc/h/ln (suggested for 60 km/h zones).

Summary of results

The results of this research (denoted 2015) are summarised in Table 3. Results are provided for all data grouped together, as well as data differentiated by positive and negative approaches and speed limit zones. Table 3 also compares base saturation flow rate (S_b) results obtained from the HCM2010, and the Bester and Meyers (2007) South African study.

Firstly, saturation flows observed in Stellenbosch in 2015 are closer to that proposed by the HCM2010 for large urban areas (defined to have a population of more than 250 000 people). Stellenbosch is a relatively small town. The population of Stellenbosch Local Municipality (including Stellenbosch, Franschhoek and Pniel) reported in 2016 was 173 419 (Statistics South Africa 2016). The definition in the HCM2010 of large urban areas is intended to provide information on commute behaviour, with more rushed, urgent driving behaviour anticipated in larger centres, leading to higher saturation

Table 3 Comparison of results

| | Study | R ² | Base S_b (pc/h/ln) | Influence of gradient (f_g) | % change in S from 1% gradient increase |
|--------------------------|--------------------------|----------------|----------------------|---------------------------------|---|
| 2015 Research | All data | 0.75 | 2 000 | $1 - (P_g/33.5)$ | 3.0% |
| | Downhill, all speeds | 0.69 | 1 900 | $1 - (P_g/20.9)$ | 4.8% |
| | Uphill, all speed limits | 0.36 | 1 900 | $1 - (P_g/106.6)$ | 0.9% |
| | 80 km/h, + and – grade | 0.94 | 2 070 | $1 - (P_g/31.9)$ | 3.1% |
| | 60 km/h, + and – grade | 0.79 | 1 880 | $1 - (P_g/39.1)$ | 2.6% |
| HCM2010 | Large urban area | | 1 900 | $1 - (P_g/200)$ | 0.5% |
| | Other areas | | 1 750 | $1 - (P_g/200)$ | 0.5% |
| Bester and Meyers (2007) | 80 km/h | | 2 246 | $1 - (P_g/71)$ | 1.4% |
| | 60 km/h | | 2 076 | | |

flow than in smaller and non-urban areas. As such, it is important to consider that Stellenbosch experiences very high congestion rates during the morning and afternoon peak commute hours, and so behaviour similar to large urban areas, as defined in the HCM2010, should be expected. Figures 2 and 3 indicate clearly that Stellenbosch exhibits saturation flows well above those defined by smaller population areas in the USA.

Secondly, it is clear that gradient has a greater influence on saturation flow than suggested by the HCM2010, corroborating previous literature that the HCM appears to underestimate the influence of gradient (Bester & Meyers 2007; Iqbal 2009). The separation of positive (uphill) and negative (downhill) gradients reveals that downhill gradients exert a greater effect on saturation flow than uphill gradients, similar to the findings of Agent and Crabtree (1982).

A single adjustment factor is proposed for both positive and negative gradients, according to Equation 10, which results in a 3.0% change in saturation flow per 1% increase in gradient (P_g is negative for downhill approaches, and positive for uphill approaches). This adjustment factor was determined for all data, as well as data separated according to speed limit. The factor proposed by Equation 8 is more conservative for both positive and negative gradients than the factors determined separately according to grade classification. Additionally, results of separated gradients as determined in this study are possibly not as reliable, due to reduced sample size.

$$f_g = 1 - \frac{P_g}{33} \quad (8)$$

Thirdly, separating data according to speed limit reveals that base saturation flow rate is influenced by speed limit, with lower speed limits resulting in lower base saturation flow rate. This is in support of previous literature (Bester & Meyers 2007). Separation of speed limit zones results in reduced variability between actual data and the regression equations. Most of the data in this research was obtained for an 80 km/h speed limit, which results in a regression equation that can account for 94% of the variation in observed data.

CONCLUSIONS AND RECOMMENDATIONS

Saturation flow rate is the maximum traffic flow of vehicles per hour that can be accommodated per approach lane of an intersection, and is used in the design and analysis of signalised intersections and traffic signal phasing plans. The most widely applied method to estimate saturation flow rate is provided by the HCM, developed by the Transportation Research Board. The universally applicable method recommended by HCM2010 to estimate saturation flow rates is accompanied by proposed default values obtained from empirical analysis in the USA, detailing typical USA traffic conditions. This research primarily considered the applicability of the HCM2010 proposed gradient estimation factors on saturation flow rate in the South African context, and commented on base saturation flow rate applicability and the influence of speed limit thereon.

The Highway Capacity Manual significantly underestimates the influence of gradient on saturation flow rate, as shown from the empirically determined results of this research, as well as previous research conducted internationally and in South Africa. A constant influence of gradient, irrespective of the approach being an uphill or downhill slope, is recommended to be 3% change in saturation flow rate per 1% change in gradient. Uphill gradients will decrease saturation flow rate, while downhill gradients will increase saturation flow rate. This influence of gradient is significantly higher than the proposed adjustment factor of the HCM2010, which results in 0.5% change in saturation flow per 1% change in gradient.

HCM methods do not take the influence of speed limit on saturation flow rate into account, which has been shown to affect saturation flow rate in a number of previous studies, and appears to be backed up by the data obtained in this research as well. It is recommended that speed limit be applied in the estimation of saturation flow rate by influencing the selection of the base saturation flow. Further research is required to determine acceptable levels of base saturation flow rate for different speed limit zones in South Africa, as the sample

size in this study was not adequate to make recommendations in this regard.

It is recommended that caution be exercised when applying base saturation flow rate values described in the HCM2010 in South African conditions. Particularly, the population size of the town in which the analysis is being conducted should not be an indication alone of base saturation flow rate. Rather, congestion conditions and driver behaviour should be used to differentiate between high- and low-base saturation flow rates. Further research in towns and cities in South Africa that do not experience the high commute volumes experienced in Stellenbosch is required to make further recommendations on this trend.

REFERENCES

- Agent, K R & J D Crabtree 1982. *Analysis of saturation flow at signalized intersections*. Lexington, KY: University of Kentucky, Kentucky Transportation Research Programme.
- Akcelik and Associates (Pty) Ltd 2016. *Sidra for HCM2010*. Available at: http://www.sidrasolutions.com/Resources/SIDRA_HCM2010 [accessed on 14 July 2016].
- Allers, S & Stander, H J 1994. *Saturation flow rates at signalised intersections in South Africa*. Report RR 88/208. Pretoria: Department of Transport.
- Bester, C J & Meyers, W L 2007. Saturation flow rates. *Proceedings*, 26th Southern African Transport Conference (SATC 2007). Pretoria: Document Transformation Technologies, pp 560–568.
- Garber, N J & Hoel, L A 2015. *Traffic and Highway Engineering*, 5th ed. Stamford, CT: Cengage Learning.
- Iqbal, M J 2009. *Estimation of saturation flow and lost time at selected intersections of Karachi (Pakistan)*. PhD thesis. Jamshoro, Pakistan: Mehran University of Engineering and Technology.
- PTV Group 2016. *PTV Products: PTV Vistro*. Available at: <http://www.vision-traffic.ptvgroup.com/en-us/products/ptv-vistro> [accessed on 14 July 2016].
- Statistics South Africa 2016. *Community survey 2016: Provinces at a glance*. Pretoria: Statistics South Africa.
- TRB (Transportation Research Board) 2010. *Highway capacity manual*. Washington, DC: National Academy of Sciences.
- Transport Simulation Systems 2015. *New features in Aimsun 8.1*. Available at: <https://www.aimsun.com/aimsun/new-features> [accessed on 14 July 2016].



JACO KOEN, who is an Associate Member of SAICE, is currently employed by the City of Cape Town as a project engineer within the Water and Sanitation Department. He obtained his BEng and MEng in Civil Engineering (*cum laude*) from Stellenbosch University in 2015 and 2017, respectively. His research interests include hydraulic structures, dam spillways and open channel hydraulics.

Contact details:

Department of Civil Engineering
Stellenbosch University
Private Bag X1, Matieland 7602, South Africa
City of Cape Town Water and Sanitation Head Office
8 Voortrekker Road, Bellville 7535, South Africa
T: +27 21 400 5777
E: jaco.koen@capetown.gov.za / jacokoen2@gmail.com



EDDIE BOSMAN obtained his BSc and BEng degrees from Stellenbosch University, and a post-graduate Diploma in Hydraulic Engineering from the International Institute for Hydraulic and Environmental Engineering in Delft, The Netherlands. He has 48 years' professional experience in research, private consulting and lecturing.

At the end of 2009 he retired from the chair in Port & Coastal Engineering in the Water Division of Stellenbosch University, and is presently practising on an ad hoc basis.

Contact details:

Water Division (Retired Lecturer)
Department of Civil Engineering
Stellenbosch University
Private Bag X1, Matieland 7602, South Africa
T: +27 21 886 4193
E: debosman@sun.ac.za



PROF GERRIT R BASSON Pr Eng, who is a Member of SAICE, is a professor in Hydraulic Engineering in the Civil Engineering Department at Stellenbosch University. He obtained a PhD from Stellenbosch University in 1996 and has more than 30 years' experience mainly in the fields of river hydraulics, fluvial morphology and the design of large hydraulic structures. He has worked on projects in 21 countries.

Contact details:

Water and Environmental Engineering Division
Department of Civil Engineering
Stellenbosch University
Private Bag X1, Matieland 7602, South Africa
T: +27 21 808 4355
E: grbasson@sun.ac.za

Keywords: stepped spillway, cavitation, aeration, flaring gate pier, crest pier

Artificial aeration of stepped spillways by crest piers and flares for the mitigation of cavitation damage

J Koen, D E Bosman, G R Basson

Stepped spillways are one of the oldest spillway designs dating back to 500 B.C. With technical advances in Roller Compacted Concrete (RCC) construction, the stepped spillway has become increasingly popular over recent decades. However, the use of this spillway is limited to a maximum safe unit discharge of $25 \text{ m}^3/\text{s}$ due to the risk of cavitation.

In order to increase the discharge capacity on stepped spillways, various crest pier designs were introduced for flow aeration, thereby reducing the risk of cavitation damage. These pier designs were investigated on two physical models, constructed on a scale of 1:15 and 1:50, both with a standard ogee crest profile which transit to a stepped spillway chute. Air concentration was recorded along the pseudo-bottom, while pressures were measured at the step riser. The results of the 1:15 scale model indicated that the implementation of a short bullnose pier increased the safe unit discharge capacity to $30 \text{ m}^3/\text{s}$. The innovative Flaring Gate Pier design, which was adapted on existing spillways in China, with reported design prototype unit discharges exceeding $200 \text{ m}^3/\text{s}$, was investigated on the 1:50 scale model. Based on the experimental results of the current study, the safe unit discharge capacity (i.e. a discharge satisfying the relevant criteria defined for this study) was increased to $50 \text{ m}^3/\text{s}$ with an X-shape Flare Gate Pier (FGP) on the spillway crest.

INTRODUCTION

A study by Nortjé (2002) attributed the main cause of dam failures to insufficient spillway capacity, which is responsible for 39% of the total dam failures in South Africa. This emphasises the need and importance for further studies of the hydraulic related characteristics of spillways in general. Typical modes of dam failure include foundation failures, flow erosion and concrete deterioration of spillways. The study of cavitation on stepped spillways, which could lead to damage of the concrete surface, is the subject of this investigation.

As excessive amounts of water discharge over the spillway crest and accelerate down the spillway face, high velocities are induced. These high velocities generate low pressure regions in which cavitation may be imminent, and which can cause major damage to the spillway or even endanger the dam's structural integrity. A pre-emptive measure to combat cavitation damage is to artificially introduce flow aeration at the pseudo-bottom. In order to aerate the flow, various crest pier aeration structures were investigated to ultimately increase the maximum safe unit discharge capacity of stepped spillways.

Flow aeration is defined as the entrainment of air bubbles and pockets that are transported within the flow. Natural air entrainment or self-aeration arises due to the growth of a turbulent boundary layer. As the turbulent boundary layer grows, a point is reached where the boundary layer breaches the free surface. If the turbulence overcomes the surface tension, air is entrained into the flow (Pfister & Hager 2011).

This study investigated the artificial aeration of piers and flares on two types of stepped spillway models, referred to as Type A and B:

- A. A standard USBR (1987) spillway with a design discharge head of 4.2 m, step height of 1.5 m, chute slope of 51.3° and transitional crest steps
- B. A standard WES (1959) spillway with a design discharge head of 17.9 m, step height of 1.0 m, chute slope of 55° and smooth ogee profile.

BACKGROUND

Experiments performed by Peterka (1953), and Russell and Sheehan (1974) indicated that a minimum air concentration of 5–8%

Table 1 Applications of the FGP design on spillways in China

| Dam | Type | Dam height (m) | Chute slope ($^{\circ}$) | Step height (m) | q_{design} (m^3/s) | q_{Check} (m^3/s) | Type of FGP |
|-------------|---------|----------------|----------------------------|-----------------|---|--|---------------------------|
| Ankang | Gravity | 128 | 51.3 | | | 254 | Y-shape FGP |
| Dachaoshan | RCC | 111 | 55 | 1 | 165 | 250 | Y-shape FGP & flip bucket |
| Shuidong | RCC | 62 | 60 | 0.9 | 100.2 | 138.7 | Y-shape FGP |
| Suofengying | RCC | 116 | 49.6 | 1.2 | 179 | 245 | X-shape FGP |

is required to protect a concrete specimen of 10–20 MPa compressive strength. A simple and effective way to prevent cavitation damage is to introduce air near the spillway surface by artificial aeration. This is achieved by installing an aerator, which would deliberately cause a large cavity or void to be formed on the underside of a high velocity jet (Khatsuria 2004). Different types of aerators exist, such as deflectors or ramps, offsets, steps, grooves, crest piers or Flaring Gate Piers (FGP). The focus of this paper was specifically aimed at the addition of piers and FGP aerators.

Crest piers

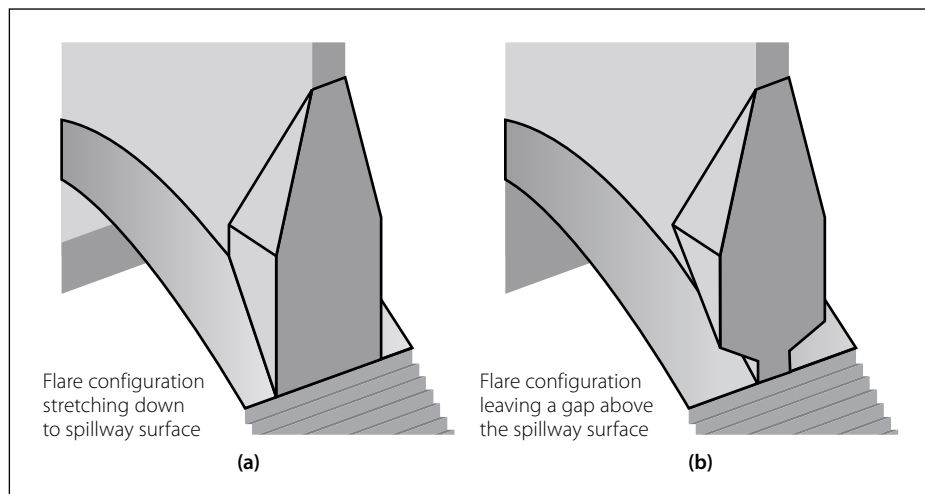
Calitz (2015) conducted a physical hydraulic model study to investigate whether the introduction of a crest pier could initiate an earlier onset of air entrainment. Two different piers were used in this study, both designed as bullnose piers, which consisted of different lengths. Calitz found that the addition of a short bullnose pier alleviated the risk of cavitation damage and the safe unit discharge capacity was increased to $30 \text{ m}^3/\text{s}$. As only one pier nose design and two pier lengths were investigated, a potential limitation was noticed. The authors attempted to optimise the pier design with alterations to the pier nose shape and pier length.

Flaring Gate Pier (FGP)

The pioneering design of flaring gate piers (FGP) was first introduced by Zhenying Gong in 1974, China. This innovation arose from simply reversing the conventional trend of gate pier design. Instead of square butt ends or tapering of the pier tail, the ends were substantially flared (Lin *et al* 1987). The design principle is to rapidly contract the flow and force it into a narrow, high-velocity jet. There are various FGP designs, such as the X-shape, Y-shape, V-shape and T-shape, but the X- and Y-shape are more commonly used.

Prototype applications of the Flaring Gate Pier

The FGP design has been applied in prototype on high head/velocity spillways

**Figure 1** Applications of the FGP design on spillways in China (Hongta Group 2017)**Figure 2** (a) Illustration of the Y-shape FGP and (b) the X-shape FGP (Ting *et al* 2011)

in China. A few of these applications are tabulated in Table 1. The design and check unit discharges of the FGP applications imply significantly increased safe unit discharges when compared to a standard stepped spillway. Both the Dachaoshan Dam (Figure 1) and the Shuidong Dam have experienced large floods close to the design unit discharge. The Dachaoshan Dam experienced a $93 \text{ m}^3/\text{s}$ flood, whereas the Shuidong Dam experienced a maximum unit discharge of $90 \text{ m}^3/\text{s}$. Both of these stepped spillways were inspected after each of the respective floods, which led to the conclusion that no significant damage had occurred (Shen 2003).

X- and Y-shape FGP

The most widely used flare design in China is the Y-shape FGP, which is located approximately a third of the way downstream from the spillway crest. This

specific flare design is characterised by frequent low or medium discharge floods. The piers constrict the flow, which result in narrow, supercritical flow past the FGP. Due to the narrowed flow width down the chute, the Y-shape FGP only uses a small area of the spillway for energy dissipation. In the case of the Dachaoshan Dam (Figure 1), only 30% of the stepped spillway surface is utilised for energy dissipation.

The X-shape FGP was designed to utilise more of the stepped spillway surface compared to the Y-shape FGP, as illustrated in Figure 2. The bottom outlet width of the X-shape FGP is wider than that of the Y-shape FGP. In the case of a low discharge, the flow is not contracted, and nearly all of the available stepped spillway surface area is used for aeration and energy dissipation. Since the flow passes mainly from the bottom outlet, at a low rate of discharge, a thin nappe develops (Bo *et al* 2007).

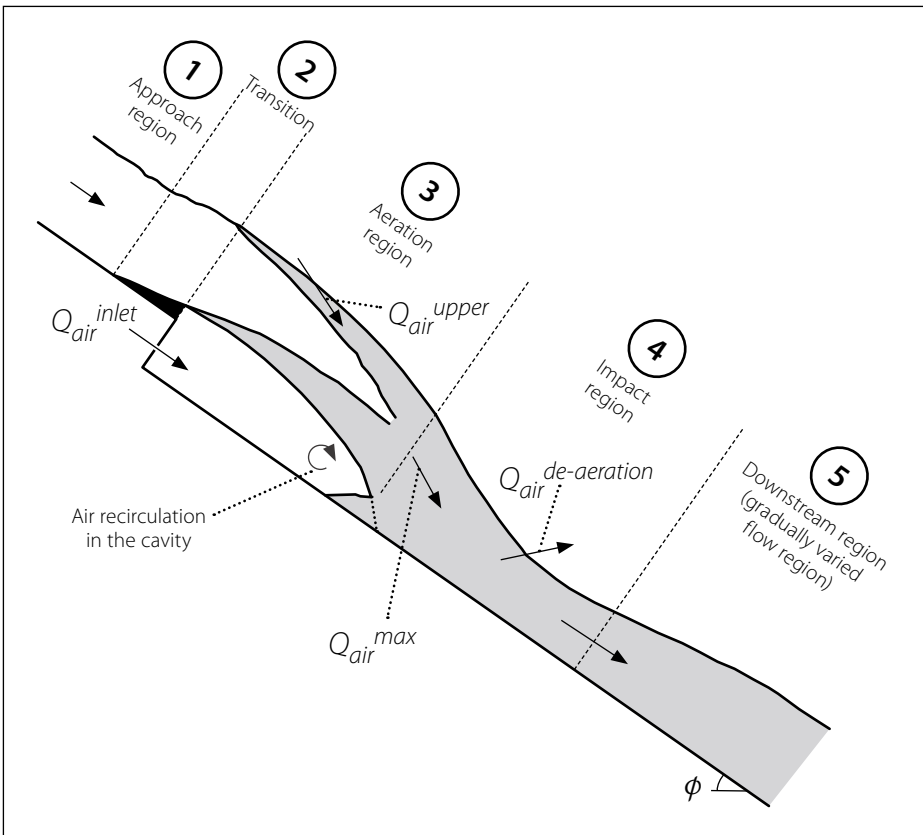


Figure 3 Deflector aerator flow regions illustrating the de-aeration of air (after Chanson 1994)

Air detrainment in impact regions

As the performance of the FGPs is characterised by the deflection of water in a ski-jump manner, an impact zone is located either on the spillway or downstream thereof. Chanson (1994) conducted a physical model investigation in which the processes of aeration and de-aeration or detrainment were identified for a bottom aeration device. As the performance of the FGP is somewhat similar to the bottom aerator, the same five distinct flow regions were introduced as illustrated in Figure 3, which are:

1. The approach flow region upstream of the aerator
 2. The transition region which coincides with the length of the aerator
 3. The aeration region downstream of the aerator
 4. The impact region
 5. The downstream flow region.
- Air is entrained at both the upper and lower air-water interfaces, as well as by plunging jet entrainment at the intersection of the jet with the recirculating pool, formed at the end of the cavity within the aeration region. Downstream of the aeration region, within the impact region, air is detrainment. This detrainment is subject to a rapid, pulsating change in pressure from a

negative to a positive pressure at the impact point. Chanson (1994) found that up to 80% of the entrained air along the jet was detrained within the impact region. The quantity of de-aeration is based on the jet velocity at impact, jet thickness at impact, gravity, angle of the jet with the spillway at impact, spillway inclination angle and the quantity of air entrained.

LABORATORY FACILITIES AND INSTRUMENTATION

The hydraulic model experiments were performed at the Civil Engineering Hydraulic Laboratory at Stellenbosch University. Both of the Type A and Type B stepped spillway models were scaled according to the Froude Model Law, as the fluid motion is predominantly influenced by gravity and a free surface gradient is present.

Instrumentation

Pressure measurement

WIKA S-10 pressure transducers were installed in the step riser to measure the pressure on the upper part of the step riser. This specific type of pressure transducer has a working range of ± 1 m and assured an accuracy of $\pm 0.5\%$. These sensors captured the pressure data at a frequency of 100 Hz and an acquisition period of 10 minutes was used. The 0.15 percentile was used as the minimum pressure parameter in the cavitation evaluation.

Air concentration

A Thermo Needle Probe system, supplied by Teletronic, was used to measure the spillway air concentration at the pseudo-bottom. The air concentration

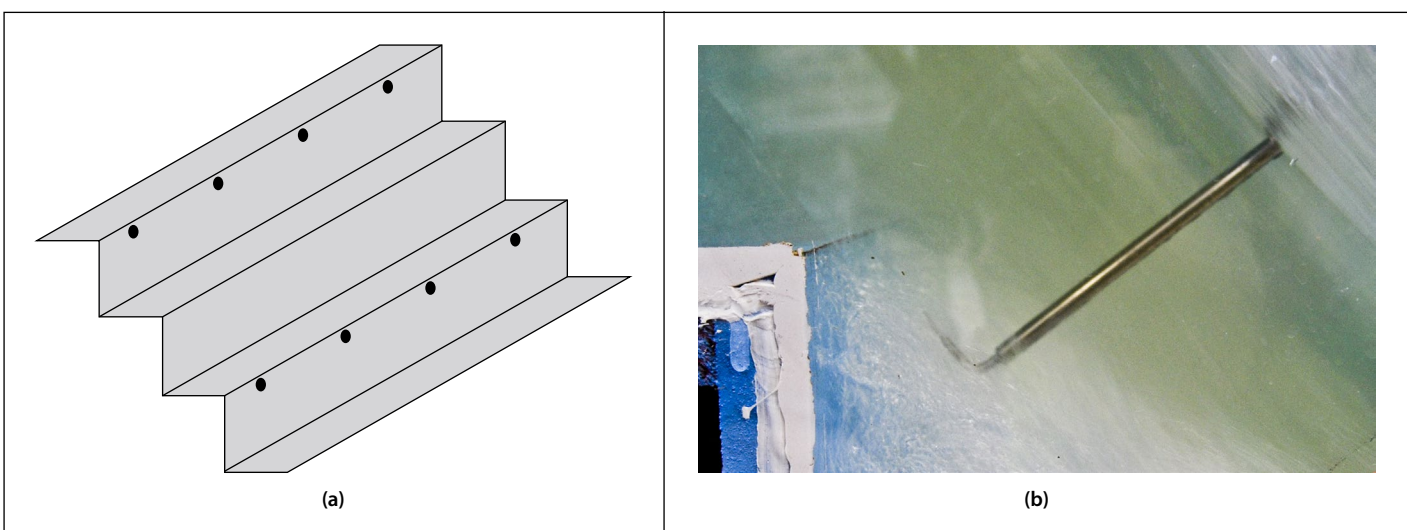


Figure 4 (a) Illustration of the pressure sensor positions and (b) Thermo Needle Probe

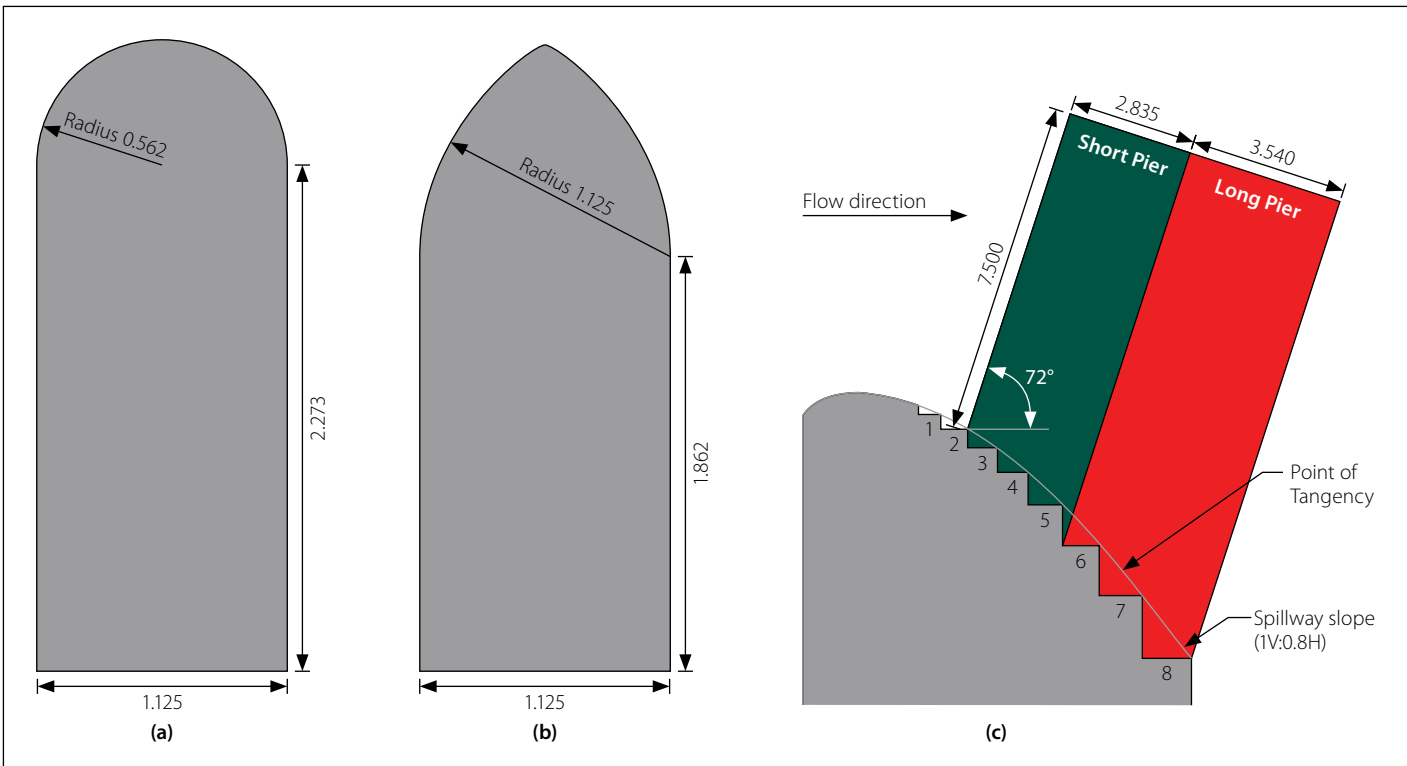


Figure 5 (a) Bullnose pier, (b) parabolic pier and (c) two different pier lengths

was recorded with a stimulation fixed frequency of 10 kHz over a sampling period of one minute. The raw data was evaluated and visualised by using the VoidWizard software package, which was supplied by HZDR innovation. The processed data provided information such as the air concentration, the conductivity of the medium and the bubble count over a preselected time step. The probe measures a different conductivity, as the medium changes between water and air. The upper conductivity threshold is characterised as the liquid phase, while the lower threshold is characterised as the gaseous phase. The difference in conductivity between subsequent measurements was thus used by the VoidWizard software package to distinguish between liquid and air. The mean air concentration was used as the air concentration parameter in the cavitation evaluation (refer to Figure 4).

Avoidance of scale effects

Various researchers such as Pinto (1984), Vischer (1982), Speerli (1999), Pegram (1999) and Boes (2000), who were all cited in Boes (2000), identified a minimum scale of 1:15 to faithfully represent the prototype behaviour of a stepped spillway. The model scale of 1:15 for the Type A stepped spillway was considered large enough to neglect the aeration scale effects.

The Type B stepped spillway model was designed with a scale of 1:50, which exceeds the recommendations of the previously mentioned researchers. Although the small scale induced aeration scale effects, the air concentration was accurately scaled and captured, as it conformed to the law of self-similarity (Chanson & Carosi 2007; Chanson 2008; Felder & Chanson 2017). The phenomenon of self-similarity is defined as the spatial distribution of properties at various instances of time and

spatial locations to be obtained from one another by a similarity transformation. Carosi, Chanson and Felder found that the void fraction remained invariant under scale changes for model Reynolds numbers greater than 8×10^4 .

EVALUATION OF CREST PIERS ON THE TYPE A STEPPED SPILLWAY

Spillway design

The 1:15 scale hydraulic model consisted of an uncontrolled ogee crest and stepped spillway. The ogee crest profile was designed according to the United States Bureau of Reclamation (USBR 1987) specifications. The spillway was constructed with a constant prototype step tread of 1.2 m and a step height of 1.5 m, resulting in an inclination angle of 51.3°, typical for RCC dams. To achieve adequate performance of the spillway for a



Figure 6 Visual performance comparison for a unit discharge of $30 \text{ m}^3/\text{s}$ comprising (a) bullnose short pier, (b) parabolic short pier and (c) a bullnose long pier

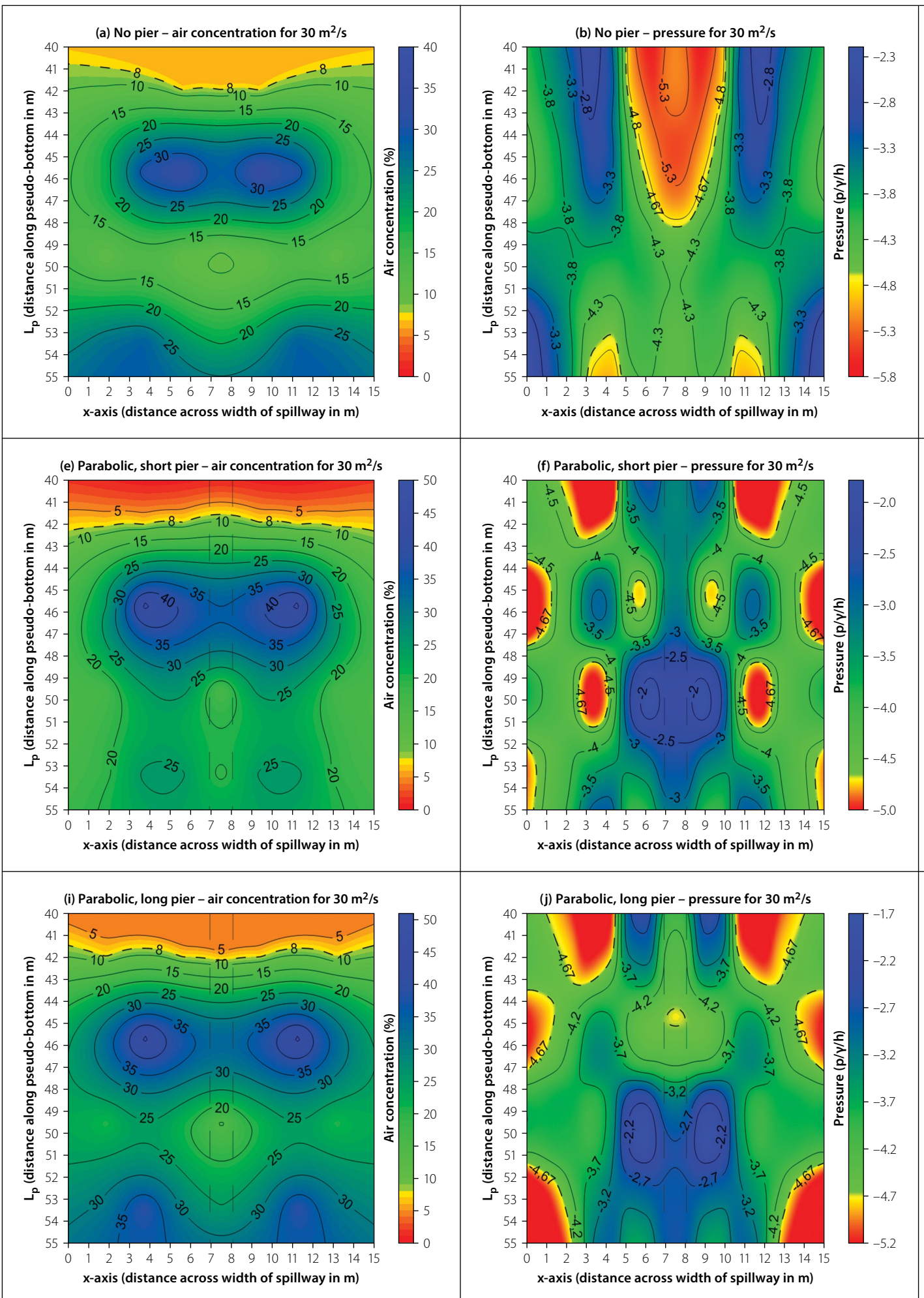
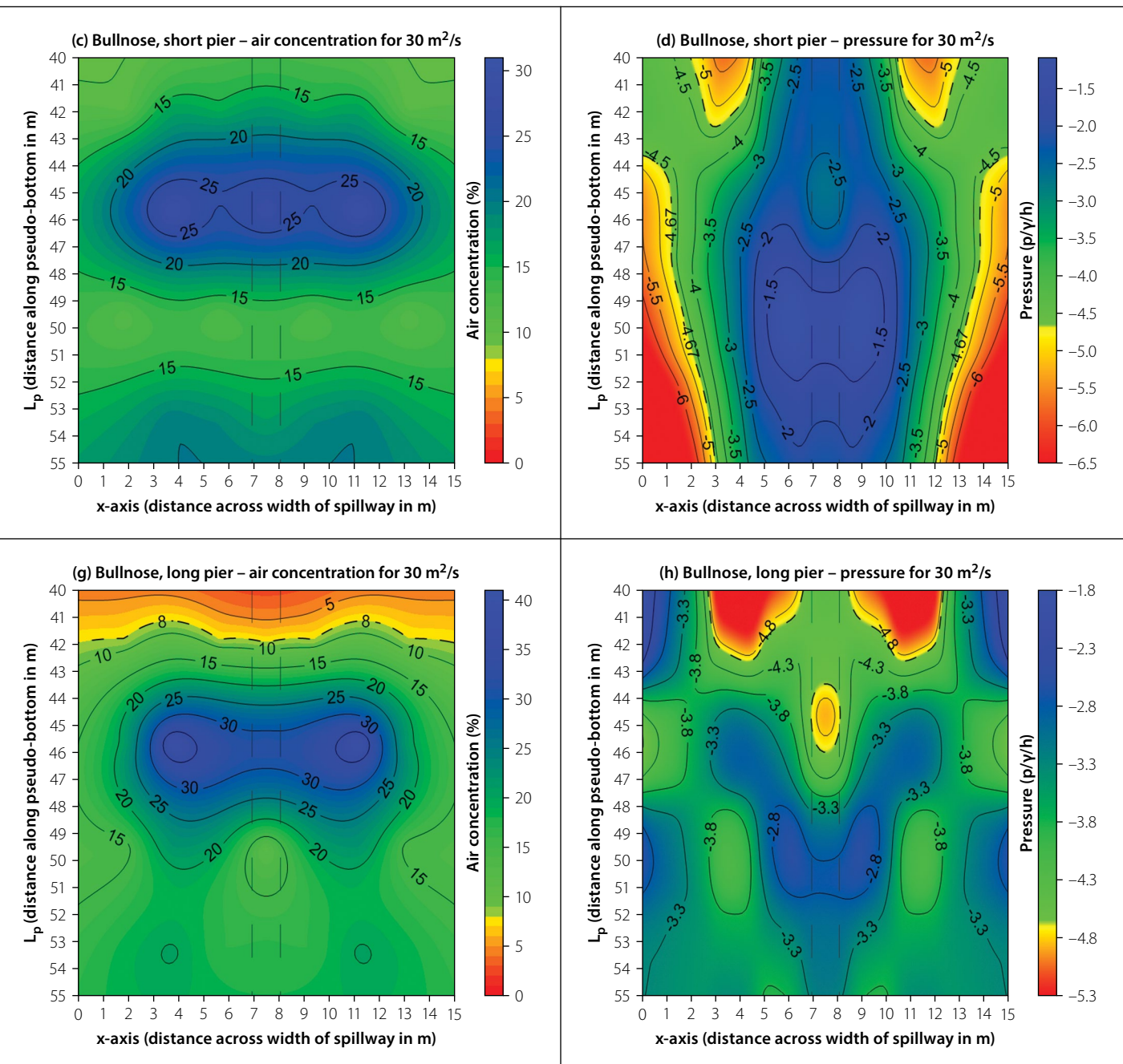


Figure 7 Cavitation analysis based on the air concentration and pressure measurements for different crest pier designs



range of discharges, a transitional step profile was introduced downstream of crest apex. The transitional profile provides increasing step treads, based on the design head, until the point of tangency is reached, whereafter a constant step design is implemented.

Crest pier design

Although crest piers are usually required to support a bridge or gates on a spillway crest, the purpose of the pier inclusion in this study was to induce artificial aeration into the flow. This paper considered variations of the pier design, comprising two different pier nose designs and two pier lengths.

The pier nose shape was designed in accordance with the guidelines provided by the American Society of Civil Engineers (ASCE 1995). A constant prototype pier

width of 1.125 m was advised in relation to the design head ($0.267 H_d$) and a bullnose and parabolic nose shape were selected. Two pier lengths were identified as suitable in order to investigate the effect thereof on the spillway aeration. The pier designs consisted of a short pier which extended 2.8 m downstream, and a long pier which extended 6.4 m downstream of the pier nose position. To ensure that the piers caused minimal additional head, they were placed downstream of the ogee crest at an angle of 72° to the horizontal. This concept was based on the pier design of the Gariep Dam in South Africa, where the piers were placed downstream of the crest, within the supercritical flow region, to eliminate any additional discharge head. Refer to Figure 5 (page 31) for a schematic illustration of the pier designs.

Model setup

The experimental area was defined to enclose the inception point, as the most severe minimum pressures had previously been measured in this location (Sánchez-Juny *et al* 2000). Four pressure sensors were installed on each measuring step, with the first sensor being installed in the middle of the spillway and subsequent sensors equally spaced. These pressure transducers were installed on the vertical step risers at a height approximately 0.9 times the step height. Due to the similarity of the model, the results were only measured on half of the spillway width. The air concentration was recorded at each of the pressure measuring positions, at the pseudo-bottom.

In order to eliminate variability in the measurements and ensure accurate results,

30% of the experiments were repeated. An average variation of 6.5% and 5% was measured for the air concentration and pressure results, respectively. The variation within the repeated experiments was considered acceptable, therefore not requiring the repetition of all tests.

Results

The experimental investigation consisted of four different pier model designs and a standard stepped spillway which acted as the control experiment. The experiments were conducted for a unit discharge of $30 \text{ m}^3/\text{s}$, as Calitz (2015) had previously established the maximum safe unit discharge capacity of a standard stepped spillway to be $25 \text{ m}^3/\text{s}$.

Visual observations

The performance of the bullnose short pier was characterised by a sharp redirection of flow, which was caused by the interaction of water on the blunt pier nose. The redirected flow allowed for a larger air void to form behind the pier, in turn permitting for a significant amount of air to be entrained. The parabolic short pier illustrated a variation in performance where the water flowing past the pier adhered to the pier sides. This was caused by the sharper pier nose which gradually redirected the flow past the pier. Adherent flow was observed for both the bullnose and parabolic long piers. The additional pier length removed the aeration which was observed on the side of the bullnose short pier, and subsequently an unaerated flow regime was experienced. Refer to Figure 6 (page 31) for the visual performance of the different crest pier designs.

Cavitation analysis

Analysis of the air concentration and pressure results was conducted to evaluate the potential of cavitation damage occurring on the spillway surface. The cavitation analysis comprised a visual presentation of the air concentration and pressure results for each of the model setups. The critical cavitation limits in terms of air concentration and pressure results were defined as 8% and -7 m , respectively. Peterka (1953) stated that a local air concentration of 8% is sufficient to avoid cavitation damage, due to the compressibility of the induced air, which absorbs the shock generated by the imploding vapour bubbles. The cavitation pressure limit of -7 m was transformed to a dimensionless pressure parameter ($p/\gamma/h$) of -4.67 , for a constant step height (h) of 1.5 m . Contour plots were used for the graphical presentation of the experimental results, which implemented a distinct colour scale where the boundary between yellow and green represented the critical cavitation limits for both the air concentration and pressure results. Refer to Figure 7 (page 32) for the air concentration and pressure results for various crest pier designs.

Through analysis of the experimental results, the bullnose short pier was identified as the best performing of the different piers in terms of air concentration, and it should be able to operate at a unit discharge of $30 \text{ m}^3/\text{s}$ without any risk of cavitation damage. This finding supports the similar conclusion of Calitz (2015). This was the only pier model to introduce an earlier onset of entrained air, compared to the control experiment. It should also be mentioned that the pressure results

indicated that the introduction of crest piers relieved the negative pressures, relative to those experienced in the control experiment, but did not remove them.

EVALUATION OF FGPs ON THE TYPE B STEPPED SPILLWAY

Spillway design

A high head, stepped spillway of the Dachaoshan Dam (Figure 1) (page 29) in China was constructed to evaluate the performance of the spillway surface with different FGP designs. The Dachaoshan Dam was constructed as an RCC gravity dam with a height of 111 m. The dam became operational in 2002 and has since experienced a large flood which resulted in a maximum unit discharge of $93 \text{ m}^3/\text{s}$. The dam discharges through five discharge bays which comprise Y-shape FGPs in combination with a slit-type flip bucket and three bottom outlets. A schematic design of the Dachaoshan Dam is illustrated in Figure 8.

The 1:50 scale hydraulic model utilised a smooth ogee crest, terminating at the downstream edge of the crest piers, whereafter it was succeeded by a stepped profile. The experiments were conducted on an uncontrolled ogee crest with the omission of radial gates between the piers. The crest design was based on a WES (1959) profile, with a vertical upstream face and four crest piers, spaced at 17 m, to form three discharge bays. The stepped spillway downstream of the crest piers was designed with a constant prototype step height of 1 m and a step tread of 0.7 m , except for the first step which had a step height of 2 m . The higher first

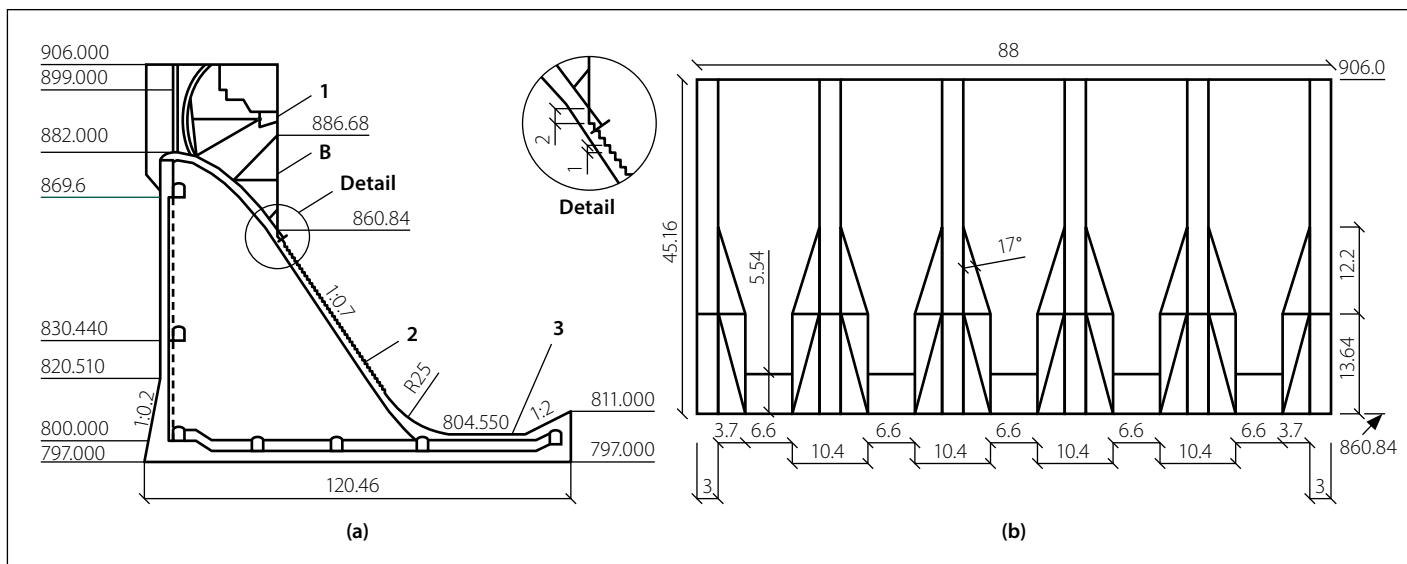


Figure 8 Schematic design of the Dachaoshan Dam indicating (a) a typical cross-section and (b) elevation as seen from the downstream side (after Nan & Rumyantsev 2014)

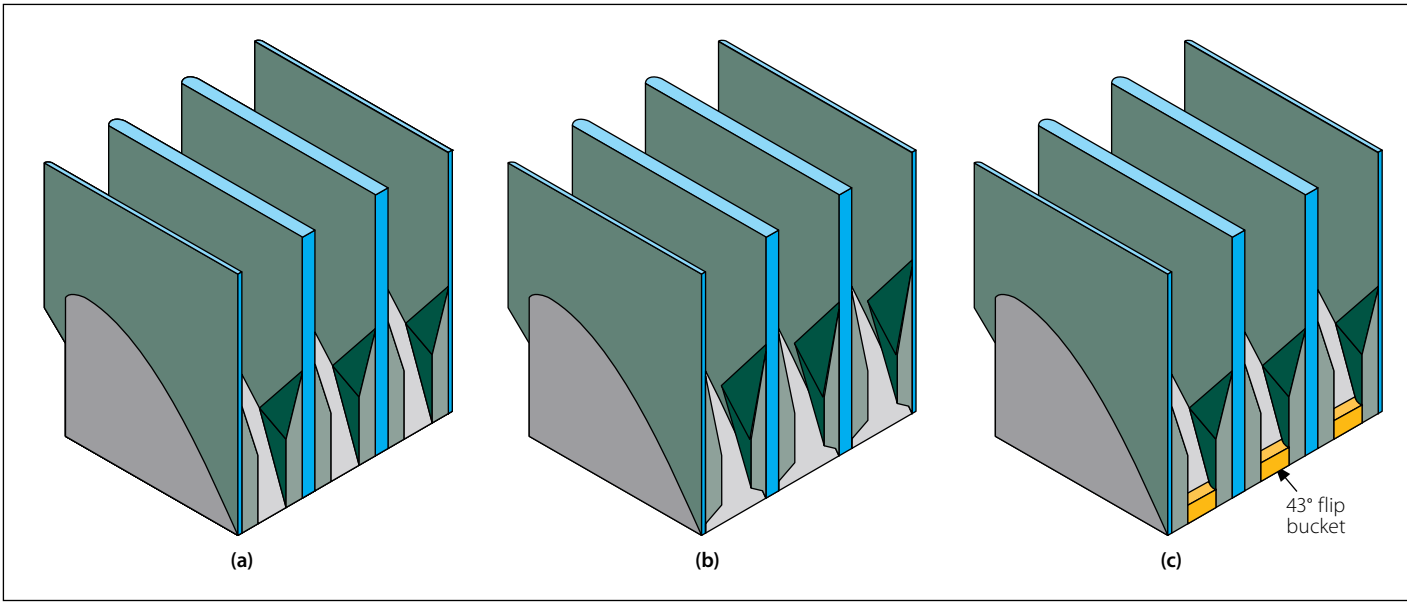


Figure 9 Schematic illustration of the (a) Y-shape FGP, (b) X-shape FGP and (c) Y-shape FGP in combination with a 43° slit-type flip bucket

step was included so that the flow would project over several steps, forming a large air cavity underneath the jet.

Flaring Gate Pier designs

The crest piers on the Dachaoshan Dam have two main functions. The first is to support the radial gates, since the dam is designed with a controlled crest. The second function is to support the FGPs, which are located at the downstream end of the crest piers, just upstream of the stepped spillway. This dam consists of six crest piers, each 45 m in length, which form five discharge bays over the crest. The pier design and spacing were based on the hydraulic design guidelines of the US Army WES (US WES 1959), i.e. a bullnose pier for high head dams which protrude upstream of the crest to increase the discharge efficiency.

The FGP designs for this model study consisted of three cases, an X-shape FGP, a Y-shape FGP and a Y-shape FGP in combination with a 43° slit-type flip bucket as indicated in Figure 9. The purpose of the flares was to contract the flow, resulting in a narrow, high-velocity jet, which created several air-water surfaces where air could be entrained. The X-shape (Figure 9(b)) has a wider bottom outlet width than the Y-shape FGP (Figure 9(a)). The wide outlet was designed to safely pass a unit discharge of 30 m³/s without the influence of the flares. At increased unit discharges the flare would contract and deflect the water. The addition of the slit-type flip bucket, in combination with the Y-shape FGP (Figure 9(c)), forces the departing jet to disperse in a vertical plane resulting in a long, narrow impact area. Scour in the downstream bed is

greatly reduced and model studies for the Dongjiang Dam, which is in the Hunan Province, China, reported a reduction of up to 80% (Lin *et al* 1987).

Model setup

The air concentration and pressure results were measured within the central discharge bay, along the length of the spillway. Three pressure sensors were located on each measuring step within the central bay, with the first sensor being installed in the middle of the bay and the two subsequent sensors equally spaced. These pressure transducers were installed on the vertical face of the step risers, at a height of approximately 0.75 times the step height. The results were measured on only half of the central discharge bay, as the similarity that was present in the physical model allowed for the mirroring of the results. The air concentration was recorded only on the centreline of the central bay, because of the time-consuming recording procedure.

To check the consistency of the model results, 40% of the experiments were repeated. An average error of 6.6% and 7.5% was recorded for the air concentration and pressure results, respectively. The repeatability of the recordings was deemed acceptable, hence all of the tests were not repeated.

Results

The experiments were conducted for unit discharges of 50, 100, 150 and 200 m³/s. The results presented in this paper are only for the 50 m³/s unit discharge, since safe unit discharges larger than 50 m³/s with the aerators were not attained experimentally. It is believed that the higher prototype

unit discharges which were experienced at both the Dachaoshan Dam (93 m³/s) and the Shuidong Dam (90 m³/s), with minimal damage to the spillway, could be due to the high tail water level generally experienced within the narrow valleys in China.

Visual observations

The Y-shape FGP's performance is characterised by large, unused spillway areas for energy dissipation and the substantial deflection (contraction and upward deflection in a ski-jump manner) of water (Figure 10(a)) (page 36). These ski-jump flow regimes were combined with longitudinal impact regions, which impinged on the stepped profile. Not only do these impact regions generate severe negative pressures, but they also lead to a decreased air concentration, according to Chanson (1994).

The design and performance of the X-shape FGP is very similar to that of the Y-shape FGP. The X-shape FGP was designed with a reduced flow blocking effect (i.e. water in the bottom part of the flow depth is not deflected) compared to the Y-shape FGP. The reduced blockage led to a decreased water deflection, as only the upper part of the flow is deflected by the flare, which is indicated in Figure 10(b) (page 36). The reduced deflection should be beneficial, since it would result in a smaller, damped, impact region. These regions where the impact had been damped would decrease the effect of impact detrainment, resulting in a higher, entrained air concentration.

The performance of the Y-shape FGP, combined with the slit-type flip bucket, was such that the water was not in contact with

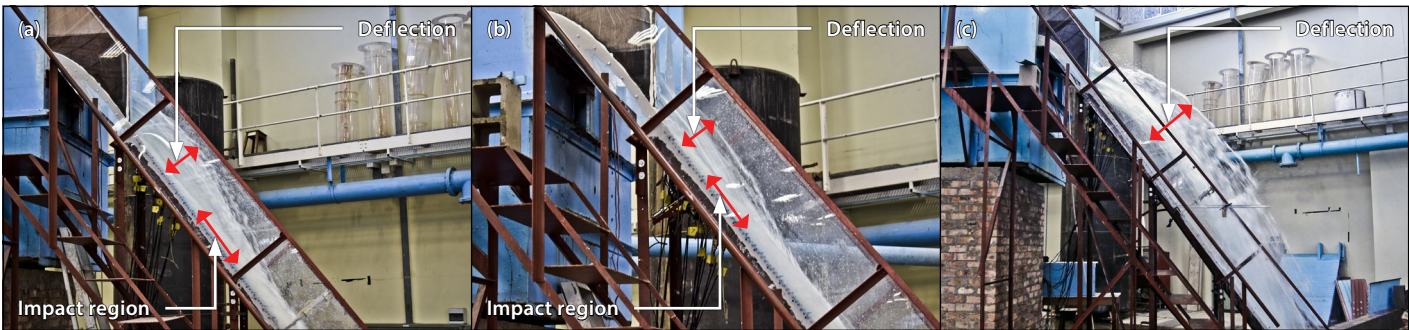


Figure 10 Visual performance comparison for a unit discharge of $50 \text{ m}^3/\text{s}$ comprising (a) a Y-shape FGP, (b) X-shape FGP and (c) Y-shape FGP in combination with a flip bucket

the stepped spillway. For all the tested unit discharges, the water was projected over the length of the spillway, as illustrated for the unit discharge of $50 \text{ m}^3/\text{s}$ in Figure 10(c). There was thus no energy dissipation by the stepped profile and the use of the steps would only be for economic benefit and the reduced construction time of RCC.

Cavitation analysis

The evaluation and interpretation of the cavitation analysis were based on the graphical presentation of the air concentration and pressure results. The cavitation analysis was based on the comparison of the air concentration and pressure results on the centreline, along the length of spillway. As the spillway pressures were recorded along the length and across the width of the spillway, pressure contour plots were used to illustrate the spillway performance. The performance for the FGPs was also compared with a stepped spillway without piers or flares, which acted as a control.

The critical air concentration and pressure values were defined as 8% and -7 m , respectively. The cavitation pressure limit of -7 m atmospheric pressure head was transformed to represent a dimensionless pressure parameter ($p/\gamma/h$) of -7 for a constant prototype step height (h) of 1 m . The contour plots implemented a distinct colour scale, where the boundary between yellow and green represented the -7 m water pressure (dashed contour). The dashed, horizontal lines on the Y- and X-shape FGP contour plots define the flare extremities on either side of the central discharge bay. The cavitation analyses of the X- and Y-shape FGPs were based on the air concentration and pressure results along the spillway centreline for a unit discharge of $50 \text{ m}^3/\text{s}$ as seen in Figure 11.

For the *no pier control case* with the unit discharge of $50 \text{ m}^3/\text{s}$, air was entrained and the pseudo-bottom inception point was located at $L_p = 88.6 \text{ m}$. The lack of air entrainment between $L_p = 50$ and 90 m was

attributed to the relatively small steps, compared to the flow depth which had a negligible effect on the development of the boundary layer. The centreline pressure results can be described as a wavy pattern, which illustrated that a portion of the flow was slightly redirected by the steps. The contour plots indicated regions of cavitation pressure which were first observed at a position approximately 80 m (L_p) downstream of the spillway crest. These regions coincided with areas of insufficient air concentration, which implies a likelihood of cavitation damage. This was observed for all the unit discharges tested.

For the *Y-shape FGP case* with the unit discharge of $50 \text{ m}^3/\text{s}$, an increased air concentration was measured as compared to the control experiment at the upstream section of the spillway. It is considered that the increased air concentration is attributable to the larger first step, in combination with the Y-shape FGP. An air cavity is formed on the first step niche, from which air is entrained at the pseudo-bottom. A decreasing trend in the air concentration was observed in a downstream direction along the length of the spillway centreline, reaching a minimum in the impact zone. Overall, the Y-shape FGP entrained more air compared to the control experiment in the zone between $L_p = 60$ and 90 m ; however, air was detrained within the impact regions. The Y-shape FGP pressure contour plot displayed two cavitation regions which occurred predominantly in the centre of the discharge bay, between the flare extremities. The cavitation evaluation identified one area ($L_p = 93$ to 113 m) which was vulnerable to cavitation damage. The overall performance of the spillway was therefore not improved with the addition of the Y-shape FGP, and the safe unit discharge capacity would be less than $50 \text{ m}^3/\text{s}$.

For the *X-shape FGP case* with the unit discharge of $50 \text{ m}^3/\text{s}$, a significant improvement in the spillway performance was noticed. Sufficient amounts of air were entrained along the entire spillway length,

whilst a minimum air concentration of 11% was recorded at $L_p = 93.6 \text{ m}$ (minimum value on the graph is an interpolation). Similar to the air concentration performance, a significant improvement in terms of the spillway pressures was noticed for the unit discharge of $50 \text{ m}^3/\text{s}$. No cavitation pressures were recorded along the length (L_p ranging from 50 to 135 m) or across the width of the discharge bay. At higher discharges, severe negative pressures were measured in the downstream region of the spillway, which are highly unfavourable. Therefore, the X-shape FGP increased the safe unit discharge capacity of the stepped spillway to $50 \text{ m}^3/\text{s}$.

Ski-jump trajectory of the Y-shape FGP in combination with a slit-type flip bucket

The ski-jump type trajectory (upper and lower edges of the projected nappe) for the Y-shape FGP in combination with the flip bucket is illustrated in Figure 12 (page 38). This combination significantly altered the flow pattern and projected all of the water over the entire length of the spillway. For the unit discharge of $50 \text{ m}^3/\text{s}$, the water was horizontally deflected by 13 m at the spillway toe. As the investigation of the impact regions downstream of the spillway toe is beyond the scope of this study, it suffices to state that a stilling basin with a minimum tail water level would probably be required in order to absorb the impact forces on the toe foundation.

CONCLUSIONS

Type A stepped spillway investigation

The most important conclusion from the Type A stepped spillway investigation is summarised as follows:

- The maximum, safe unit discharge capacity of a stepped spillway without crest piers was previously determined to be $25 \text{ m}^3/\text{s}$ (Calitz 2015). The implementation of the short, bullnose pier at

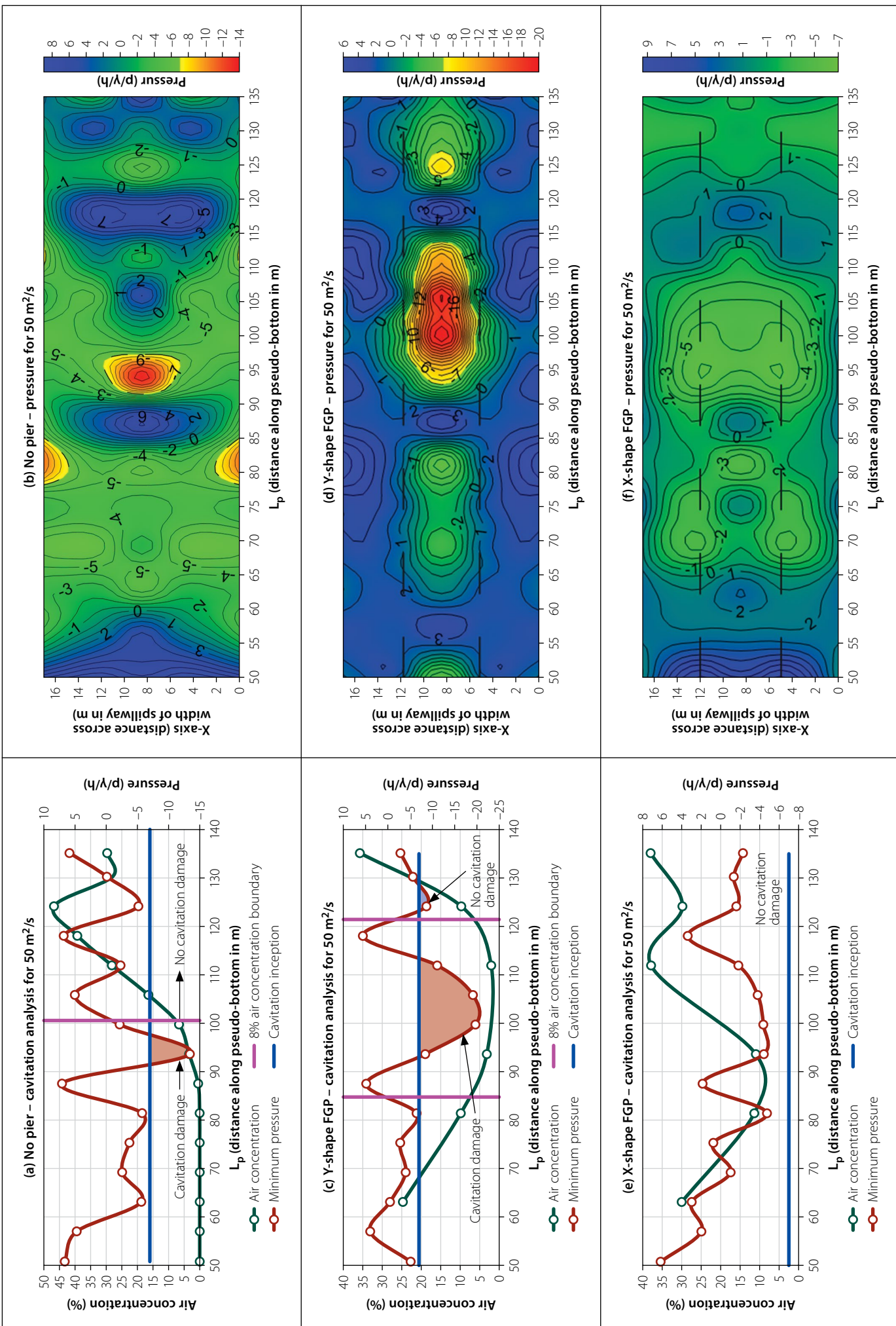


Figure 11 Cavitation analysis based on the air concentration and pressure measurements for the no pier control experiment, Y-shape FGP and X-shape FGP

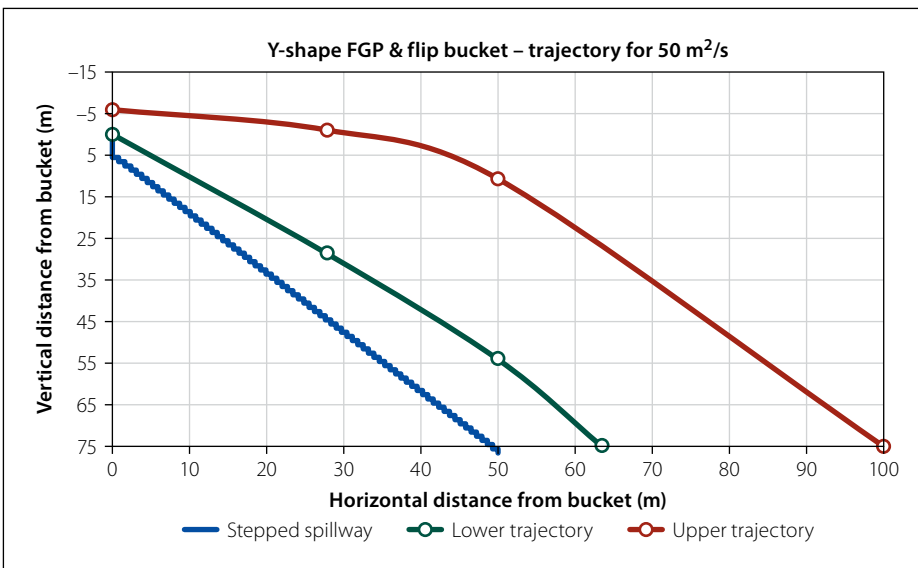


Figure 12 Ski-jump trajectory for the Y-shape FGP in combination with a slit-type flip bucket

the spillway crest increased the safe unit discharge capacity to $30 \text{ m}^3/\text{s}$, by eliminating the risk of cavitation damage. This was the only crest pier design that increased the discharge capacity.

Type B stepped spillway investigation

The Type B stepped spillway was investigated to determine how the existing, high unit discharge, stepped spillways in China performed with respect to aeration and pressure on the pseudo-bottom for each of the aeration structures. The conclusions are summarised as follows:

- The most notable improvement was the increase of the safe unit discharge capacity to $50 \text{ m}^3/\text{s}$ in the case of the X-shape FGP. Air concentrations above the 8% limit were recorded along the length of the spillway, whilst the entire spillway area ($L_p = 50 \text{ m}$ and $L_p = 135 \text{ m}$) was free of cavitation pressures. This design is not advised for higher unit discharges, since it generated severe negative pressures at $L_p = 135 \text{ m}$.
- The spillway performance of the Y-shape FGP was the most consistent, irrespective of the unit discharge. Not only were the air concentration and pressure results similar, but at higher unit discharges, the Y-shape FGP outperformed the X-shape FGP. However, cavitation regions were observed in a small section on the downstream end of the spillway ($L_p = 91 \text{ m}$ to 135 m). Future research is required to determine the tail water level, which would

prevent cavitation damage in the downstream region.

- The Y-shape FGP, together with the slit-type flip bucket, projected the flow over the entire length of the stepped spillway for all the tested unit discharges ($50 \text{ m}^3/\text{s}$ to $200 \text{ m}^3/\text{s}$). As no water was discharged via the stepped spillway, it was free of exposure to cavitation damage.
- The Type B stepped spillway investigation did not improve the safe unit discharge capacity to the design capacity of $200 \text{ m}^3/\text{s}$ like some of the Chinese Dams. Nonetheless, the results were of value, as they enhanced the understanding of the FGP performance and design. The impact regions should ideally be located downstream of the spillway toe, to avoid the de-aeration of the flow and the accompanying cavitation pressures on the step edges.

REFERENCES

- ASCE (American Society of Civil Engineers) 1995. *Hydraulic Design of Spillways*. Reston, VA: ASCE.
- Boes, R M 2000. Scale effects in modelling two-phase stepped spillway flow. *International Workshop on Hydraulics of Stepped Spillways*. Leiden, Netherlands: Balkema, 53–60.
- Bo, W, Chao, W, Hu, Y & Mo, Z 2007. Relationship of first step height, step slope and cavity in X-shaped flaring gate piers. *Journal of Hydrodynamics*, 19: 349–355.
- Calitz, J 2015. *Investigation of air concentration and pressures of a stepped spillway equipped with a crest pier*. MEng Dissertation. Stellenbosch University.
- Chanson, H 1994. Aeration and deaeration at bottom aeration devices on spillways. *Canadian Journal of Civil Engineering*, 21: 404–409.
- Chanson, H 2008. Physical modelling, scale effects, and self-similarity of stepped spillway flows. *World Environment and Water Resources Congress*, 1–10.
- Chanson, H & Carosi, G 2007. Turbulent time and length scale measurements in high-velocity open channel flows. *Experiments in Fluids*, 42: 385–401.
- Felder, S & Chanson, H 2017. Scale effects in microscopic air-water flow properties in high-velocity free surface flows. *Experimental Thermal and Fluid Science*, 83: 19–36.
- Hongta Group 2017. *Dachaoshan Dam*. Available at: http://www.hongta.com/language/en/aboutus/hcty/20110/t20111012_148018.htm [accessed on 1 January 2017].
- Khatsuria, R M 2004. *Hydraulics of Spillways and Energy Dissipators*. Boca Raton, FL: CRC Press.
- Lin, B, Li, G & Chen, H 1987. Hydraulic research in China. *Journal of Hydraulic Engineering*, 113: 47–60.
- Nan, F & Rumyantsev, I 2014. Modelling of flood routing through stepped spillway of water reservoir dam. *Proceedings*, 11th International Conference on Hydroinformatics (HIC 2014), 8 January, New York. CUNY Academic Works. Available at: http://academicworks.cuny.edu/cc_conf_hic/375.
- Nortjé, J 2002. Dam safety legislation and programme in the Republic of South Africa. In *Design and Rehabilitation of Dams*. Short course presented by the Institute for Water and Environmental Engineering, Stellenbosch University.
- Peterka, A J 1953. *The Effect of Entrained Air on Cavitation Pitting*. Reston, VA: ASCE, 507–518.
- Pfister, M & Hager, W H 2011. Self-entrainment of air on stepped spillways. *International Journal of Multiphase Flow*, 37(2): 99–107.
- Russell, S & Sheehan, G 1974. Effect of entrained air on cavitation damage. *Canadian Journal of Civil Engineering*, 1(2): 97–107.
- Sánchez-Juny, M, Pomares, J & Dolz, J 2000. Pressure field in skimming flow over a stepped spillway. In Minor, H E & Hager, W H, *Proceedings*, International Workshop on Hydraulics of Stepped Spillways, 22–24 March, Zurich, Switzerland, Rotterdam: Balkema, pp 137–146.
- Shen, C 2003. RCC dams in China. *Proceedings*, 4th International Symposium on Roller Compacted Concrete, 17–19 November, Madrid, Spain.
- Ting, Z, Chao, W & Qi, Z 2011. Comparison on somatotype of X- and Y-shape flaring gate pier connected with stepped spillway. *Advanced Materials Research*, 3661–3665.
- US WESS (US Army Waterways Experimental Station) 1959. *Hydraulic Design Criteria*. Ficksburg, MS: US WESS.
- USBR (United States Bureau of Reclamation) 1987. *Design of Small Dams*. Water Resources Technical Publication No. 2. Washington, DC: USBR.

Understanding public transport needs in Cape Town's informal settlements: a Best-Worst-Scaling approach

M Teffo, A Earl, M H P Zuidgeest

A poor understanding of the needs of people living in informal settlements has often resulted in these needs being assumed and misunderstood due to the lack of proper public consultation or participation. Because of this, South Africa's transport sector, and by extension many other public sectors, faces various challenges. Knowing that public transport is the dominant mode of transport in informal settlements, a better understanding of its challenges as experienced by its commuters is essential for the development of informal settlement upgrading policies. The research in this paper uses Best-Worst-Scaling (BWS) – part of the family of discrete choice models – as a survey and analysis tool for rating and ranking public transport-related challenges of 290 randomly selected commuters from six different informal settlements in Cape Town. The most important features deduced from the public transport experience (PTE) study include (1) Walking Safety, (2) Personal Safety, (3) Unsafe Driving, (4) Overcrowding and (5) Walking Distance. There is no apparent trend in the variance between the choices of men and women. However, there is a significant variance of choices across the respective locations, and – for most attributes – between mode users. This suggests that, with respect to public transport infrastructure upgrading, contextual factors, determined by one's environment, dominate experiences and perceptions, rather than socio-demographic factors.

BACKGROUND

South Africa, like many developing countries, is experiencing a rapid population growth, with an increasing demand for travel. Most inhabitants still rely on public transport to gain access to economic, social, educational, medical, recreational and cultural activities. In 2013, 91.4% of people in the lowest income group in the country were reliant on public transport, with 5.7% using trains, 23.6% buses and 62.1% minibus taxis (Statistics SA 2013a). Public transport thus remains an absolute necessity to low-income inhabitants. The public transport system of South Africa, however, is in a bad state, at least in part because "... there has been a very poor post-apartheid government response to the escalating mobility needs of low-income travellers, who constitute the vast majority of South Africa's urban population (Lucas 2011 pg 1320)." Lucas (2011) gives four key causes for the level of transport poverty we see in South Africa today, namely: (1) low access to private and public transport services, (2) affordability issues connected to over-reliance on minibus taxis, (3) the legacy of apartheid planning on contemporary

housing developments and (4) over-reliance on walking. Lucas (2011) furthermore found that, for urban low-income residents, the use of formalised public transport is often not an option due to their location of residence and the times of the day when they require public transport. Because of this, and because of the existence of an extensive, informal, minibus taxi industry, many commuters from low-income areas have become captive users of this form of paratransit. This in a context where Statistics SA (2013b) reports that the lowest income population group spends on average up to 66.6% of their income on transport, with the second and third lowest income groups spending 41.9% and 29.4% respectively, instead of the internationally accepted target of 10%, which is also adopted by South Africa in its 1996 White Paper on Transport Policy (Department of Transport 1996), and which shows the urgency to address the mobility needs of the poor.

South Africa's hopes of finding a solution to these transport problems are placed upon Bus Rapid Transit (BRT) systems, which are currently being rolled out in most major cities in South Africa. Progress

TECHNICAL PAPER

JOURNAL OF THE SOUTH AFRICAN INSTITUTION OF CIVIL ENGINEERING

ISSN 1021-2019

Vol 61 No 2, June 2019, Pages 39–50, Paper 0083



MONERI TEFFO is an engineer at the Transnet Group Capital (Transnet SOC Ltd) Civils and Perway Design Office, Johannesburg. He graduated with a BSc (Hons) (Civil Engineering) from the University of Cape Town in 2016, and has an interest in Transportation Engineering and Planning, particularly the interaction thereof with the socio-economic indices of urban areas.

Contact details:
Transnet Group Capital
9 Country Estate Drive
Waterval 5-Ir
Midrand 1662
South Africa
T: +27 11 308 1283
E: moneri.teffo@transnet.net



ANDREW EARL is currently pursuing a double Master's (Ma and MSc) in Innovation Design Engineering between the Royal College of Art and Imperial College London. Prior to undertaking his Master's, he graduated (BSc (Hons)) from the University of Cape Town Civil Engineering Department in 2016. He maintains a keen interest in urban issues, particularly those around transport in the South African context. During his time in the United Kingdom he is learning new approaches to problem solving in a variety of contexts and aims to bring this knowledge home after graduating.

Contact details:
Imperial College London
United Kingdom
Flat 7, Oxford Court
Bolingbroke Walk
SW11 3NJ, London
United Kingdom
T: +44 77 8012 6131
E: andrew.earl@network.rca.ac.uk / a.earl17@imperial.ac.uk



PROF MARK H P ZUIDGEEST is a member of SAICE, and is the SANRAL Chair of Transportation Planning and Engineering at the University of Cape Town. He graduated with an MSc (Civil Engineering) from the University of Twente, The Netherlands, in 1997, and a PhD from the Netherlands Research School for Transport, Infrastructure and Logistics (TRAIL) in 2005. His fields of interest include land use – transport systems analysis, with an emphasis on questions around sustainability, equity and accessibility.

Contact details:
Centre for Transport Studies
Department of Civil Engineering
University of Cape Town
Private Bag X3
Rondebosch 7701
South Africa
T: +27 21 650 4756
E: mark.zuidgeest@uct.ac.za

Keywords: public transport satisfaction, informal settlements, best-worst-scaling, Cape Town

has been slow, however, mainly due to conflicts between the developers of the BRT system and the existing minibus taxi industries (Schalekamp & Behrens 2010), and financial challenges associated with the building and operating of full-fledged BRT systems. Because of these and many other reasons, it has been acknowledged that the minibus taxi industry should actually form part of the solution to the transport problems faced by South Africa's urban poor (see Lucas 2011; Del Mistro & Behrens 2015; Ferro & Golub 2012), for example by operating minibus taxis as feeders of the formalised transit trunk routes (Golub *et al* 2009; Ferro Salazar & Behrens 2015).

Such hybrid systems would require more formalised infrastructure and regulations that also cater for the minibus taxi industry in low-income areas, such as informal settlements. Pertinently, Mahapa and Mashiri (2001) argued that transport policy-makers in South Africa have been preoccupied with technological solutions and efficiency savings rather than focusing on 'local beneficiary' communities, claiming that, with a focus on the latter, transport solutions would have been less expensive and more context- and gender-specific. Furthermore, Potgieter *et al* (2006, p 35) suggest that there is a "... need for a national qualitative and quantitative study that provides insight and baseline data on how issues of transport are gendered and the consequences on the quality of lives of women." Potgieter *et al*'s argument is especially relevant in view of the statement by Statistics SA (2013c) that, in general, women are more reliant on public transport in South Africa than men. Thus, should the development of transport infrastructure in low-income areas occur, the infrastructure and regulations provided must be context- and gender-specific.

To get a better understanding of the public transport-related experiences and associated needs of the urban poor in South Africa's informal settlements, this paper seeks to apply an innovative survey method and analysis based on principles of choice modelling and stated choice survey design for the collection of such data in the context of informal settlements.

LITERATURE REVIEW

Literature regarding user satisfaction and service quality in public transport describes how consumers evaluate the quality of a

public transport service, i.e. public transport service attributes including, but not limited to, safety, availability and travel fares. Furthermore, and of significance to transport authorities, the relative importance of these attributes is typically evaluated (Beirão & Sarsfield Cabral 2007).

User satisfaction and service quality studies come in many forms, either qualitative, quantitative or as a mixed-methods approach (de Oña & de Oña 2014). Qualitative studies have typically taken two forms. In-depth interviews such as those conducted by Beirão and Sarsfield Cabral (2007), or focus group discussions as seen in Guiver (2007). The advantage of such qualitative studies is that they yield nuanced and detailed information regarding the field of study. The more quantitative survey methods in service quality and user satisfaction in public transport typically use Likert scales (Donoso *et al* 2013), which is an approach used to scale responses comparable with a 3, 5 or 7-point rating scale. See for example Sam *et al* (2017) for a study on public transport experiences in Ghana, Wong *et al* (2017) for a study on public transport satisfaction of elderly citizens in Hong Kong, and Efthymiou and Antoniou (2017) for a study on changing public transport satisfaction in Greece during the economic crisis. There are clearly two main approaches by which these studies assess the relative importance of service attributes. The first approach, referred to as an indirect method, uses statistical models of correlation and regression after collecting the respondents' surveys to ascertain the relative importance of service quality or transport attribute information. The second approach, referred to as a direct method, is characterised by finding attribute importance and service quality directly from the interviews or surveys. There is still debate as to whether direct or indirect measures are more effective (Schalekamp & Behrens 2010). While these survey methods are useful due to their ubiquity, the Likert scale is prone to response biases, mainly socially desirable responding, acquiescence and extremity bias (Paulhus 1991). Furthermore, the focus in these studies is largely on identifying important user satisfaction of particular service attributes and not the relative importance of them (Behrens & Schalekamp 2010). In studies that aim for capturing the relative importance of attributes rating scales, researchers mostly use rating scales that do not force respondents to discriminate between items, allowing them

to state that multiple items are of similarly high importance of satisfaction/dissatisfaction (Flynn & Marley 2014), whilst in some cases only the preferred item is identified and thus little is understood of the relative ranking of attributes for a given respondent. The Best-Worst-Scaling technique used in this paper to elicit public transport related experiences in Cape Town's informal settlements, is a direct method that overcomes both shortcomings of the commonly used rating scales.

Best-Worst-Scaling (BWS)

BWS is a statistical research tool, a theory for data collection, and a modelling technique for eliciting ranked preferences of respondents. Surveys conducted using the BWS technique allow respondents to indicate their most important attribute and their least important attribute in a set of choices. The BWS technique thus allows the surveyor to get a full ranking of terms, rather than just the most preferred item/s as is common in, for example, stated preference survey design. In addition, BWS can be applied to many more than seven attributes, where many other ranking methods are known to suffer from accuracy and consistency when numbers of attributes increase beyond seven (see for example Bettman *et al* 1990).

The BWS technique has predominantly been applied in the marketing, health and social sciences fields, and is relatively new to the field of transport planning and engineering, with only a handful known applications dealing with preferences for electric vehicle choice in Germany and Australia (Hinz *et al* 2015; Beck *et al* 2016) and for assessing public transport experience in Australia (Beck & Rose 2016).

First proposed in the 1980s by Professor Jordan Louviere, it was initially called the method of maximum difference scaling or MaxDiff. It was introduced to capitalise on a human's tendency to be more reliable and accurate at identifying extreme options, rather than options placed on a graded scale (Louviere *et al* 2015). BWS provides a theoretical framework within which to measure latent, subjective quantities that produce measurement values that can be presented nominally and compared. The principles underlying the analysis of BWS choice data are similar to those in a discrete choice experiment and are based on random utility theory (RUT).

RUT assumes that people make errors, but when choosing repeatedly, their choice

frequencies give an indication of how much they value the items under consideration, i.e. how often item A is picked over item B gives an indication of how much item A is preferred over item B.

The first step in applying the BWS technique is to decide how many attributes will be compared, and then to develop survey designs using that number of attributes. There are three different case types that are used in BWS designs, each for different reasons.

BWS Case Types

Case 1 analysis, also referred to as the object case, is the simplest and most commonly used of the three BWS design methods. This type of analysis derives the relative values associated with each object in a list of comparable objects (Louviere *et al* 2015) such as modes of transport. The value scale being used, such as degree of concern or effectiveness, is up to the discretion of the researcher. Thus, category rating scales, such as the aforementioned Likert scale, can easily be substituted within a BWS design (Flynn & Marley 2014).

Case 2 analysis, which is also referred to as the profile case, asks the respondent to choose the attribute within a profile, which is defined as a set of attributes with attribute levels, that is the best and the one that is the worst (Louviere *et al* 2015). Presenting different profiles with different attribute levels now ensures trade-off between attributes. The difference between Case 1 and Case 2 analyses is illustrated in Table 1.

Finally, a Case 3 analysis is referred to as the multi-profile case, which is a logical extension of the Case 2 type and looks most like a common choice experiment, except that the respondent is asked to choose the worst/least attractive profile and the best/most attractive profile from a set of three or more profiles (Louviere *et al* 2015). This case type allows for the estimation of multinomial logit models (Flynn & Marley 2014).

An in-depth review of the different cases and their uses, amongst others the estimation of logit models from BWS outputs, as well as their position in the field of choice modelling and discrete choice experiments, is beyond the scope of this paper. See Hess and Daly (2014) for a review of choice modelling methods, and Louviere *et al* (2015) for more details on BWS itself.

In this paper we apply a Case 1 BWS design to capture public transport experiences (PTE) of commuters in informal

Table 1 Example of Best-Worst-Scaling Case Types 1 and 2

| Example of Type 1: Object case | | |
|--------------------------------|--------------------------|------------------|
| Most Concerning | Public Transport Feature | Least Concerning |
| | Travel delays | |
| | Overcrowding | |
| ✓ | Personal Safety (crime) | |
| | Availability | ✓ |

| Example of Type 2: Profile case | | |
|---------------------------------|--|------------------|
| Most Concerning | Public Transport Feature and Level | Least Concerning |
| | Some problems finding the bus station | |
| ✓ | No waiting time at the station | |
| | Extremely crowded during the commute | ✓ |
| | Moderately loud inside mini-bus taxi | |

settlements based on a set of defined features (attributes) of the public transport experience, such as overcrowding, travel delays, personal safety and availability. These can be meaningfully compared in an object analysis. A Case 2 or 3 analysis would have been more appropriate when dealing with preferences rather than experiences.

BWS balanced incomplete block designs

Early executions of Case 1 analyses were conducted using so-called 2^J designs (Flynn & Marley 2014), so named because for J objects there are 2^J best-worst choice sets that are possible. Issues around using this format of choice set design arise only from psychological phenomena, as the size of the choice sets is not constant; for instance, respondents can view choice sets with a small number of objects as the more important ones (Louviere *et al* 2015). To avoid these problems, Balanced Incomplete Block Designs (BIBD), which stem from combinatorial mathematics, are most commonly used now. A BIBD guarantees that the occurrence and co-occurrence of all objects (or attributes) is constant, therefore reducing the propensity of respondents to make assumptions regarding the relative significance of objects.

A BIBD has the following characteristics (see Table 2):

- Each task contains the same number of items.
- First order balance or frequency balance: each item occurs the same number of times across tasks.
- Second order balance or orthogonality: each item appears equally often with every other item.

- Positional balance: each item should appear an equal number of times in the first, second, third and n -th positions within the sets to avoid order-bias.
- Connectivity: each item should be directly/indirectly compared to every other item in the study to allow for all the items to be compared on a common scale (Peitz & McEwan 2016).

Table 2 A BIBD design example of four attributes; attribute numbers fill the cells

| | Attribute number | | |
|--------------|------------------|------------|------------|
| | Position A | Position B | Position C |
| Set 1 | 1 | 2 | 3 |
| Set 2 | 2 | 3 | 4 |
| Set 3 | 3 | 4 | 1 |
| Set 4 | 4 | 1 | 2 |

Practice with BWS designs revealed that four to six items per choice is optimal for most respondents and most tasks. If the item labels are long, such as positioning statements, then fewer than six items should be used. Respondents can typically undertake up to 20 choice sets, though anecdotal evidence suggests that boredom sets in after about 10 to 12 choice sets (Chrzan & Peitz 2015).

RESEARCH DESIGN

For this study attributes related to a commuter's public transport experience within the context of Cape Town's informal settlements were used to design the choice sets of

the survey. The attributes were formulated through a literature review (including Beirão & Sarsfield Cabral 2007; Behrens & Del Mistro 2010; Donoso et al 2013; Lucas 2011; de Oña & de Oña 2014; and Transport for Cape Town 2013), field reconnaissance visits and semi-structured interviews with township dwellers, and a pilot survey. Formal surveys were conducted after the pilot survey to obtain the BWS data. The choice data was accordingly statistically analysed to develop the most concerning and least concerning choice clusters. The most concerning and least concerning public transport experience attributes were then used to draw relationships across the boundaries of locations and gender.

Pilot survey

The preliminary design of the BWS attributes was developed based on the literature review, including priorities highlighted in the City of Cape Town's comprehensive integrated transport plan (Transport for Cape Town 2013), semi-structured interviews with community organisations, and discussions with 32 randomly selected respondents from the University of Cape Town (UCT) and the Thandokhulu High School in Rondebosch, who presently live in informal settlements, or in areas that have historically been on the urban periphery of Cape Town. The respondents were asked to describe (in their own words) some of the challenges they experience when accessing and using public transport. The respondents were also asked to comment on transport infrastructure elements that they feel are lacking. A draft final attribute list was then established.

In a pilot survey a provisional Case 1 BWS design was tested to see whether the chosen attributes were understandable to the respondents. This pilot survey was again conducted with randomly selected students and staff at UCT and Thandokhulu High School. At each of these locations, a total of five respondents were asked to complete the BWS questionnaire. It was observed, in this case, that some respondents became agitated by the repetition of attributes in the different choice sets. Respondents would very seldom ask that a certain attribute be explained to them, as they were confident in their understanding of the attribute. However, most respondents responded well when the BWS method was explained. In some cases, respondents preferred that the questionnaire should be filled out for them

Table 3 Final list of attributes

| Attribute | Descriptive Question |
|--|---|
| Travel Delays | Are there frequent delays when you travel? |
| Overcrowding | Is there overcrowding/overloading? |
| Personal Safety (mugging/abuse) | Is there criminal activity such as mugging, assault, or abuse that makes you feel unsafe using the transport? |
| Availability | Is transport readily available and in operation during the course of the week? |
| Frequency (waiting time) | Do you have to wait long for the transport? |
| Unsafe Driving | Do you have experience of unsafe/dangerous driving when using road-based public transport? |
| Travel Costs | Are public transport fares affordable? |
| Protest Action (strikes) | Do strikes/protests often affect normal operations of public transport? |
| Unclean Conditions | Is public transport clean and/or comfortable? |
| Walking Distance (to/from access point) | Is access to public transport far? |
| Walking Experience/Safety (to/from access point) | Do you feel unsafe or uncomfortable when accessing public transport? |
| Lack of Disability Services | Are disabled people struggling to use the transport? |
| Traffic Congestion/Jams | Is there frequently congestion when travelling with the road-based public transport? |

while they provided the relevant answers. This procedure seemed to be more effective, as the inferences from the respondents' own interpretation of the study were reduced, making the responses more consistent. Lessons learned from the pilot survey were incorporated in the final BWS questionnaire design and survey approach.

Table 3 shows the final attribute list for the study, which comprises questions around public transport use as well as access conditions. Most attributes are self-explaining. Walking Safety for example refers to how safe a respondent feels when walking to the public transport stop, whilst Personal Safety refers to how safe a person feels whilst using the mode of public transport. All terms were, however, explained to each respondent prior to the completion of the survey.

BWS survey design

In the BWS survey, participants choose their 'most concerning' and 'least concerning' feature related to the use of and access to public transport. The features presented were negative challenges related to the use of the various public transport modes used by participants and made up the BWS list of attributes. In choosing a feature as 'most concerning', the participant acknowledged that the challenge in question was significantly troubling or unsettling. Conversely, in choosing a feature as 'least concerning',

the participant acknowledged that the challenge experienced was insignificantly troubling or insignificantly unsettling relative to the other attributes.

BWS choice set generation and design

Sawtooth Software Inc (SSI) implements a BIBD BWS survey design and was used to develop the BWS choice sets. The following additional considerations compared to the five listed before were considered when determining the choice sets:

- A maximum of four items per choice set to avoid choice task fatigue
- Each item appears at least three times per survey, following a recommendation by Peitz and McEwan (2016).

Equation 1 was used to determine the number of choice sets (*tasks*) for the BWS design:

$$\frac{\text{tasks} \times \text{size}}{\text{items}} = r, \text{ with } r \geq 3 \quad (1)$$

With a task size of four items (*size*) per choice set, 13 items (*items*) in total, and a minimum repetition of three times per survey, a minimum of 10 choice sets (*tasks*) had to be generated, all in accordance with the BIBD principles. The final design is depicted in Appendix A on page 50.

BWS analysis

XLSTAT software was then used to analyse the BWS data. So-called raw scores were

calculated by subtracting the number of times an item has been chosen as the worst (least concerning) choice from the number of times the same item has been chosen as the best (most concerning) choice. Equation 2 shows how the raw scores are obtained:

$$\mathcal{O}_i = B_i - W_i \quad \forall i \in I \quad (2)$$

where \mathcal{O}_i is the raw score (per item i), B is the number of times an item i is chosen as best (most important/concerning), and W is the number of times an item i is chosen as worst (least important/concerning). The set of items is depicted as I .

The raw scores are then converted to average B-W scores $\tilde{\mathcal{O}}_{av,i}$ by dividing the raw score of an item by the number of respondents R and the number of times each item appeared in the choice sets, r :

$$\tilde{\mathcal{O}}_{av,i} = \frac{\mathcal{O}_i}{R \times r} \quad \forall i \in I \quad \text{with } r = 3. \quad (3)$$

The conversion of the raw scores to $\tilde{\mathcal{O}}_{av,i}$ helps to simplify the interpretation of the results on an interval scale $[+1.0 \dots -1.0]$. The items chosen as best (most concerning) more than they have been chosen as worst (least concerning) will have a value $\tilde{\mathcal{O}}_{av,i} > 0$. Conversely, the items chosen as worst (least concerning) more than they have been chosen as best (most concerning) will have a value $\tilde{\mathcal{O}}_{av,i} < 0$.

An item with a score of 1.0 is higher (more important) than an item with a score of 0.5, for example. But, when interpreting these scores, it cannot be said that the item with a score of 1.0 is twice as preferred as an item with a score of 0.5. To do that, the raw scores $\tilde{\mathcal{O}}_{av,i}$ first have to be transformed to a positive probability scale that supports ratio operations, which is discussed next. In literature, the $\tilde{\mathcal{O}}_{av,i}$ scores are also referred to as utility scores.

There are a number of ways to transform scores from a discrete choice experiment (such as this BWS study) into comparable utility scores – see Green *et al* (2001). Of the different methods in BWS surveys, the one mostly used is the Hierarchical Bayes method. The Hierarchical Bayes method is a hierarchical model using Bayesian statistics to create individual utilities for each respondent. A description of the method is beyond the scope of this paper, but the reader is referred to Howell (2009) or Gustafsson *et al* (2003) for a review of Hierarchical Bayes applied in

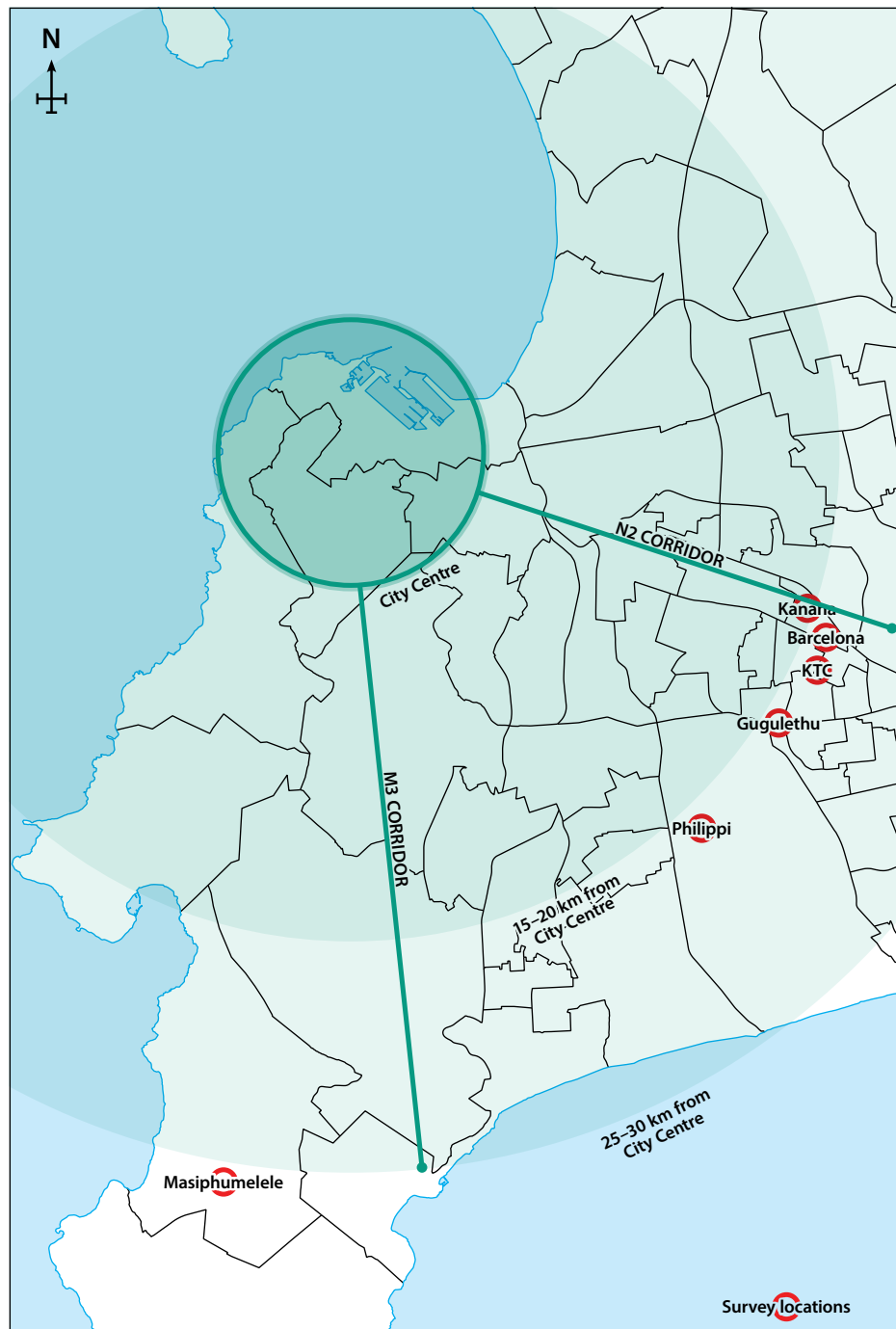


Figure 1 Locations of surveyed informal settlements (Data source: City of Cape Town Open Data Portal Map (2016))

choice modelling. Both SSI and XLSTAT have implemented Hierarchical Bayes routines to get the utility scores $\tilde{\mathcal{O}}_{av,i}$.

Survey

The actual survey was conducted in six informal settlements situated in the Southern Peninsula, Cape Flats and Mitchells Plain districts of Cape Town. All six settlements were chosen based on their proximity to township areas with developed public transport infrastructure, including taxi ranks, bus terminals and train stations, as well as their closeness to high-volume transport corridors connecting the city centre. Five informal

settlements are situated along the N2 freeway corridor and the Metrorail central line, both carrying high volumes of public transport commuters to and from the urban business centres. The other informal settlement is situated in the Southern Peninsula along another high-volume corridor (the M3, Main Road and the Metrorail Southern Suburbs line). The informal settlements sampled were (1) Gugulethu, (2) Kanana, (3) Barcelona, (4) KTC and (5) Philippi in the Cape Flats and Mitchells Plain area, and (6) Masiphumelele in the Southern Peninsula. Figure 1 indicates the locations of the six informal settlements relative to the high-volume corridors.

Ethics approval was obtained from the University of Cape Town. The objective was to obtain a minimum of 50 participants from each settlement. In total 334 participants across the six settlements were finally recruited. Initial questions included age, location of residence, occupation and regular mode of transport they use. Eventually, 44 of the questionnaires were omitted, due to crucial missing information or because respondents were not living in the area, leaving 2 900 (290×10 choice sets) useable responses for the BWS analysis. The selection of respondents across the locations was done using a gender-stratified sampling during weekdays, targeting a 50/50% split between men and women. There were always three to five trained surveyors in each area. The surveyors would split into opposite directions to conduct door-to-door surveys, interviewing one individual who was at least 18 years of age per household. Surveyors would systematically approach every third dwelling in a street or the following house in case of no response or when none of the qualifying household members were willing to participate. In some informal settlements, particularly in Masiphumelele, the main roads were replete with pedestrian thoroughfare. Surveyors would take advantage of this by conducting the interviews along the length of the road, approaching pedestrians (of 18 years and older) in each stratum (male/female), in addition to the systematic sampled door-to-door surveys, until meeting their quota. We are confident that this way the sample is representative enough to infer lessons about public transport needs of informal settlement dwellers.

RESULTS

Sample statistics

In total, 51% of the 290 respondents were female, close to the target strata of 50%. This suggests that the overall result will not have a gender bias. There was a larger disparity in the percentage respondents with respect to age groups. Most participants were young (aged 18–34) and made up 65% of the total respondents (~28% of the South African population is in this age group (Statistics SA 2013d)). The middle-agers (35–54) made up 32% (against ~22% in South Africa (Statistics SA 2013d)) of the total respondents, followed by the senior citizens at 3% (against ~12% of the South African population (Statistics SA

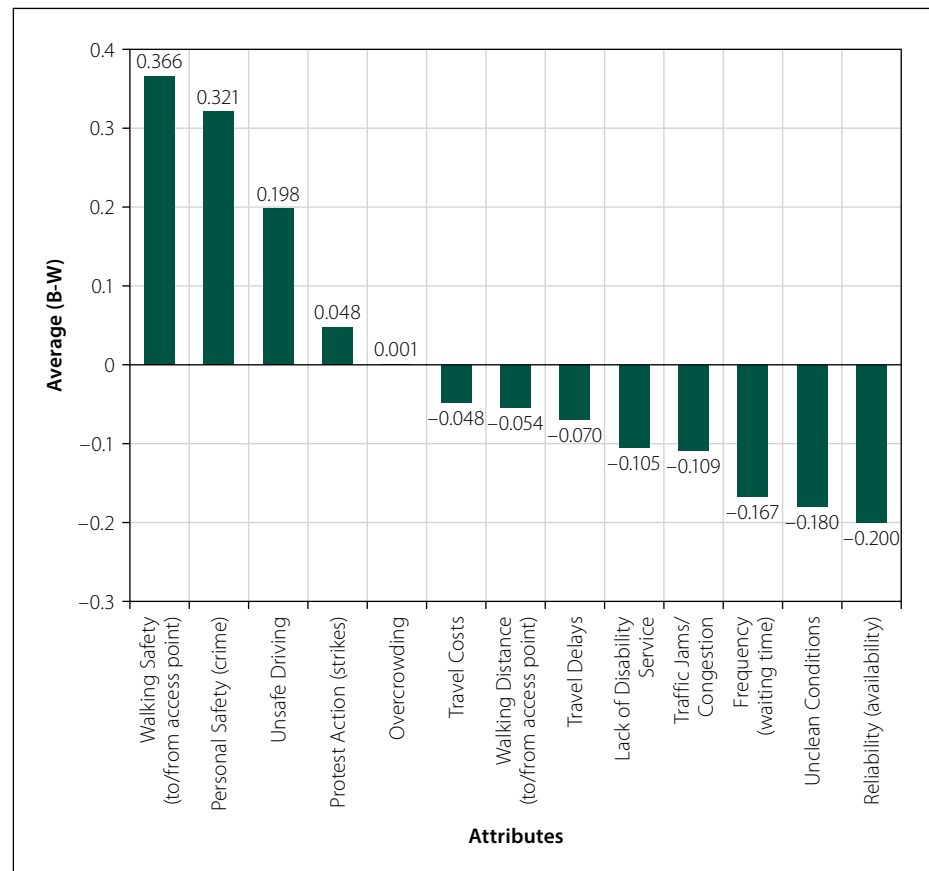


Figure 2 Average B-W scores ($\tilde{\varnothing}_{av,i}$) for overall PTE

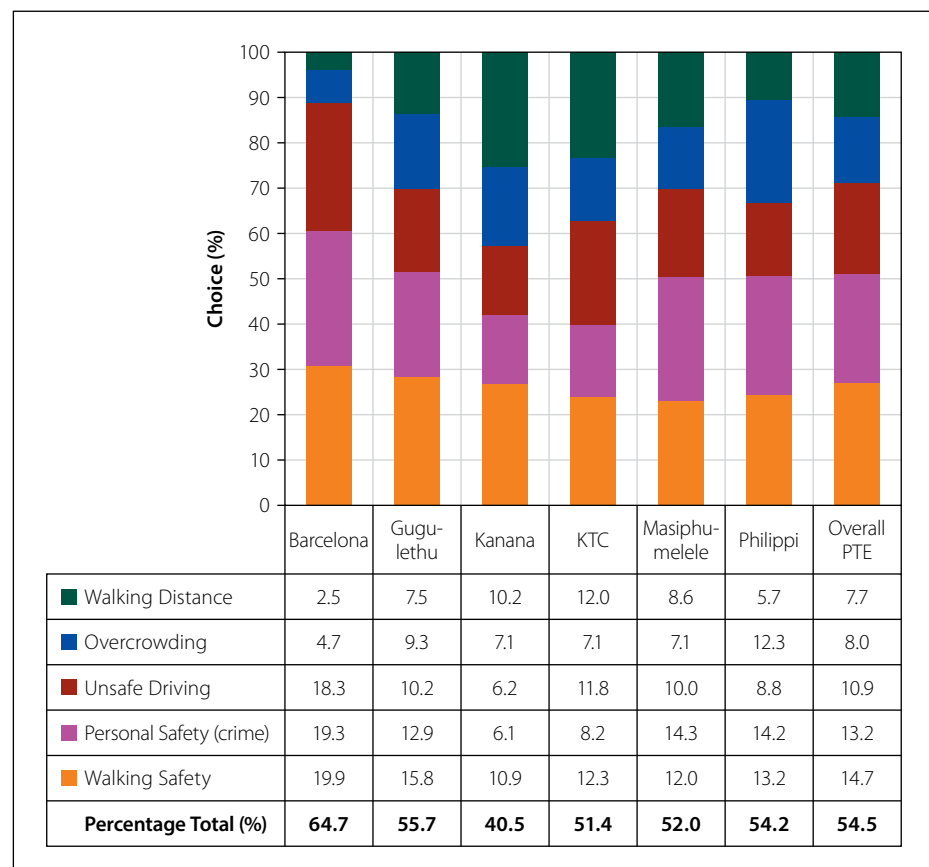


Figure 3 The top five most concerning choices for overall PTE in the various areas

2013d)). Only in three of the six informal settlements senior citizens (age ≥ 55 years) participated. The analysis may therefore have a bias towards the youth.

Most of the respondents in the sample are from the Kanana informal settlement making up 19% of the participants. This is followed by Philippi, Barcelona and

Table 4 One-way ANOVA table showing the variance in means between areas for each attribute, $\alpha = 0.05$

| Source of variation | | SS | df | MS | F | P-value | F crit. | α |
|--|----------------|-----------|-----|----------|-------|----------|---------|----------|
| Walking Safety (to/from access point) | Between groups | 2 705.28 | 5 | 541.06 | 80.22 | < 0.0001 | 2.25 | 0.05 |
| | Within groups | 1 915.53 | 284 | 6.74 | | | | |
| Travel Costs | Between groups | 5 294.03 | 5 | 1 058.81 | 34.63 | < 0.0001 | 2.25 | 0.05 |
| | Within groups | 8 683.60 | 284 | 30.58 | | | | |
| Personal Safety (crime) | Between groups | 5 779.36 | 5 | 1 155.87 | 31.43 | < 0.0001 | 2.25 | 0.05 |
| | Within groups | 10 443.95 | 284 | 36.77 | | | | |
| Walking Distance (to/from access point) | Between groups | 2 820.11 | 5 | 564.02 | 27.10 | < 0.0001 | 2.25 | 0.05 |
| | Within groups | 5 911.19 | 284 | 20.81 | | | | |
| Frequency (waiting time) | Between groups | 1 709.21 | 5 | 341.84 | 22.29 | < 0.0001 | 2.25 | 0.05 |
| | Within groups | 4 354.90 | 284 | 15.33 | | | | |
| Travel Delays | Between groups | 1 804.23 | 5 | 360.85 | 22.29 | < 0.0001 | 2.25 | 0.05 |
| | Within groups | 4 597.67 | 284 | 16.19 | | | | |
| Unclean Conditions | Between groups | 2 960.17 | 5 | 592.03 | 19.58 | < 0.0001 | 2.25 | 0.05 |
| | Within groups | 8 585.51 | 284 | 30.23 | | | | |
| Availability | Between groups | 738.81 | 5 | 147.76 | 19.29 | < 0.0001 | 2.25 | 0.05 |
| | Within groups | 2 175.68 | 284 | 7.66 | | | | |
| Unsafe Driving | Between groups | 4 270.25 | 5 | 854.05 | 19.21 | < 0.0001 | 2.25 | 0.05 |
| | Within groups | 12 627.37 | 284 | 44.46 | | | | |
| Protest Action (strikes) | Between groups | 2 121.49 | 5 | 424.30 | 15.28 | < 0.0001 | 2.25 | 0.05 |
| | Within groups | 7 887.89 | 284 | 27.77 | | | | |
| Overcrowding | Between groups | 1 664.14 | 5 | 332.83 | 10.61 | < 0.0001 | 2.25 | 0.05 |
| | Within groups | 8 906.46 | 284 | 31.36 | | | | |
| Lack of Disability Service | Between groups | 916.44 | 5 | 183.29 | 10.37 | < 0.0001 | 2.25 | 0.05 |
| | Within groups | 5 018.91 | 284 | 17.67 | | | | |
| Traffic Jams/ Congestion | Between groups | 483.36 | 5 | 96.67 | 2.79 | 0.0176 | 2.25 | 0.05 |
| | Within groups | 9 834.21 | 284 | 34.63 | | | | |

KTC with 17% of the participants coming from each of these areas. Gugulethu and Masiphumelele make up 16% and 14% of the participants respectively. The proportion of the participants, with respect to location, is thus relatively balanced.

In total, 46% of the total respondents are taxi users. This is followed by bus and train users at 30% and 24% respectively, while less than 1% of respondents are MyCiti (BRT) users. This data is consistent with 'Cape Town's Transport Picture 2015', which revealed that transport users of minibus taxis, buses and trains make up 44%, 33% and 23% of these forms of public transport respectively (Transport for Cape Town 2013). Furthermore, 58% of bus users are male and 56% of taxi users are female.

Area-based public transport experience

The following results are derived from the 2 900 responses from the 290 qualifying surveys. Figure 2 gives the overall average B-W scores, $\bar{Q}_{av,i}$, following Equation 3.

Walking Safety has the highest average B-W score, while Availability comes out with the lowest average B-W score.

The results of the top five most concerning utility scores ($\bar{Q}_{av,i}$) are shown for each of the choice clusters in Figure 3, and can be compared ordinally between areas. The most concerning clusters are summarised in 'percentage stacked column' graphs to compare, on a scale of one to 100%, i.e. the performance of these attributes in the various locations/study areas. Figure 3 identifies that Walking Safety, Personal Safety, Unsafe Driving, Overcrowding and Walking Distance are the top five most concerning features in the various areas. Walking Safety is the most concerning attribute, with an average utility score of 14.7%. This means that, overall, Walking Safety is seen as almost twice as important as Walking Distance. Walking Safety, Personal Safety and Unsafe Driving are most concerning in Barcelona, scoring 19.9%, 19.3% and 18.3% respectively. Overcrowding is most concerning

in Philippi with a utility score of 12.3%. Finally, Walking Distance is most concerning in KTC, which scored 12.0%.

Summing these top five features in the overall study generates a score of 54.5%, meaning that the other eight features contribute 45.5% to the total importance, illustrating their relative insignificance. Figure 3 also shows that these five features are of greater concern in Barcelona where they scored an overall BWS mean value of 64.7%, whereas in Kanana these features scored 40.5% cumulatively. Overall, the least concerning features include Availability and Frequency which scored 3.3% and 4.3% respectively, in line with the results in Figure 2.

Next, a one-way ANOVA test was conducted to test the variance of means for each of the attributes between the six informal settlements. First, Table 4 shows that for all the attributes, the p -values are much lower than the significance level, $\alpha = 0.05$, with the smallest difference being in Traffic Jams/Congestion, which has a p -value of 0.018. The null hypothesis (that

there is no difference between means) is thus rejected in all cases, i.e. there are significant differences in the perceptions of importance of PTE attributes between the six informal settlements

Figure 4 shows the top five most concerning features between users of different modes across the locations. For bus users Walking Safety comes out as the most concerning attribute, with a scoring of 16% on average, while Unsafe Driving was the most concerning attribute for taxi drivers, scoring 14.6%. For train users Personal Safety was most concerning with a score of 13.9%. Walking Safety was the second most concerning attribute for both taxi and train users, scoring 13.6% and 13.2% respectively. For bus users this is Unsafe Driving.

Further statistical tests (not shown here) revealed that, in general, between the different modes, for each attribute, the p -values are lower than the significance level, $\alpha = 0.05$. The null hypothesis (that there is no difference between means) is thus rejected in most cases, i.e. there are significant differences in the perceptions of importance of PTE attributes between the different modes. However, perceptions around Personal Safety, Travel Costs, Unclean Conditions and Walking Distance are found to be similar between taxi and train users. Similarly, train and bus users

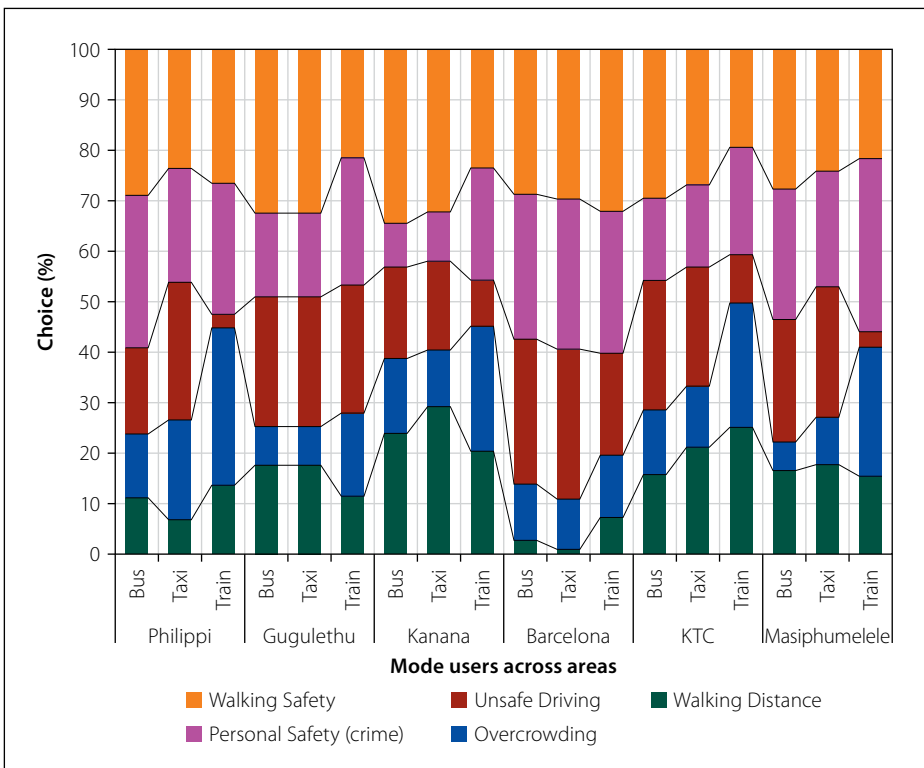


Figure 4 The top five most concerning choices for overall PTE between different mode users across the areas

feel similarly about Lack of Disability Service, Overcrowding, Personal Safety, Unclean Conditions and Walking Distance. Finally, taxi and bus users are equally concerned about Personal Safety, Unclean Conditions and Unsafe Driving.

Gender-based public transport experience

Figure 5 gives the overall average B-W scores for the 290 respondents, arranged such that the scores of men and women can be compared. For women, personal

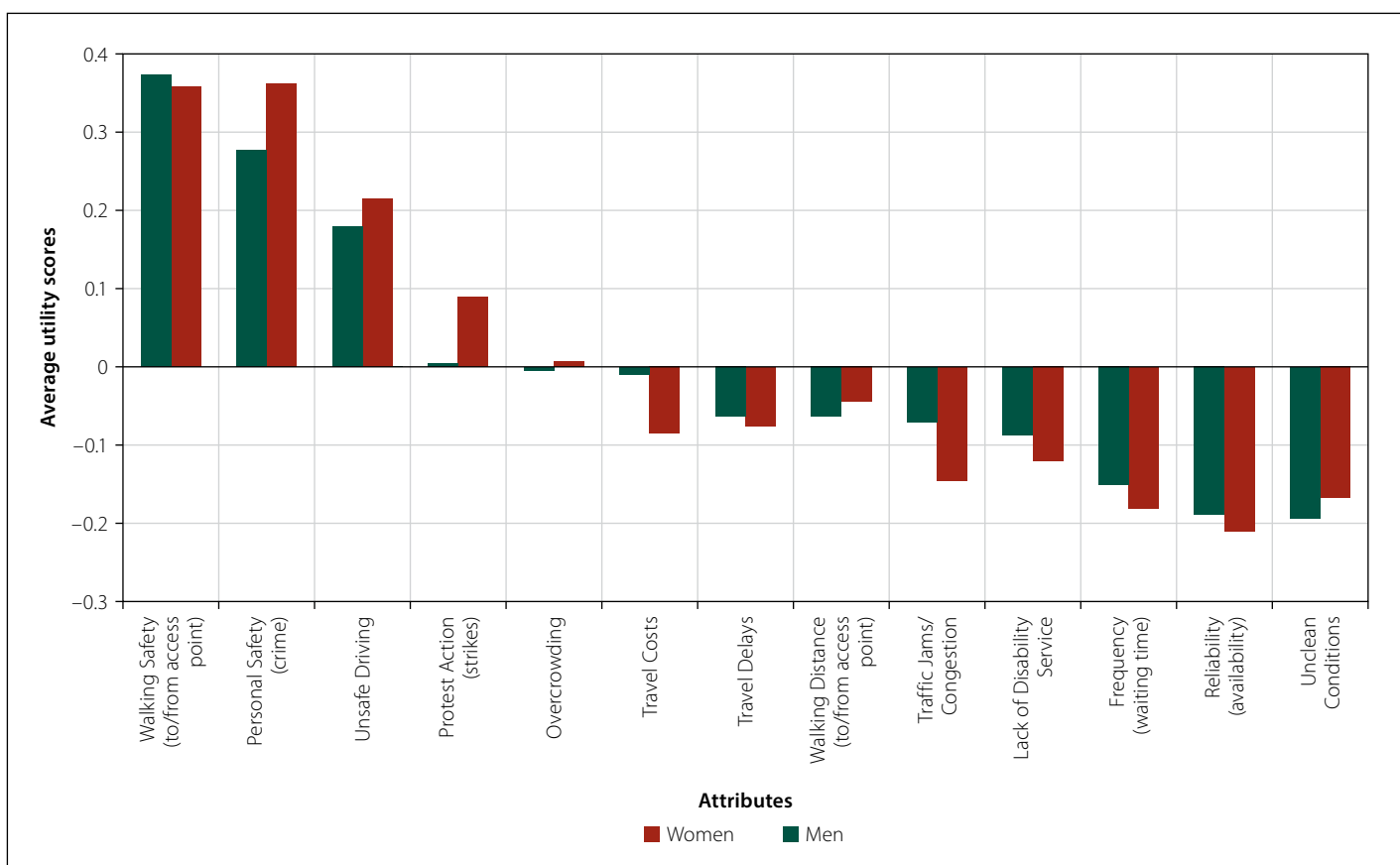


Figure 5 Average utility scores ($\bar{o}_{av,i}$) comparing men and women's PTE

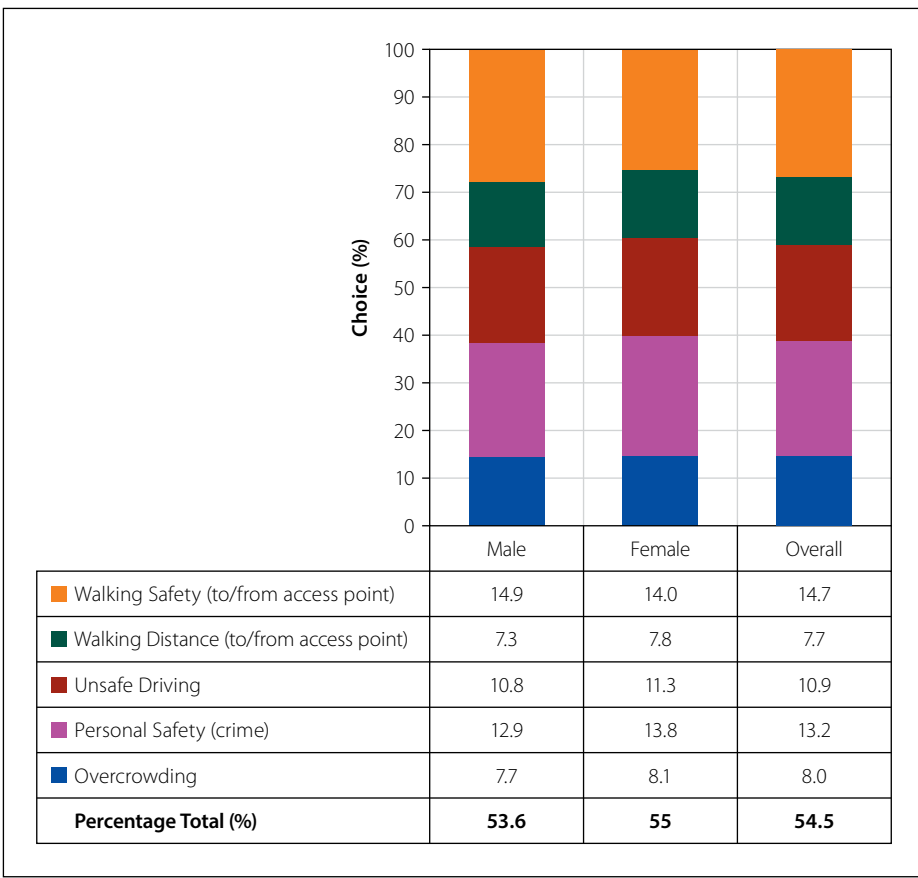


Figure 6 The top five most concerning choices for men, women and the overall PTE

safety has the highest average B-W score, while availability has the lowest average B-W score. For men, Walking Safety has the highest average B-W score, while Unclean Conditions has the lowest average B-W score.

Figure 6 shows the top five choice clusters for men, women and overall. The most concerning features are Walking

Safety, Personal Safety, Unsafe Driving, Overcrowding and Walking Distance, with Walking Safety being the most concerning attribute for both men and women. Walking Safety is more concerning for men (14.9%) than women (14.0%), while Personal Safety on public transport is more important for women (13.8%) than men (12.9%).

Finally, Table 5 shows the results of the two-sample *T*-test comparing the means of all attributes between men and women. The null hypothesis was set as there being no difference between the means. Overall there was little variance in the means of choices between men and women. The only significant variances found, where the *p*-value is less than the significance level $\alpha = 0.05$, were in the means of Frequency (waiting time), Protest Action (strikes) and Traffic Jams (congestion). These attributes are all relatively unimportant, as none of them are of the top five most important attributes. Hence it can be said that there is no significant difference in the perception of importance of PTE attributes between men and women in the surveyed informal settlements.

DISCUSSION

From the results we can surmise that Walking Safety, Personal Safety, Unsafe Driving, Overcrowding and Walking Distance are the most concerning features for the overall PTE. These features make up the most concerning choice cluster with a cumulative BWS mean value of 55%. Walking Safety to access public transport is consistently the most concerning in all the locations, with scores ranging from 12% (Masiphumelele) to 20% (Barcelona). The least concerning features across all locations have been identified as Availability and Frequency. It is assumed that, because of the multiplicity of minibus taxis, travellers assume a readily available minibus

Table 5 T-test describing variance of means between men and women for each attribute, $\alpha = 0.05$

| Attribute | T-test for equality of means | | | | | |
|---|------------------------------|--------------------|---------------------|-----|----------------------|----------|
| | Difference | t (Observed value) | t (Critical value) | DF | p-value (Two-tailed) | α |
| Frequency (waiting time) | -0.867 | -2.065 | 1.968 | 288 | 0.040 | 0.05 |
| Lack of Disability Service | -0.426 | -0.924 | 1.968 | 288 | 0.356 | 0.05 |
| Overcrowding | 0.460 | 0.712 | 1.968 | 288 | 0.477 | 0.05 |
| Personal Safety (crime) | 0.919 | 0.938 | 1.968 | 288 | 0.349 | 0.05 |
| Protest Action (strikes) | 1.225 | 2.159 | 1.968 | 288 | 0.032 | 0.05 |
| Availability | 0.393 | 1.453 | 1.968 | 288 | 0.147 | 0.05 |
| Traffic Jams/Congestion | -1.287 | -2.300 | 1.968 | 288 | 0.022 | 0.05 |
| Travel Costs | 0.233 | 0.312 | 1.968 | 288 | 0.755 | 0.05 |
| Travel Delays | -0.814 | -1.673 | 1.968 | 288 | 0.095 | 0.05 |
| Unclean Conditions | 0.003 | 0.005 | 1.968 | 288 | 0.996 | 0.05 |
| Unsafe Driving | 0.477 | 0.520 | 1.968 | 288 | 0.603 | 0.05 |
| Walking Distance (to/from access point) | 0.556 | 0.995 | 1.968 | 288 | 0.321 | 0.05 |
| Walking Safety (to/from access point) | -0.871 | -1.888 | 1.968 | 288 | 0.060 | 0.05 |

taxi, and thus availability is seen as least concerning, despite the service quality and delivery levels.

All the attributes seem to have significant variance across the different locations. Personal Safety for example ranges from 6% (Kanana) to 19% (Barcelona), while Unsafe Driving ranges from 6% (Kanana) to 18% (Barcelona), Overcrowding ranges from 5% (Barcelona) to 12% (Philippi), and finally Walking Distance ranges from 3% (Barcelona) to 12% (KTC).

The differences between mode users are less pronounced, with some attributes differing significantly between the modes, such as frequency and travel delays, and some attributes being of concern to all mode users, such as personal safety and unclean conditions.

Combining these findings there are obviously differences between mode users in the different areas, for example Walking Safety for minibus taxi users ranges from 11.9% in KTC to 3.9% in Philippi. For train users Travel Delays range between 12% in Masiphumelele to 4.1% in Barcelona. Nevertheless, for certain attributes, regardless of area and mode, there will be similarities in perception. Analysis shows that the context of actual realities on the ground is a driving factor in people's perception of public transport experience. It is thus important to make site-specific considerations when designing any public transport infrastructure in informal settlements.

As illustrated in Figure 5 and 6, Walking Safety, Personal Safety, Unsafe Driving and Overcrowding have all been regarded as most concerning in the same order of importance by both women and men. Attributes pertaining to safety (Walking Safety and Personal Safety) are the two most concerning for men and women and make up 27.8% of the overall importance. For comparison's sake, a combination of the next two most concerning features, Unsafe Driving and Overcrowding, makes up only 19%.

The only distinct difference in choices between men and women concerns Frequency (waiting time), Protest Action (strikes) and Traffic Jams (congestion). Men considered congestion slightly more concerning than women did, with the former having a score of 7.3% and women having a score of 6%. Women viewed Protest Action more important than men did, with the former having a score of 7.8% and men having a score of 6.5%. This can be explained by the known gender differences between

men and women when it comes to risk perception and risk taking (for a meta-study on this see Byrnes *et al* (1999)). Finally, men found Frequency more important than women, with the latter having a score of 4% and the former having a score of 4.8%.

CONCLUSIONS AND RECOMMENDATIONS

This paper implemented the BWS technique using Case 1 type of analysis and a BIBD survey design to obtain meaningfully comparable data regarding public transport priority needs of people living in informal settlements around Cape Town. The attributes used were based on literature, conversations in the community and with students of the University of Cape Town and Thandokhulu High School in Cape Town. Interviews were conducted with 334 participants in total across six informal settlements in Cape Town. The data of the interviews was analysed using the Hierarchical Bayes clustering routine provided by XLSTAT to make useful comparisons of the most important attributes ascertained by the BWS survey. An ANOVA table was then generated to ascertain whether there was significant variance in the means of the results generated for each attribute between each area. Statistical tests were conducted to assess whether there are significant differences in perceptions of attribute importance between men and women.

The study found that Walking Safety, Personal Safety, Unsafe Driving, Overcrowding and Walking Distance are, overall, the most concerning features for public transport users in the informal settlements surveyed. The least concerning features across all locations have been identified as Availability and Frequency. In addition, there is no apparent trend in the variance between the choices of men and women. Yet, there is significant variance across the different locations, and generally there is significant variance between mode users.

Walking Safety is considerably and consistently important across all the locations and genders. Personal Safety during the use of public transport is of high importance for both genders, and across all locations. Walking Safety and Personal Safety are highly important, but relate to two different settings. Walking Safety relates to a respondent's environment when accessing the public transport, and

Personal Safety relates to a respondent's environment whilst using the public transport. Their high importance reflects daily anxieties that plague both men and women in the informal settlements surveyed, posing the question: are both the public transport user's walking safety to and from the infrastructure and the user's safety on board the public transport the responsibility of the transport authority? Thus, a complementary study would be one that investigates the pedestrian experience of a traveller's commute with regard to his/her safety.

With Availability and Frequency of public transport having a low perceived importance, while Unsafe Driving and Overcrowding have a much higher perceived importance, it seems that travellers are easily able to find a means of transport, but are unhappy with the quality of service being provided. Pertinent to the argument of Mahapa and Mashiri (2001), it is clear from the results that all informal settlements are unique, as there are significant differences in the results obtained from different areas. Infrastructure interventions must thus be case-sensitive to be effective.

From a methodological perspective, this paper demonstrates the ability of the BWS technique to yield clear and accessible data regarding public transport priorities for people living in informal settlements. This research has room for expansion, however, as a larger sample size would generate data that is perhaps more statistically representative. The research could also be spatially compressed, as it could be useful to generate a larger sample size from just three informal settlements to allow for more effective comparisons regarding which attributes are more important and why. Alternatively, a survey could be implemented that targets specific age groups to facilitate design that cater for the most vulnerable in terms of age. The attributes used for this study might not include all features that are important for public transport users – further studies could be done to nominally understand the transport needs of the urban poor, before assessing them in terms of priority. Furthermore, a complementary survey could focus on the pedestrian experiences of public transport users in informal settlements. A final recommendation is to implement further analysis regarding variance in modal choice in the six informal settlements.

This study proves that the BWS technique can be an effective tool for rating and

ranking preferences in the civil engineering domain and provides an opportunity for more studies of this nature to be conducted. The research has also shown that the BWS method can be an effective way to engage with communities to understand their prioritised areas of needs and to identify specific areas of concern.

REFERENCES

- Beck, M J & Rose, J M 2016. The best of times and the worst of times: A new best-worst measure of attitudes toward public transport experiences. *Transportation Research Part A – Policy and Practice*, 86: 108–123.
- Beck, M J, Rose, J M & Greaves, S P 2016. I can't believe your attitude: A joint estimation of best worst attitudes and electric vehicle choice. *Transportation*, 44(4): 753–772.
- Behrens, R & Del Mistro, R 2010. Shocking habits: Methodological issues in analyzing changing personal travel behavior over time. *International Journal of Sustainable Transportation*, 4(5): 253–271.
- Behrens, R & Schalekamp, H 2010. Public transport mode satisfaction in Cape Town: Findings of a passenger intercept survey. *Proceedings, 29th Southern African Transport Conference, 18–19 August, Pretoria*, pp 733–748.
- Beirão, G & Sarsfield Cabral, J A 2007. Understanding attitudes towards public transport and private car: A qualitative study. *Transport Policy*, 14(6): 478–489.
- Bettman, J R, Johnson, E J & Payne, J W 1990. A componential analysis of cognitive effort in choice. *Organizational Behavior and Human Decision Processes*, 45(1): 111–139.
- Byrnes, J P, Miller, D C & Schafer, W D 1999. Gender differences in risk taking: A meta-analysis. *Psychological Bulletin*, 125(3): 367–383.
- Chrzan, K & Peitz, M 2015. Advanced MaxDiff Topics. *Sawtooth Software Webinar*. Available at: <https://www.sawtoothsoftware.com/.../webinars/1606-webinar-advanced-maxdiff-topics>.
- Del Mistro, R & Behrens, R 2015. Integrating the informal with the formal: An estimation of the impacts of a shift from paratransit line-haul to feeder service provision in Cape Town. *Case Studies on Transport Policy*, 3(2): 271–277.
- de Oña, J & de Oña, R 2014. Quality of service in public transport based on customer satisfaction surveys: A review and assessment of methodological approaches. *Transportation Science*, 49(3): 605–622.
- Department of Transport (South Africa) 1996. *National Transport Policy White Paper*. Available at: <http://www.gov.za/documents/National-transport-policy-white-paper>.
- Donoso, P, Munizaga, M & Rivera, J 2013. Measuring user satisfaction in transport services: methodology and application. In: Zmud, J. (Ed.), UK, *Transport Survey Methods: Best Practice for Decision Making*, Bingley, UK: Emerald Group, 603–623.
- Efthymiou, D & Antoniou, C 2017. Understanding the effects of economic crisis on public transport users' satisfaction and demand. *Transport Policy*, 53: 89–97.
- Ferro, P S & Golub, R B A 2012. Planned and paratransit service integration through trunk and feeder arrangements: An international review. *Proceedings, 31st Southern African Transport Conference, 8–11 July, Pretoria*, pp 604–618.
- Ferro Salazar, P & Behrens, R 2015. From direct to trunk-and-feeder public transport services in the urban south: Territorial implications. *Journal of Transport and Land Use*, 8(1): 123–136.
- Flynn, T N & Marley, A A J 2014. Best worst scaling: Theory and methods. In Hess, S (Ed.), *Handbook of Choice Modelling*, 178–199. Available at: <https://www.unisa.edu.au/Global/business/centres/i4c/docs/papers/wp12-002.pdf> [accessed on 4 May 2017].
- Golub, A, Balassiano, R, Araújo, A & Ferreira, E 2009. Regulation of the informal transport sector in Rio de Janeiro, Brazil: Welfare impacts and policy analysis. *Transportation*, 36(5): 601–616.
- Green, P E, Krieger, A M & Wind, Y 2001. Thirty years of conjoint analysis: Reflections and prospects. *Interfaces*, 31(3): 56–73.
- Guiver, J W 2007. Modal talk: Discourse analysis of how people talk about bus and car travel. *Transportation Research Part A: Policy and Practice*, 41(3): 233–248.
- Gustafsson, A, Herrmann, A & Huber, F (Eds.) 2003. *Conjoint Measurement : Methods and Applications*. Dordrecht, Germany: Springer. Available at: https://books.google.co.za/books?id=meQFCAAAQBAJ&dq=hierarchical+bayes+conjoint+analysis&lr=&source=gbs_navlinks_s [accessed on 8 May 2017].
- Hess, S & Daly, A J 2014. *Handbook of Choice Modelling*, 1st ed. Cheltenham, UK: Edward Elgar. Available at: <http://www.e-elgar.com/shop/eep/preview/book/isbn/9781781003152> [accessed on 4 May 2017].
- Hinz, O, Schlereth, C & Zhou, W 2015. Fostering the adoption of electric vehicles by providing complementary mobility services: A two-step approach using best-worst scaling and dual response. *Journal of Business Economics*, 85(8): 921–951.
- Howell, J R 2009. CBC/HB for Beginners. *Sawtooth Software–Research Paper Series*, 98382(360): 1–6.
- Louviere, J J, Flynn, T N & Marley, A A J 2015. *Best-Worst Scaling: Methods and Applications*. Cambridge, UK: Cambridge University Press.
- Lucas, K 2011. Making the connections between transport disadvantage and the social exclusion of low income populations in the Tshwane Region of South Africa. *Journal of Transport Geography*, 19(6): 1320–1334.
- Mahapa, S M & Mashiri, M 2001. Social exclusion and rural transport: Gender aspects of a road improvement project in Tshitwe, Northern Province. *Development Southern Africa*, 18(3): 365–376.
- Paulhus, D L 1991. Measurement and control of response bias. In Robinson, J P, Shaver, P R, Wrightsman, L S & Andrews, F M (Eds), *Measures of Personality and Social Psychological Attitudes*, San Diego, CA, 17–59.
- Peitz, M & McEwan, B 2016. An Introduction to Max Diff. *Sawtooth Software Webinar*. Available at: <https://www.sawtoothsoftware.com/.../webinars>.
- Potgieter, C-A, Pillay, R & Rama, S 2006. *Women, Development and Transport in Rural Eastern Cape, South Africa*. Cape Town: Human Sciences Research Council. Available at: <http://uloitopob.ru/hityq.pdf>.
- Sam, E F, Hamidu, O & Daniels, S 2017. SERVQUAL analysis of public bus transport services in Kumasi metropolis, Ghana: Core user perspectives. *Case Studies on Transport Policy*, 6(1): 25–31.
- Schalekamp, H & Behrens, R 2010. Engaging paratransit on public transport reform initiatives in South Africa: A critique of policy and an investigation of appropriate engagement approaches. *Research in Transportation Economics*, 29(1): 371–378.
- Statistics SA 2013a. *National Household Travel Survey February to March 2013*. Pretoria: Statistics South Africa, 1–179.
- Statistics SA 2013b. *Measuring household expenditure on public transport: In-depth analysis of the National Household Travel Survey 2013 data*. Pretoria: Statistics South Africa.
- Statistics SA 2013c. *Gender Series Volume III : Gender patterns in transport*. Pretoria, Statistics South Africa.
- Statistics SA 2013d. *Population Census 2011*. Pretoria: Statistics South Africa. Available at: <http://www.statssa.gov.za>.
- Transport for Cape Town 2013. Comprehensive Integrated Transport Plan 2013–2018. p 407. Available at: [http://www.tct.gov.za/docs/categories/1258/CTIP 2013-2018 \(20131112\)1.pdf](http://www.tct.gov.za/docs/categories/1258/CTIP 2013-2018 (20131112)1.pdf).
- Wong, R C P, Szeto, W Y, Yang, L & Li, YC 2017. Elderly users' level of satisfaction with public transport services in a high-density and transit-oriented city. *Journal of Transport & Health*, 7(B): 209–217.

Please turn over for Appendix A

APPENDIX A

Which of the following public transport mode features most concerns you and which concerns you the least?

(1 of 10)

| Most Concerning | Feature | Least Concerning |
|-----------------|----------------------------|------------------|
| | Travel Delays | |
| | Overcrowding | |
| | Personal Safety (crime) | |
| | Reliability (availability) | |

(6 of 10)

| Most Concerning | Feature | Least Concerning |
|-----------------|---|------------------|
| | Protest Action (strikes) | |
| | Unclean Conditions | |
| | Walking Distance (to/from access point) | |
| | Walking Safety (to/from access point) | |

(2 of 10)

| Most Concerning | Feature | Least Concerning |
|-----------------|--------------------------|------------------|
| | Frequency (waiting time) | |
| | Unsafe Driving | |
| | Travel Costs | |
| | Protest Action (strikes) | |

(7 of 10)

| Most Concerning | Feature | Least Concerning |
|-----------------|----------------------------|------------------|
| | Personal Safety (crime) | |
| | Reliability (availability) | |
| | Frequency (waiting time) | |
| | Unsafe Driving | |

(3 of 10)

| Most Concerning | Feature | Least Concerning |
|-----------------|---|------------------|
| | Unclean Conditions | |
| | Walking Distance (to/from access point) | |
| | Walking Safety (to/from access point) | |
| | Lack of Disability Service | |

(8 of 10)

| Most Concerning | Feature | Least Concerning |
|-----------------|----------------------------|------------------|
| | Lack of Disability Service | |
| | Traffic Jams/Congestion | |
| | Travel Delays | |
| | Overcrowding | |

(4 of 10)

| Most Concerning | Feature | Least Concerning |
|-----------------|-------------------------|------------------|
| | Traffic Jams/Congestion | |
| | Travel Delays | |
| | Overcrowding | |
| | Personal Safety (crime) | |

(9 of 10)

| Most Concerning | Feature | Least Concerning |
|-----------------|---|------------------|
| | Travel Costs | |
| | Protest Action (strikes) | |
| | Unclean Conditions | |
| | Walking Distance (to/from access point) | |

(5 of 10)

| Most Concerning | Feature | Least Concerning |
|-----------------|----------------------------|------------------|
| | Reliability (availability) | |
| | Frequency (waiting time) | |
| | Unsafe Driving | |
| | Travel Costs | |

(10 of 10)

| Most Concerning | Feature | Least Concerning |
|-----------------|---------------------------------------|------------------|
| | Walking Safety (to/from access point) | |
| | Lack of Disability Service | |
| | Traffic Jams/Congestion | |
| | Travel Delays | |

Stormwater runoff quality on an urban highway in South Africa

A Robertson, N Armitage, M H P Zuidgeest

Roadway sediment and stormwater runoff were sampled from a 15 km section of the R300 freeway located in the greater Cape Town area, South Africa. Grab samples were collected over a four-month period in 2016 and analysed for metals, hydrocarbons and nutrients.

The metal concentration profiles were similar in sediment and runoff samples. The primary pollutants identified in the highway runoff were aluminium, copper, lead, manganese, nitrogen, phosphorus, zinc, total suspended solids (TSS), and oil and grease. The concentrations of each of these elements, barring lead, exceeded the national effluent water quality guidelines. Large volumes of macro pollutants such as cigarettes, plastic and packaging were also observed. The results of this research indicate that Sustainable Drainage Systems (SuDS) should be used in conjunction with highways, particularly where runoff may influence a sensitive or valuable aquatic ecosystem, as it can be a significant non-point source of pollution.

INTRODUCTION

Highway drainage presents a high risk of non-point source pollution when compared to other urban land use areas, introducing heavy metals, suspended solids and hydrocarbons to urban waterways (Ellis *et al* 2012). The composition and volume of contaminants depend on a variety of factors, such as climate, rainfall event intensity and duration, and traffic characteristics (Crabtree *et al* 2006). Whilst there is a large body of international work describing the impacts and water quality characteristics of highway runoff (Sartor *et al* 1974; Opher & Friedler 2010; Barbosa *et al* 2012), the profile and extent of pollution emanating from South African highways remain largely unknown.

Suspended solids are the most common constituent in highway runoff (Kayhanian *et al* 2007). Fine suspended particles (<200 µm) transport pollutants such as heavy metals and hydrocarbons, and account for a large portion of the overall pollution potential (Sartor *et al* 1974; Vaze & Chiew 2002). Several studies report a strong correlation between total suspended solids and heavy metal concentrations (Shinya *et al* 2000; Han *et al* 2006; Desta *et al* 2007).

Copper, iron, lead and zinc are the most commonly reported heavy metals found in highway runoff waters (Opher & Friedler 2010). The concentration of lead has decreased worldwide with the introduction of unleaded fuel (Khan *et al* 2006), and current

reported values are approximately 10% of those reported prior to the 1970s (Opher & Friedler 2010). Other widely reported metals include cadmium, chromium, magnesium and nickel (Göbel *et al* 2007).

Organic matter such as oils and greases, volatile organic compounds (VOCs) and polycyclic aromatic hydrocarbons (PAHs) are a common constituent in highway runoff waters. Organic substances originate from vehicle fluids such as oils, fuel, brake fluid, wear and tear of rubber elements and engine emissions (Legret & Pagotto 1999).

Knowledge of pollutant concentrations in highway runoff is necessary to assess and control the impact of stormwater on the urban natural environment. Stormwater management in South Africa largely focuses on flow quantity management, with little, if any, consideration for environmental consequences (Armitage *et al* 2013). There are no national or provincial policies addressing pollutant removal from stormwater, leaving stormwater management to be regulated at a local level. The City of Cape Town, where this study was conducted, requires the treatment and attenuation of stormwater from developments within the city, and proposes Sustainable Drainage Systems (SuDS) as a means to achieve this (CSRM 2009).

Internationally, SuDS are recognised as best practice to realise holistic stormwater management (Marsalek & Chocat 2002). SuDS, also known as Low Impact Design



ABBY ROBERTSON works as a design and development engineer at BVi Consulting Engineers. She graduated with an MSc in Civil Engineering from the University of Cape Town in 2017. Her interests are in urban water management, sustainable drainage systems, and using Python to augment engineering design processes.

Contact details:

BVi Consulting Engineers
Block B2
Edison Square
corner Edison Way & Century Avenue
Century City
Cape Town 7441
South Africa
T: +27 21 527 7000
E: robertson.abby@gmail.com



PROF NEIL ARMITAGE Pr Eng, who is a Fellow of SAICE, is Professor in Water Engineering in the Department of Civil Engineering at the University of Cape Town (UCT). His main research interest is urban drainage. He led the team that developed the South African Guidelines for Sustainable Drainage Systems (SuDS), published by the Water Research Commission (WRC) of South Africa (TT 558/13, May 2013). He is Deputy Director of the 'Future Water' Research Institute at UCT.

Contact details:

Department of Civil Engineering
University of Cape Town
Private Bag X3
Rondebosch 7701
South Africa
T: +27 21 650 2589
E: neil.armitage@uct.ac.za



PROF MARK H P ZUIDGEEST is a member of SAICE, and is the SANRAL Chair of Transportation Planning and Engineering at the University of Cape Town. He graduated with an MSc (Civil Engineering) from the University of Twente, The Netherlands, in 1997, and a PhD from the Netherlands Research School for Transport, Infrastructure and Logistics (TRAIL) in 2005. His fields of interest include land use – transport systems analysis, with an emphasis on questions around sustainability, equity and accessibility.

Contact details:

Centre for Transport Studies
Department of Civil Engineering
University of Cape Town
Private Bag X3
Rondebosch 7701
South Africa
T: +27 21 650 4756
E: mark.zuidgeest@uct.ac.za

Keywords: highway runoff, heavy metals, pollutants, water quality, SuDS

(LIDs), Water Sensitive Urban Design (WSUD) and Best Management Practices (BMPs), are structural and process controls that attenuate surface flows and improve water quality by means of infiltration, filtration, adsorption, bioaccumulation and percolation *inter alia*. Examples of SuDS elements include swales (vegetated broad shallow channels), infiltration trenches (excavated pits that are filled with coarse aggregate and often lined with a geotextile) and constructed wetlands (Armitage *et al* 2013). The stormwater quantity and quality characteristics determine the type, size and number of SuDS elements required to manage stormwater to the desired standard.

The objectives of this study were to identify the primary contaminants in the R300 surface runoff, determine the range of concentrations of the primary contaminants, determine if there is a significant difference between the highway runoff quality and ambient levels of pollution, and to propose an appropriate stormwater management system in the context of the R300 freeway in Cape Town.

METHOD

The R300, a freeway in Cape Town that links National Roads N1 and N2, was chosen as an appropriate study site (Figure 1). Not only is this highway heavily trafficked – thus likely to demonstrate high stormwater pollutant levels – but it is operated and maintained by the South African National Roads Agency Limited (SANRAL), who funded this study and facilitated data collection.

Sediment and runoff were sampled from three locations on the freeway and one location of undeveloped land adjacent to the R300. The latter sample location was chosen as an environmental control site to distinguish between the ambient levels of contamination and the contaminants present due to road use activities. The sampling sites were distributed along a 15 km section of the freeway in order to mitigate localised effects. The samples were analysed for heavy metals, hydrocarbons and nutrients at an independent laboratory. Contaminants included aluminium, arsenic, cadmium, chromium, copper, lead, manganese, nickel, zinc, phosphorus, nitrogen, oils and grease, and total suspended solids (TSS). Additionally, various catchpits were monitored before and after rainfall events to identify the macro pollutants transported by

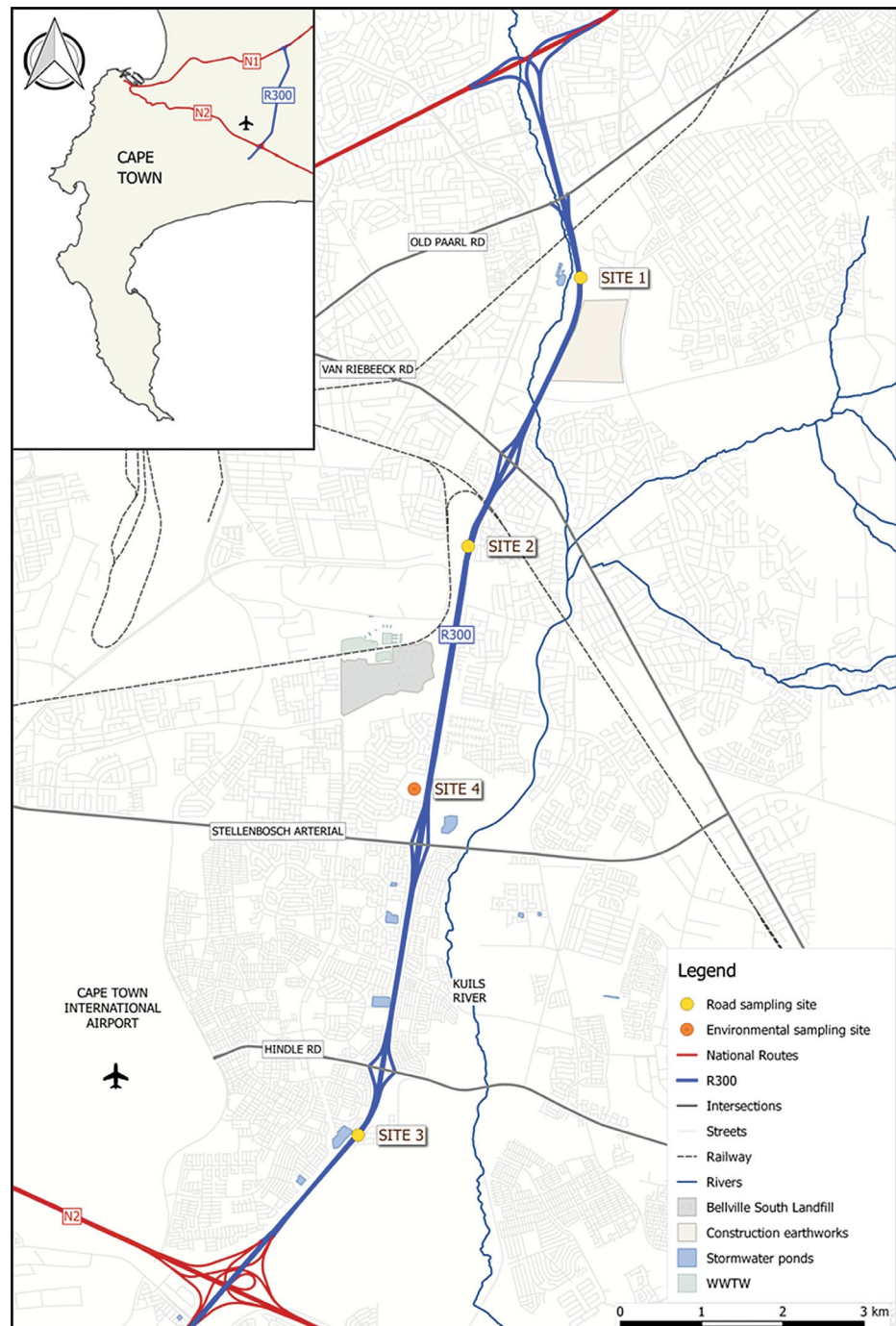


Figure 1 Location map of the R300 and sample positions

stormwater from the road surface to the surrounding environment.

Site description

The R300 is an asphalt freeway consisting of three lanes in each direction with a speed limit of 120 km/h. There are mixed land use areas surrounding the road, including low-income formal and informal housing, and commercial and industrial areas. The annual average daily traffic (AADT) is approximately 49 500 vehicles/direction/day (SANRAL 2013). Traffic is bimodal on weekdays, with peak volumes from 07:00–08:00 and 16:00–17:00, and the average speed for light vehicles is 93 km/h (SANRAL 2013). The highway crosses the Kuils River and

lies adjacent to floodplains, wetlands and the Driftsands Nature Reserve. The climate is moderate, with warm, dry summers (December to February) and moderate, wet winters. Annual rainfall ranges between 348 and 707 mm, with a mean annual precipitation (MAP) of 492 mm based on data obtained from the Cape Town International Airport weather station, which lies approximately 5 km west of the R300 freeway.

Sample collection

Grab samples of sediment and runoff from the highway were collected over a four-month period from March to June 2016. As an example of typical conditions, Figure 2 shows (a) a highway sample location,

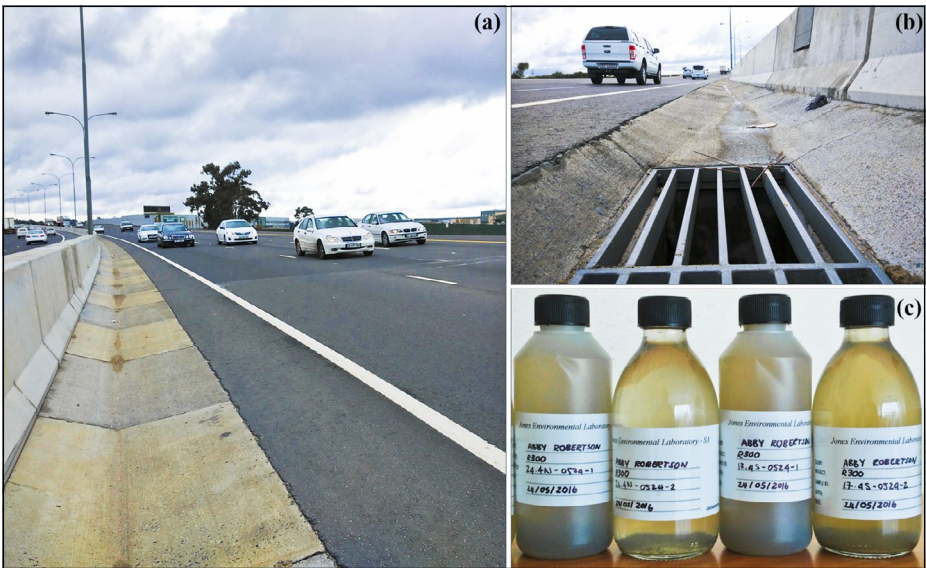


Figure 2 (a) Highway sample location, (b) catchpit inlet, (c) runoff samples

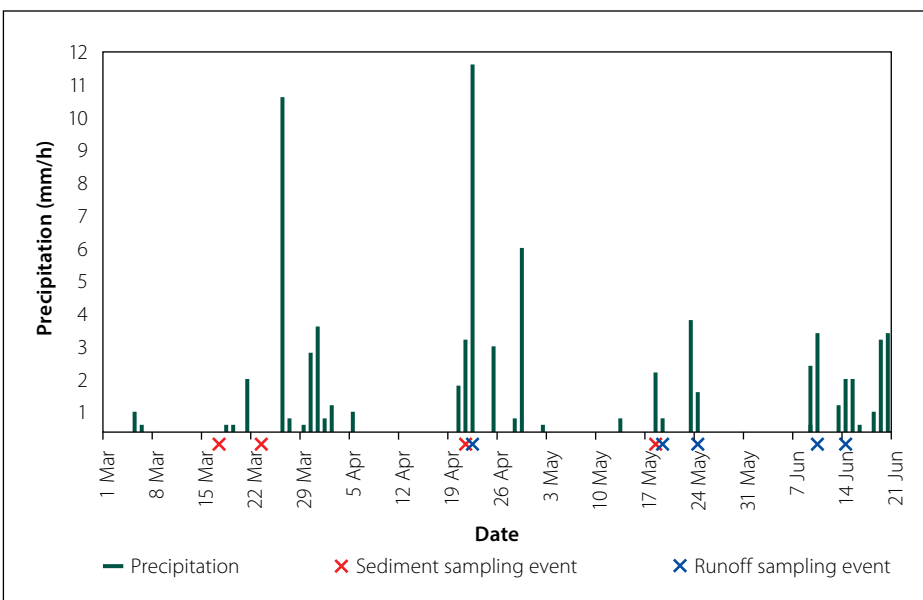


Figure 3 Time series of sampling events and precipitation from March to June 2016

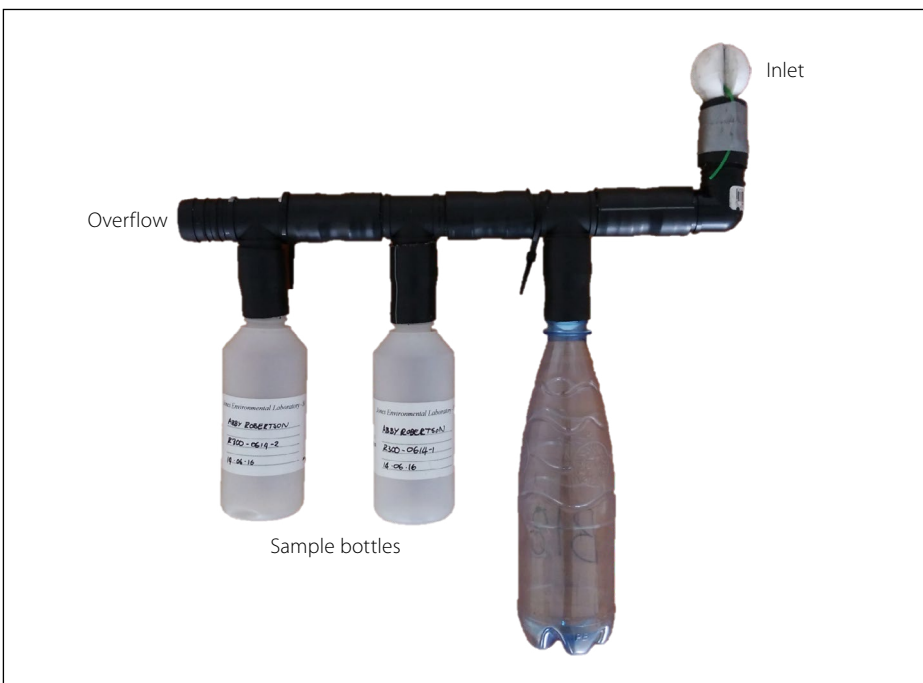


Figure 4 Custom-made sampling device

(b) a catchpit inlet, and (c) some of the runoff samples collected. Figure 3 shows a time series of the sample events and precipitation on the R300 during the research period.

Sediment samples were swept with a horsehair brush into a polypropylene dustpan and transferred to amber glass sample jars on site. Care was taken to include the fines fraction in the sample volume as this fraction adheres to the surface of the sampling equipment and has been shown to contain the highest concentration of contaminants (Zafra *et al* 2011).

Runoff samples were collected using a custom-made sampling device (Figure 4). The device was designed to sit in the catchpit and capture an extended grab sample of the runoff entering the drain. The device has a flow limiting inlet that samples a small fraction of the incoming runoff, which is channelled to the sample containers through a polypropylene pipe manifold. The extended grab sample collected by this device is a composite sample obtained over a period of 15 minutes to 1 hour, depending on the rate of runoff. The sample containers are sealed by a buoyant stopper once full. Ma *et al* (2009) showed that this sampling technique reduces the error in estimating mean concentrations by approximately 50% when compared to instantaneous grab sampling. Research by Deletic (1998) indicates that road surfaces could have a first flush effect, where the runoff is more polluted during the first period of a rainfall event. Therefore, in order to obtain a sample concentration closer to the true mean, the sampling device included a 500 ml storage volume to capture the initial stormwater runoff prior to filling the sample containers. Rainfall was collected in modified PET bottles attached to the top of wooden fence poles, approximately 10 m from the highway to provide an indication of the baseline pollution levels.

Upon collection, liquid samples were stored in clear glass bottles for oil and grease analysis, and clear plastic containers for metals, nutrients and TSS analysis. Both liquid and sediment samples were subsequently refrigerated and couriered to the laboratory in polystyrene chests with ice packs to preserve the sample.

Analysis

Sample analysis was conducted according to standard methods at an accredited laboratory (ISO 2005). TSS was determined using the gravimetric method, where the sample is filtered and the resulting residue is dried and weighed.

COD was tested for by hot digestion with potassium dichromate and measured spectrophotometrically. Oils and greases were determined gravimetrically after petroleum ether extraction. Metal elements were measured by inductively coupled plasma – optical emission spectrometry (ICP-OES). For sediment analysis, samples were dried, ground and digested using *aqua regia* before ICP-OES.

The particle size distribution of road sediment was determined according to the British Standard 1377-2:1990, Dry Sieving Method (BS 1990). Composite samples were created at each sampling event and manually sieved through nylon and metal sieves ranging from 5.00 mm down to 0.02 mm.

RESULTS

Based on visual inspection, the volume of solids accumulated in each catchpit between storm events ranged between 0 and 0.5 m³. Following rainfall events, however, the catchpits were typically scoured clean. The solid waste collected in the catchpits included sand; plant matter such as leaves and grass cuttings; cigarette butts; food packaging such as soda cans; chip packets; sweet wrappers and fast-food containers; and miscellaneous items such as polystyrene, plastic, cardboard and paper.

Table 1 provides the sample mean and range of contaminant concentrations in the sediment and runoff samples. The confidence interval was generated for a 90% confidence level, calculated using the t-distribution which is suitable for small sample sets ($n < 30$) (Field 2013). In the absence of water quality guidelines that specify constituent concentrations for stormwater, the results were compared to both the Department of Water and Sanitation's guidelines for preventing toxic effects in aquatic ecosystems (DWS 1996) and the Department of Environmental Affairs' requirements for effluent water quality (DEA 1984). The sample mean concentrations of copper, zinc, phosphorus and nitrogen exceeded both the aquatic ecosystem and effluent water quality standards. The sample mean concentrations of aluminium and lead exceeded the aquatic ecosystem guidelines, while the sample mean concentrations of manganese, oil and grease, COD and TSS exceeded the effluent standards. The concentrations of chromium, arsenic and cadmium were, however, within the permissible limits for maintaining health and biodiversity.

There was no significant spatial variation in the contaminant concentrations between

Table 1 Concentration of the measured contaminants in the R300 freeway sediment and runoff

| Sediment | | | | | | | Runoff | | | | | |
|--------------------|-------|----------------|-------|-------|---------------|------------------|--------|----------------|-------|--------|-----------------------------|-------------------|
| Contaminant | Unit | No. of samples | Min | Max | Mean* | Contaminant | Unit | No. of samples | Min | Max | Aquatic ecosystem standard# | Effluent standard |
| Aluminium | mg/kg | 6 | 2 213 | 5 348 | 3 440 ± 1 120 | Total aluminium | µg/l | 11 | 3 088 | 41 770 | 9 478 ± 6 021 | 100 |
| Arsenic | mg/kg | 6 | 1 | 5 | 3 ± 1 | Total arsenic | µg/l | 11 | 0 | 29 | 6 ± 5 | 130 |
| Cadmium | mg/kg | 12 | 0 | 0 | 0 ± 0 | Total cadmium | µg/l | 11 | 0 | 0 | 0 ± 0 | 6 |
| Chromium | mg/kg | 12 | 24 | 169 | 72 ± 24 | Total chromium | µg/l | 11 | 14 | 250 | 50 ± 37 | 340 |
| Copper | mg/kg | 12 | 24 | 83 | 45 ± 10 | Total copper | µg/l | 11 | 67 | 389 | 143 ± 50 | 46 |
| Lead | mg/kg | 12 | 17 | 191 | 52 ± 25 | Total lead | µg/l | 11 | 32 | 316 | 80 ± 45 | 7 |
| Manganese | mg/kg | 6 | 68 | 322 | 144 ± 77 | Total manganese | µg/l | 11 | 84 | 909 | 246 ± 125 | 1 300 |
| Nickel | mg/kg | 6 | 4 | 12 | 7 ± 2 | Total nickel | µg/l | 11 | 5 | 50 | 14 ± 7 | none |
| Zinc | mg/kg | 12 | 70 | 266 | 151 ± 29 | Total zinc | µg/l | 11 | 232 | 2 826 | 698 ± 399 | 36 |
| Phosphorus | mg/kg | 12 | 281 | 484 | 375 ± 34 | Total phosphorus | µg/l | 11 | 333 | 14 930 | 2 660 ± 2 295 | 250 |
| Total Nitrogen | % | 6 | 0 | 0 | 0 ± 0 | Total nitrogen | mg/l | 11 | 3 | 97 | 19 ± 16 | 10 |
| Fats, oil & grease | mg/kg | 12 | 119 | 265 | 202 ± 24 | Oil and grease | mg/l | 11 | 0 | 746 | 144 ± 127 | none |
| COD | | | | | | COD | mg/l | 14 | 12 | 320 | 148 ± 49 | none |
| TSS | | | | | | TSS | mg/l | 11 | 0 | 354 | 146 ± 60 | none |
| | | | | | | | | | | | 90 | |

* Confidence interval at a 90% confidence level
The concentration above which up to 5% of the species in the aquatic community are expected to experience acute toxic effects

Table 2 t-Test parameters for the difference in contaminant concentrations between the R300 road surface and surrounding environment

| | | Road surface | | Environment | | | | | |
|----------|--------------------|--------------|--------|-------------|-----|-----|--------|---------|---------|
| | | mean | SD | mean | SD | df | t-stat | p-value | |
| Sediment | Heavy metals* | mg/kg | 2 116 | 2 093 | 227 | 231 | 12 | 3.1 | 0.005 |
| | Total phosphorus | mg/kg | 375 | 65 | 204 | 19 | 14 | 8.2 | 5.4E-07 |
| | Fats, oil & grease | mg/kg | 202 | 46 | 0 | 0 | 11 | 15.3 | 4.7E-09 |
| Runoff | Heavy metals* | µg/l | 10 715 | 12 223 | 539 | 447 | 10 | 2.8 | 0.01 |
| | Total phosphorus | µg/l | 2 660 | 4 199 | 46 | 3 | 10 | 2.1 | 0.03 |
| | Oil & grease | mg/l | 144 | 233 | 80 | 161 | 10 | 0.5 | 0.3 |
| | TSS | mg/l | 146 | 110 | 0 | 0 | 10 | 4.4 | 0.001 |

* aluminium, arsenic, cadmium, chromium, copper, lead, manganese, nickel and zinc

the three sample locations on the highway. The data was grouped into 'highway' and 'environmental' categories to determine whether the highway land use contributes significantly to the stormwater quality characteristics. Two-sample t-tests assuming unequal variances were performed to assess whether there is a statistically significant difference between (a) highway and environmental sediment contamination, and (b) highway runoff and rainwater quality characteristics (Table 2). This assessment showed that the sediment collected from the R300 freeway was significantly more contaminated with heavy metals, phosphorus and fats, oils and greases than the surrounding environmental sediment. Similarly, the concentrations of heavy metals, total phosphorus and TSS were significantly greater in the road runoff compared with rainwater from the same location. Based on the sample results, it was not possible to establish whether the oil and grease concentration was different in road runoff and rainwater collected at the environmental sample location.

The metal contaminant concentration profile was similar for both the sediment and runoff on the R300 freeway. Figure 5 shows the distribution of sample mean metal concentrations, indicating the relative concentration of each contaminant. Aluminium, phosphorus, zinc and manganese were present in the highest concentrations, while arsenic and nickel were found in low concentrations, and the concentration of cadmium was below the detectable limit. These results support the notion that sediment analysis provides useful information regarding runoff water quality.

The highway sediment particle size ranged between 0.02 mm and 5 mm, with an 85th percentile size of 0.83 mm. This compares to other highway sediment studies (Vaze & Chiew 2002; Anta *et al* 2007; Zafra *et al* 2011). Figure 6 shows the average

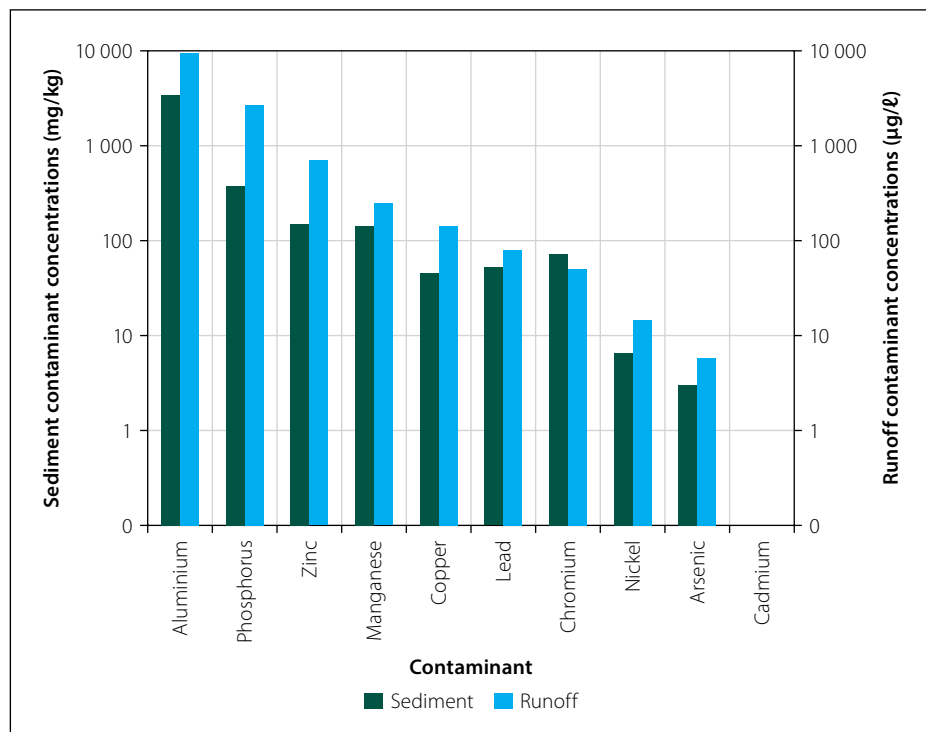


Figure 5 Relative mean metal contaminant concentrations in sediment and runoff

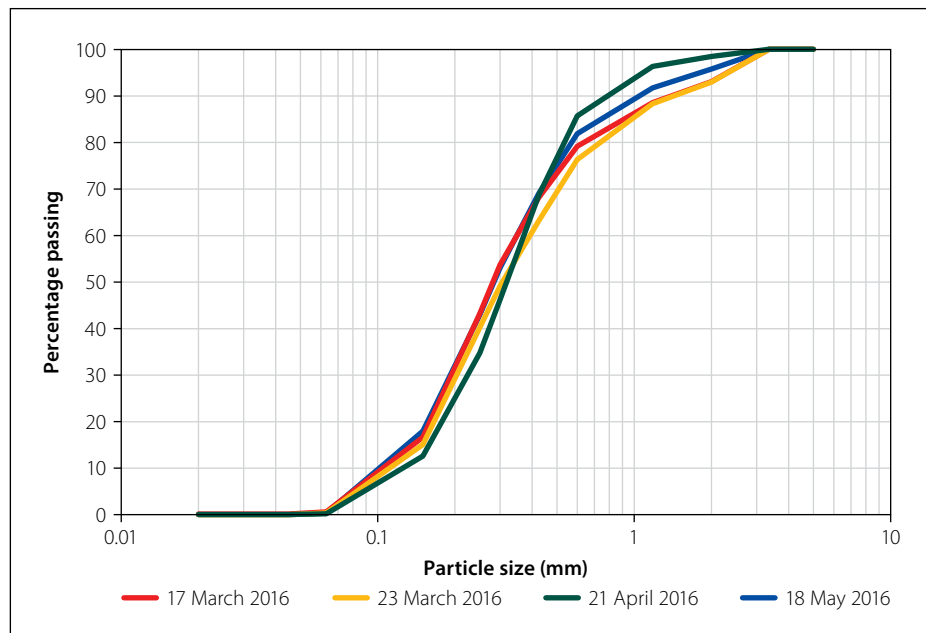


Figure 6 Particle size distribution of sediment on the R300 freeway

particle size distribution of composite samples taken from the three highway sampling locations for four sampling events. The particle size envelope is small, indicating a relatively homogenous and consistent particle size distribution in the surface sediment on the R300. This has implications for drainage design and controlling sedimentation. Research has shown that a large fraction of the pollutant load is attached to particles, therefore sediment removal is one of the primary means by which to improve surface runoff quality (Woods-Ballard *et al* 2007).

DISCUSSION AND CONCLUSIONS

The primary contaminants in the R300 surface water were aluminium, copper, lead, phosphorus, zinc, TSS, and oil and grease. Additionally, large volumes of macro pollutants including cigarettes, plastic and packaging material, were transported by the stormwater system from the highway to the surrounding environment.

The metal contaminant concentration profile is similar in sediment and runoff from the R300 freeway. The results for the surface runoff, however, show a higher level of variability than the sediment samples. Based on this observation, sediment sampling, which is easier and more cost-effective to conduct, can be used to provide an indication of the metal contamination in highway surface runoff.

Based on the magnitude of the solid waste, heavy metal, TSS and oil and grease concentrations in the R300 runoff waters, it is recommended that highway runoff is treated where the water quality may influence a sensitive or valuable aquatic ecosystem. International best management practices and local legislation suggest Sustainable Drainage Systems (SuDS) to ameliorate stormwater runoff quality and assist in controlling solid waste.

The SuDS elements and configuration required to meet performance and site conditions can be determined by modelling the stormwater system using computational decision support software such as PCSWMM (Ahiablame *et al* 2012). Pollutant modelling can be implemented by specifying an average pollutant concentration in the runoff, which is suitable for long-term modelling where event-to-event errors are not problematic. This approach is widely used, and approximate values are readily attainable in the literature. The mean concentration should, however, be informed by local conditions, as it may otherwise misrepresent the total pollutant loading.

The outcomes of this research indicate that stormwater runoff from urban highways can be a significant source of pollution, and further studies are required to investigate the temporal and spatial variation of pollutant loading across South Africa.

ACKNOWLEDGEMENT

The authors gratefully acknowledge the South African National Roads Agency Ltd (SANRAL) for their financial support of this project.

REFERENCES

- Ahiablame, L M, Engel, B & Chaubey, I 2012. Effectiveness of low impact development practices: Literature review and suggestions for future research. *Water, Air, and Soil Pollution*, 223: 4253–4273.
- Anta, J, Peña, E, Suárez, J & Cagiao, J 2007. A BMP selection process based on the granulometry of runoff solids in a separate urban catchment. *Water SA*, 32(3). Available at: <http://www.hdl.handle.net/10520/EJC116337> [accessed on 13 July 2015].
- Armitage, N, Vice, M, Fisher-Jeffes, L, Winter, K, Spiegel, A & Dunstan, J 2013. *The South African Guidelines for Sustainable Drainage Systems*. WRC Report TT558/12. Pretoria: Water Research Commission.
- Barbosa, A, Fernandes, J & David, L 2012. Key issues for sustainable urban stormwater management. *Water Research*, 46(20): 6787–6798.
- BS (British Standard) 1990. *Methods of Test for Soils for Civil Engineering Purposes. Part 2: Classification Tests*. London: British Standards Institution.
- Crabtree, B, Moy, F, Whitehead, M & Roe, A 2006. Monitoring pollutants in highway runoff. *Water and Environment Journal*, 20(4): 287–294.
- CSRM 2009. *Management of urban stormwater impacts policy*. City of Cape Town, Roads and Stormwater Department Catchment, Stormwater and River Management (CSRM) Branch. Available at: <https://www.capetown.gov.za/en/CSRM/Pages/Policiesandstrategy.aspx> [accessed on 16 February 2016].
- DEA (Department of Environmental Affairs) 1984. *General and Special Standards: Requirements for the purification of waste water or effluent*. Available at: https://www.dwa.gov.za/Dir_WQM/docs/Legis.asp [accessed on 7 May 2015].
- Deletic, A 1998. The first flush load of urban surface runoff. *Water Research*, 32(8): 2462–2470.
- Desta, B M, Bruen, M, Higgins, N & Johnston, P 2007. Highway runoff quality in Ireland. *Journal of Environmental Monitoring*, 9(4): 366–371.
- DWS (Department of Water and Sanitation) 1996. *South African Water Quality Guidelines. Volume 7: Aquatic ecosystems*. Pretoria: Government Printer.
- Ellis, J B, Revitt, D M & Lundy, L 2012. An impact assessment methodology for urban surface runoff quality following best practice treatment. *Science of the Total Environment*, 416: 172–179.
- Field, A 2013. *Discovering Statistics using IBM SPSS Statistics*, 5th ed. London: SAGE.
- Göbel, P, Dierkes, C & Coldewey, W G 2007. Storm water runoff concentration matrix for urban areas. *Journal of Contaminant Hydrology*, 91(1–2): 26–42.
- Han, Y H, Lau, S L, Kayhanian, M & Stenstrom, M K 2006. Correlation analysis among highway stormwater pollutants and characteristics. *Water Science and Technology*, 53(2): 235–243.
- ISO (International Organization for Standardization) 2005. *ISO 17025:2005. General Requirements for the Competence of Testing and Calibration Laboratories*. Geneva: ISO.
- Kayhanian, M, Suverkropp, C, Ruby, A & Tsay, K 2007. Characterization and prediction of highway runoff constituent event mean concentration. *Journal of Environmental Management*, 85(2): 279–295.
- Khan, S, Lau, S-L, Kayhanian, M & Stenstrom, M K 2006. Oil and grease measurement in highway runoff – Sampling time and event mean concentrations. *Journal of Environmental Engineering*, 132(3): 415–422.
- Legret, M & Pagotto, C 1999. Evaluation of pollutant loadings in the runoff waters from a major rural highway. *Science of the Total Environment*, 235(1–3): 143–150.
- Ma, J-S, Kang, J-H, Kayhanian, M & Stenstrom, M K 2009. Sampling issues in urban runoff monitoring programs: Composite versus grab. *Journal of Environmental Engineering*, 135(3): 118–127.
- Marsalek, J & Chocat, B 2002. International report: Stormwater management. *Water Science and Technology*, 46(6–7): 1–17.
- Opher, T & Friedler, E 2010. Factors affecting highway runoff quality. *Urban Water Journal*, 7(3): 155–172.
- SANRAL 2013. *SANRAL Yearbook 2013*. Pretoria (Unpublished).
- Sartor, J, Boyd, G & Agardy, F 1974. Water pollution aspects of street surface contaminants. *Water Pollution Control Federation*, 46(3): 458–467.
- Shinya, M, Tsuchinaga, T, Kitano, M, Yamada, Y & Ishikawa, M 2000. Characterization of heavy metals and polycyclic aromatic hydrocarbons in urban highway runoff. *Water Science and Technology*, 42(7–8): 201–208.
- Vaze, J & Chiew, F H 2002. Experimental study of pollutant accumulation on an urban road surface. *Urban Water*, 4(4): 379–389.
- Woods-Ballard, B, Kellagher, R, Martin, P, Jefferies, C, Bray, R & Shaffer, P 2007. *The SuDS manual*. London: Construction Industry Research and Information Association (CIRIA).
- Zafra, C, Temprano, J & Tejero, I 2011. Distribution of the concentration of heavy metals associated with the sediment particles accumulated on road surfaces. *Environmental Technology*, 32(9): 997–1008.

The collapsible nature of residual granite soils of the Cape Granite Suite

N Fouché, S Y Asante

INTRODUCTION

Where residual granite soils of the Cape Granite Suite, located in the Western Province of South Africa, are identified on-site during a geotechnical investigation, the potential risk of collapse settlement should not be overlooked and will, in all instances, require investigative measures to determine the likelihood and extent of sudden and excessive settlement. The majority of research pertaining to collapsible soils has focused on the problematic basement complex granites situated in the northern part of the country, with much less attention paid to the weathered Cape granites. However, the research carried out on these, often troublesome, Cape granite soils at Stellenbosch University has allowed the researchers to gain valuable insight into their collapse behaviour.

This paper focuses on the nature of the Cape granite soils and presents recent findings with regard to their collapse potential using traditional methods, as well as innovative new techniques such as X-ray computed tomography (CT-scanning) and scanning electron microscopy (SEM).

THE NATURE OF COLLAPSIBLE SOILS

When any open-textured silty or sandy soil with a low dry density (high void ratio) and relatively high shear strength at a low moisture content (due to suction and the presence of bridging colloidal material) is identified during a geotechnical investigation, a soil with collapse potential should be suspected. In the South African context, soils with a collapsible fabric are common in various transported soils (including hill-wash, gulley wash and aeolian and littoral deposits), and in a number of residual soils present in regions where quartz-rich rocks such as granite or feldspathic sandstone have undergone chemical weathering to produce intensely leached residual soils (such as residual granite from the Basement

Complex and the Berea Red Sands from Quaternary calcarenites) (Schwartz 1985).

When a partially saturated transported or residual soil with a collapsible fabric wets up under load, the bridging colloids and salts lose strength and stiffness and, as a result, the soil particles are forced into a denser state of packing (termed collapse of the soil structure) (Schwartz 1985).

Cape granite soils have, in the past, frequently been overlooked by engineers and engineering geologists as problem soils with regard to their potential to collapse. In addition, these soils occasionally do not present with the characteristic honeycomb-like structure (for example high void ratio and low clay content), and may therefore appear stable. Upon saturation the soil often loses strength and undergoes a substantial decrease in volume. An additional applied load is mostly required to initiate collapse. The potential severity of the problem therefore often goes unnoticed, leading to structural damage, either aesthetically displeasing (for example hairline cracks) and/or structurally significant (for example distortion).

Exposures of Cape Granite Suite rocks are typically restricted to the South Western Cape and daylights in areas such as Stellenbosch, Paarl, Darling, Greyton, Swellendam and the Cape Peninsula (Brink 1981). The widespread occurrence of Cape granites gives an indication of the possible extent of the collapse problem in the South Western Cape.

RESEARCH OBJECTIVES

The main objectives of the research pertaining to the collapse phenomenon were to:

- Determine the occurrence and extent of collapse settlement in residual and reworked residual Cape granite in the Stellenbosch, Paarl and Darling areas
- Establish the mechanisms of collapse in residual Cape granite



NANINE FOUCHE graduated in 2008 with a Bachelor's degree in Earth Science from Stellenbosch University. Thereafter she continued her studies and completed a Post-Graduate Diploma and MScEng in Geotechnical Engineering. Nanine gained valuable experience as an engineering geologist at Aurecon South Africa,

undertaking geotechnical and foundation investigations for a wide range of projects. Her passion for teaching and the academics led her to a career in teaching and research at the Civil Engineering Department of Stellenbosch University. Nanine is currently teaching geotechnical courses, providing support to geotechnical research students and completing her PhD.

Contact details:
 Department of Civil Engineering
 Stellenbosch University
 Private Bag X1
 Matieland 7602
 South Africa
 T: +27 21 882 9441
 E: naninef@sun.ac.za



SAMUEL YAW ASANTE is currently a PhD student at Zhejiang University, Hangzhou, China. He holds an MEng in Civil Engineering (Geotechnical option) and a BSc in Geological Engineering from Stellenbosch University, South Africa, and the University of Mines and Technology, Ghana, respectively. His interests lie in soil behaviour, microstructure characterisation of soil and methane hydrate-bearing sediments, as well as geotechnical laboratory techniques. Since graduation he has worked for a number of companies in Ghana.

Contact details:
 D Block
 RM 725
 Zhejiang University
 Zijingang Campus
 Hangzhou
 China
 T: +23 3541030717
 E: samuelasanteyaw@gmail.com

- Develop a test procedure to investigate the microstructure of soils to aid in identifying potentially collapsible soils
- Provide insight with regard to the properties and behaviour of the collapsible Cape granite soils, i.e. possible explanations about the collapse behaviour.

Detailed field investigations comprising disturbed and undisturbed soil sampling and profiling were carried out by the researchers within the demarcated study areas. A soil testing phase followed, encompassing standard testing methods such as collapse potential tests and newer techniques such as SEM and CT-scanning. Both residual granite (defined as the weathering product of granite parent rock occurring directly above the parent rock) and reworked residual granite (defined as residual granite reworked in-situ by termites) from the investigated areas were included in the study.

DEMARCATED STUDY AREAS

Selected study areas within the towns of Stellenbosch, Paarl and Darling, all located within the mapped extent of the Cape Granite Suite, formed part of the research area. An additional site in Paarl, underlain by residual Malmesbury shale (which is known to be non-collapsible), was investigated to aid as a control. The following sites make up the greater research area:

- Four sites along the R44 between Stellenbosch and Somerset West: These sites are underlain (partly or entirely) by residual granite and reworked residual granite derived from coarse-grained porphyritic granite of the Kuils River – Helderberg pluton. Various sampling locations were selected within each chosen site, resulting in a total of 17 sampling localities and 18 large undisturbed block samples for laboratory testing.
- Nine sites, of which five are situated at the foot or on the side slopes of the Paarl Pluton within the Paarlberg Reserve, and four sites at the foot of the southern and eastern side slopes of the same Pluton: The sampling areas are underlain by residual granite derived from the Bretagne Granite, Laborie Granite or Montvieu Granite. One sample was collected from each of these locations, resulting in a total of nine undisturbed block samples.
- Five sites on farmland in the northern outskirts of Darling: These sites are situated within the boundaries of the

Darling Batholith and are underlain by residual biotite granite. One large undisturbed block sample was collected from each of the sites.

Six undisturbed soil samples comprising residual Malmesbury shale were also sampled from a quarry site in Paarl. These residual Malmesbury soils do not develop a collapsible, honeycomb-like structure and were sampled to compare and to better understand the influence of the soil microstructure on collapsibility of the residual soils.

EXPERIMENTAL WORK METHODOLOGY

The experimental work carried out by the researchers entailed extensive laboratory testing, including both standard procedures such as consolidometer testing and index type tests (e.g. particle size analysis) and newer, non-destructive techniques, such as CT-scanning and electron microscopy.

The research objectives mentioned before and the corresponding testing methods used in achieving each objective are summarised in Table 1.

The collapse potential of a soil is governed by its microstructure, that is, the porosity, particle and pore size distribution, particle morphology and mineralogy. The use of non-destructive techniques such as CT-scanning and scanning electron microscopy (SEM) to examine the microstructure of soils is currently showing promising progress, with further development in such research techniques. CT-scanning enables the visualisation of the internal structure of objects (such as soils) by converting measured X-ray computed tomography signals to two-dimensional (2D) or three-dimensional (3D)

images, whereas SEM operates on optical principles, generating images by scanning the soil surface with a focused beam of electrons. By examining the microstructure of potentially collapsible soils with these techniques, the influence of the various components of the soil microstructure on the behaviour of collapsible soils can be studied. By creating a better understanding of these mechanisms, collapsible soils can potentially be identified by examination of the soil microstructure. CT-scanning and SEM, which formed the basis of the experimental research aimed at developing a test procedure to identify potentially collapsible soils, are briefly discussed below.

CT-scanning involves the visualisation of the internal structure of soils without disturbing the soil structure. The porosity, particle size distribution and pore size distribution of soils can be determined by analysing two- and three-dimensional X-ray images obtained via data acquisition and image reconstruction. To obtain the 3D X-ray images, the General Electric Phoenix V-TomeX L240 X-ray micro-computed tomography scanner (microCT) and NanoCT were used for the experimental work in conjunction with VGStudio Max and Avizo Fire Image analysis software. As part of the experimental work multiple scans were performed on reworked residual and residual granite from Stellenbosch, as well as the residual Malmesbury shale from Paarl (functioning as a control). To investigate the soils' microstructure after collapse, a number of reworked residual and residual granitic soil samples were also scanned after completion of the single oedometer testing. An advantage of CT-scanning is the non-destructive nature of the technique, allowing samples to be scanned and subsequently analysed several times.

Table 1 Experimental work to achieve research outcomes

| Research objectives | Testing methods to achieve objective |
|---|---|
| To determine the occurrence and extent of collapse settlement in the residual Cape granite in the Stellenbosch, Paarl and Darling areas | Consolidometer tests including collapse potential, single oedometer and double oedometer tests (in accordance with ASTM D2435 (ASTM 2011), and Jennings and Knight (1975)) |
| To develop a test procedure to investigate the microstructure of soils to aid in identifying potentially collapsible soils | CT-scanning and scanning electron microscopy |
| To confirm the mechanism(s) of collapse settlement in residual Cape granite soils | |
| To provide insights with regard to the properties and behaviour of the collapsible Cape granite soils, i.e. possible explanations concerning the collapse behaviour | Standard laboratory procedures (TMH1 1986) to determine particle size distribution, Atterberg limits and dry density, and X-ray diffraction, CT-scanning and scanning electron microscopy |

As a result of its higher resolution and magnification power, SEM has been used to investigate soil microstructure (Remley & Bradford 1989). It is considered an effective and reliable technique to determine soil mineralogy and particle morphology, which play a significant role in processes such as collapsibility. The SEM generates images by scanning a focused electron beam over the soil surface to create an image. The ZEISS EVO MA15 scanning electron microscope at the Centre for Analytical Facility at Stellenbosch University was used to determine the mineral composition and morphology of the reworked residual and residual granite from Stellenbosch, Paarl and Darling, and the residual Malmesbury shale from Paarl. A total of 170 images were obtained during the experimental work. Appropriate methods and software packages were used to determine the mineral composition and morphology from these images. The disadvantages of SEM are the time-consuming nature of preparing samples for the microscopy study, lens aberration and long analytical time.

Soil mineral composition can also be determined by means of X-ray diffraction (XRD) and X-ray fluorescence spectrometry (XRF). The clay content and soil fabric of the residual granite sampled from Paarl

and Darling were examined by means of X-ray diffraction. However, considering the disadvantages associated with XRD and XRF – such as the limiting depth of X-ray penetration and the influence of water content on the performance and reliability of the results – scanning electron microscopy is the preferred method to determine soil mineralogy (Asante 2015).

Table 2 Guiding values of collapse potential (Jennings & Knight 1975)

| Collapse potential | Severity of problem |
|--------------------|---------------------|
| 0% – 1% | No problem |
| 1% – 5% | Moderate trouble |
| 5% – 10% | Trouble |
| 10% – 20% | Severe trouble |
| >20% | Very severe trouble |

EXPERIMENTAL FINDINGS

Standard laboratory methods

Double-oedometer, single-oedometer and collapse potential tests confirmed the presence of collapsible soils at the majority of sampling locations underlain by reworked residual and residual granite in the Stellenbosch, Paarl and Darling areas. The reworked residual and residual soils sampled from the demarcated study areas in Stellenbosch are typically moderately collapsible and collapsible, with collapse potential values mostly between 1.7% and 10% (maximum 18.4%). Table 2 provides the descriptive terms associated with the values of collapse potential. The collapse potential test results obtained for a number of reworked residual specimens sampled from a particular site near Stellenbosch are

shown in Figure 1. From the figure it is evident that, once a critical value of moisture content is exceeded, the fine silt bridges are no longer able to resist deformation, resulting in a sudden and large decrease in soil volume. A slight bow in the compression curves is noted at a vertical stress of about 50 kPa, and a slight, but uncharacteristic increase in void ratio between 100 and 200 kPa. The cause of these unusual volume changes is uncertain, but it can possibly be ascribed to temperature variations in the soils laboratory bringing about changes in soil moisture.

The residual granites sampled from various sites in Paarl and Darling displayed collapse potential values ranging from < 1% (not collapsible) to 5.7% (collapsible), and between < 1% and 3% (moderately

Table 3 Summary of experimental findings from standard laboratory tests on reworked residual and residual Cape granite soils
(compiled from Gildenhuys 2010; Muteb 2013; Asante 2015)

| Sampling area | Collapse potential (%) (number of samples per category) | Soil type | Moisture content range (average) (%) | Dry density range (average) (kg/m ³) | Void ratio range (average) | Clay content range (average) (%) |
|---------------|---|--|--|---|----------------------------|----------------------------------|
| Stellenbosch | <1 (4) | sandy clay clayey silty sand clayey sand | 13.4–27.3 (22.3) | 1 414 – 1 902 (1 581) | 0.32–0.87 (0.71) | 21–41 (29) |
| | 1–5 (7) | clayey silty sand clayey sand silty sand sandy clay | 5.5–25.5 (15.9) | 1 441 – 2 022 (1 654) | 0.34–0.92 (0.63) | 9–43 (29) |
| | 5–10 (7) | clayey sand silty sand | 14.2–18.7 (16.6) not determined for all samples | 1 507 – 1 834 (1 628) not determined for all samples | 0.51–1.69 (1.18) | 3–27 (16) |
| | 10–20 (3) | silty sand | not determined | not determined | 0.96–0.99 (0.98) | 1 |
| Paarl | <1 (4) | silty sand silt clayey sand | 11.8–25.7 (17.9) | 1 310 – 1 574 (1 455) | 0.71–1.0 (0.85) | 16–33 (21.7) |
| | 1–5 (5) | clayey sand silty sand | 10.8–20.1 (15) | 1 343 – 1 458 (1 411) | 0.85–1.0 (0.91) | 14–28 (19.5) |
| | 5–10 (1) | clayey sand | 10.9 | 1 486 | 0.81 | 28 |
| Darling | <1 (3) | clayey sandy gravel clayey sand | 11.9–13.6 (12.7) | 1 665 – 1 731 (1 698) | 0.56–0.62 (0.59) | 29–33 (31) |
| | 1–5 (5) | clayey sand silty sand sandy gravel | 10.5–17.1 (14.6) | 1 380 – 1 603 (1 460) | 0.68–0.95 (0.85) | 3–32 (14.6) |

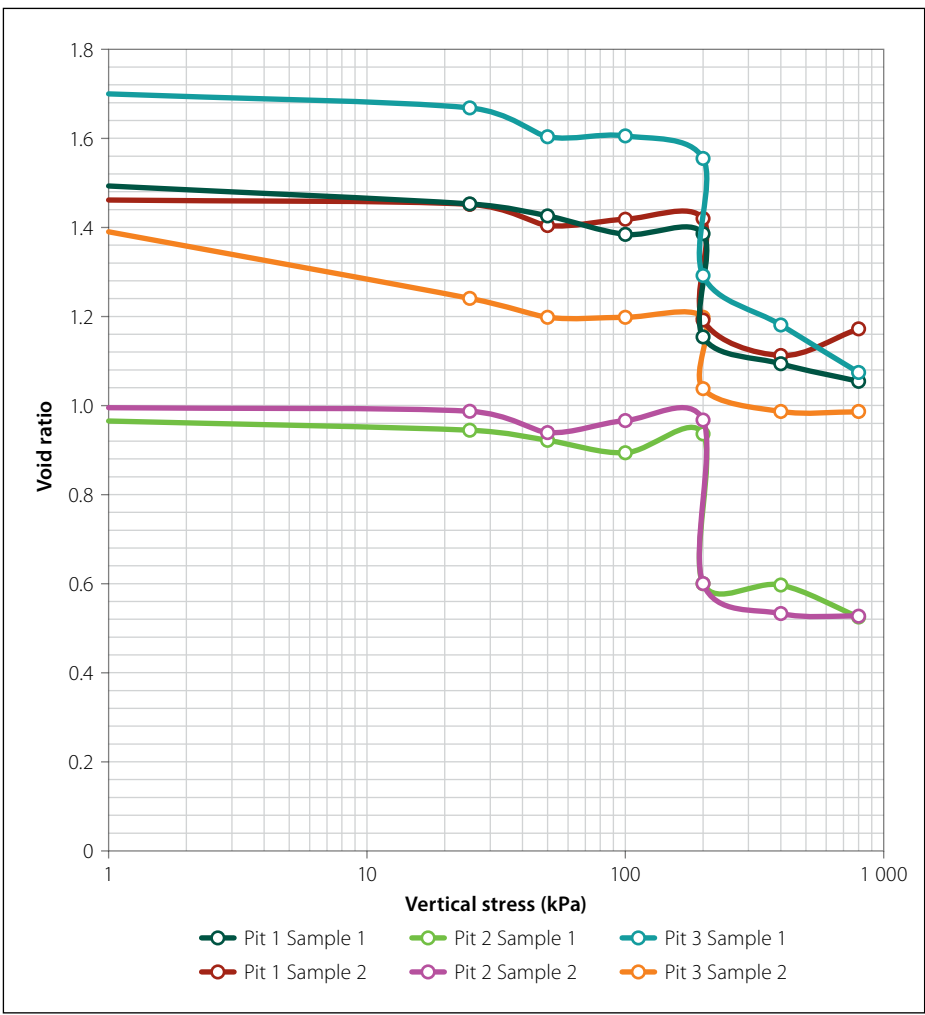


Figure 1 Stellenbosch collapse potential test results (Asante 2015)

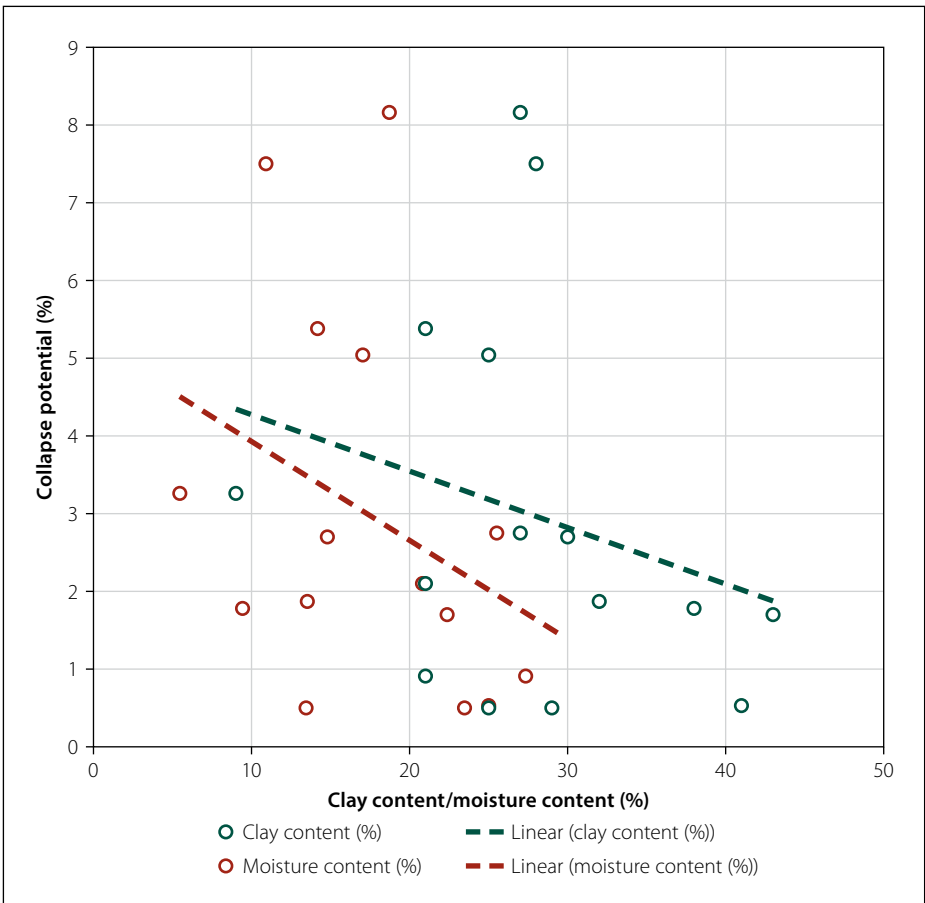


Figure 2 Collapse potential versus clay and moisture content for Cape granite soils

collapsible), respectively. Collapse potential tests confirm that the residual Malmesbury shales sampled from Paarl are not collapsible.

A summary of the characteristics of all reworked residual and residual granite soils sampled from the study areas is presented in Table 3. The parameters were obtained by means of standard laboratory procedures. The collapse potential values given in Table 3 originate from three separate research studies, and are thus an amalgamation of collapse potential, single-oedometer and double-oedometer test results. In addition, both residual and reworked residual specimens were included in the study; however, no distinction is made between the outcomes associated with these two soil types.

From Table 3 the following conclusions can be drawn:

- With an increasing collapse potential (%), the average clay content and in-situ moisture content (MC) obtained for each collapse potential category tend to decrease (see Figure 2). Notwithstanding this, outliers were observed, particularly at high and low values of collapse potential.
- No clear correlation between dry density and collapse potential could be found; thus accentuating the fallacy in assuming that all soils with a low dry density will have a tendency to collapse, and vice versa. The large range in dry density and void ratio values observed in some instances in the table shows that soil stability is not consistently represented by dry density.
- The average void ratios determined for each collapse category typically increase with increasing collapsibility (see Figure 3). The high collapse potential values (17.11% and 18.4%) associated with the two specimens with void ratios of 0.96 and 0.99, can possibly be explained by the interconnectedness of the soil voids and/or the particle morphology. These aspects will be discussed as part of the microstructure analysis.
- The tabulated results demonstrate that collapsible residual granite does not necessarily possess typical characteristics associated with collapse, such as a low dry density and clay content.

Microstructure analysis

The distribution of particle sizes in ten samples of reworked residual granite was determined from CT-scanned images using

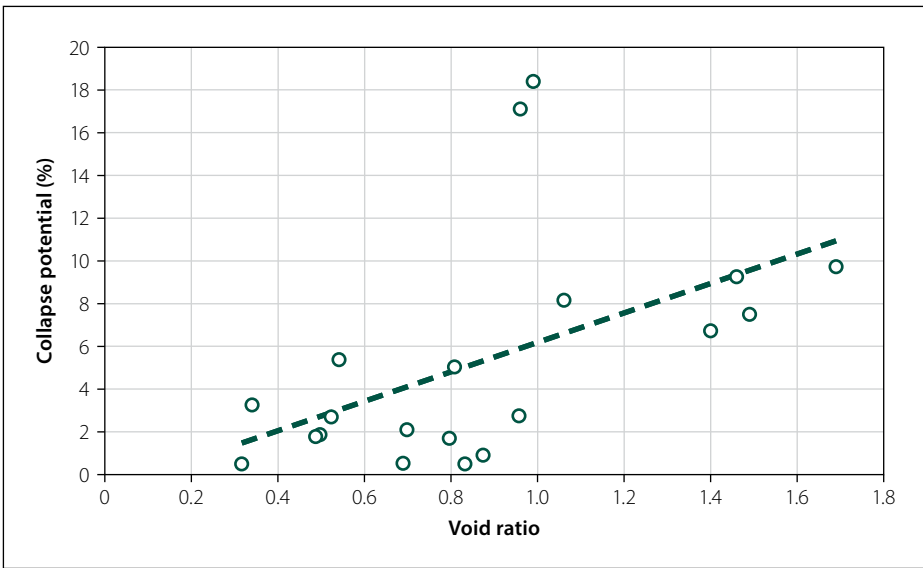


Figure 3 Variation in void ratio with degree of collapse in Cape granite soils

an image processing technique termed granulometry. A typical particle size distribution (PSD) curve is shown in Figure 4. The PSD curve for the same material, but determined by means of mechanical sieving and hydrometer analysis, is also shown on the figure. The mechanical analysis was carried out on the same ten samples in accordance with TMH1 Methods A1, A5 and A6 (TMH1 1986). The minor discrepancy noted for the finer soil particles can be attributed to the tendency of these particles to clump together, subsequently being seen as a single homogenous particle in the digital CT-scan image produced.

This phenomenon, termed bleeding, results in the finer, measured CT-scan particles (silt and clay size) appearing larger than their counterparts measured by means of mechanical sieving and hydrometer analysis. Conversely, an advantage of the CT-scan method is the ability to determine the volume and surface area of the individual particles from which the actual diameter can be calculated. This allows a more accurate size distribution of coarse particles. The more prominent difference in the distribution of coarse particle sizes can thus be ascribed to the inaccuracies of the mechanical sieving method. The

CT-scan method is therefore considered marginally superior with regard to the determination of soil particle sizes, providing slightly more accurate and reliable grading results. Notwithstanding this, the gradations obtained from the traditional and CT-scanning methods are sufficiently similar, providing comparable textural descriptions to aid in identifying a collapsible fabric.

From the CT-scanned images, the porosity of the reworked residual granite and residual Malmesbury shale was studied. This entailed determination of the average volumetric change within the different pore size classes given by Brewer (1964) during collapse of the soil structure. Figure 5 shows the voids present in a scanned image of reworked residual granite before (a) and after collapse (b) of the soil structure. A significant reduction in the volume of coarse macropores (indicated in pink) upon saturation is shown, with the formation of fine and medium macropores (indicated in blue) as the particles rearrange. The results showed a direct correlation between the average volume of connected pores (specifically coarse macropores of 75 – >5 000 µm) and the volumetric change within these pores, and the magnitude of collapse. It was found that the average volume of connected coarse macropores and volumetric change within the non-collapsible residual Malmesbury shale were significantly lower than within

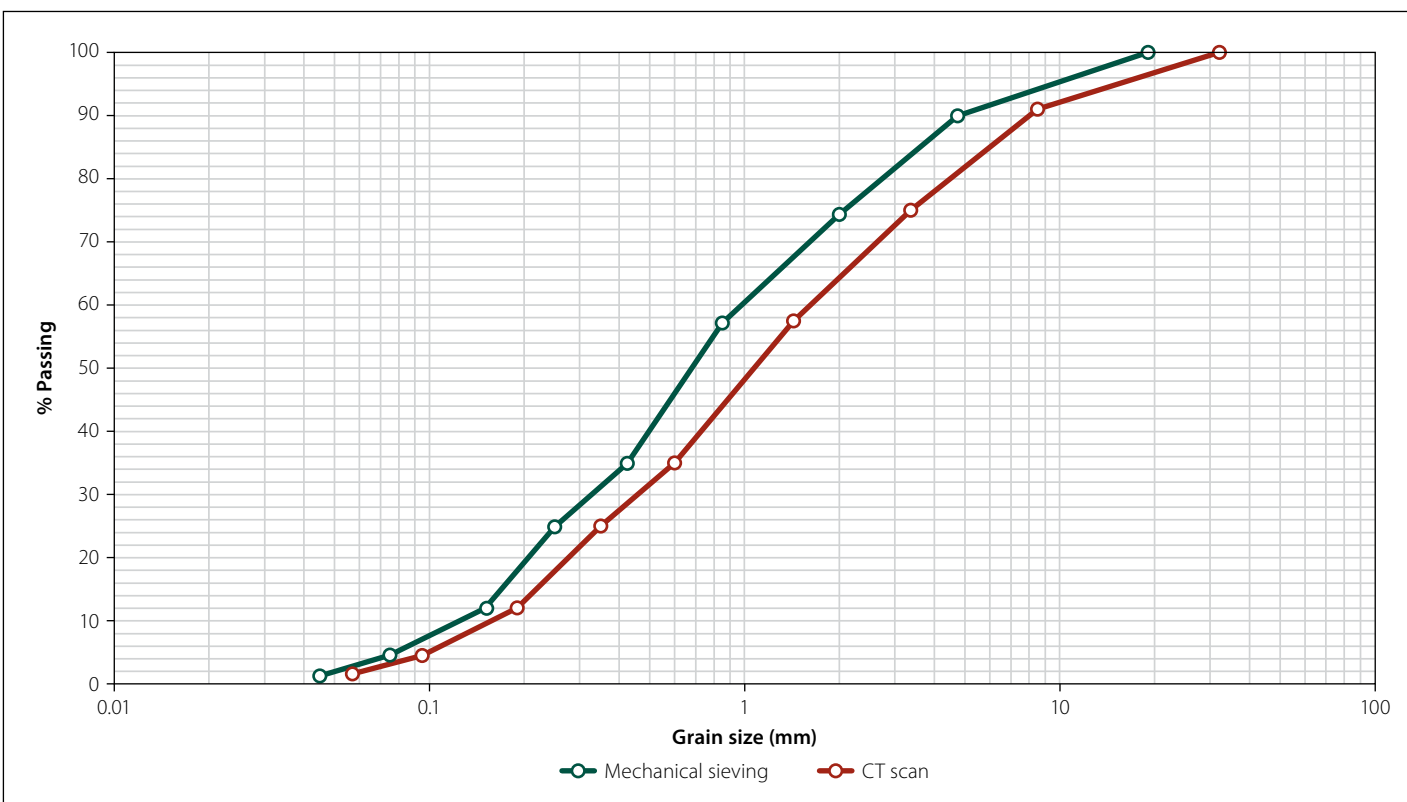


Figure 4 Comparative plot of PSD by mechanical sieving and CT-scanning (Asante 2015)

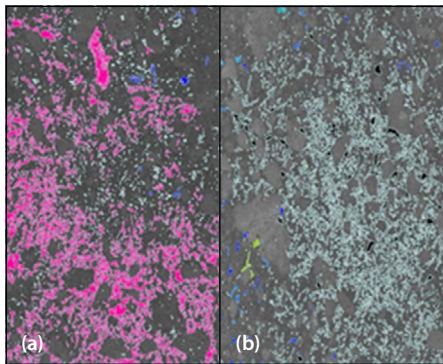


Figure 5 Thresholding (void analysis) applied to a sliced two-dimensional image of reworked residual granite showing volumetric change in pores following collapse (Asante 2015)

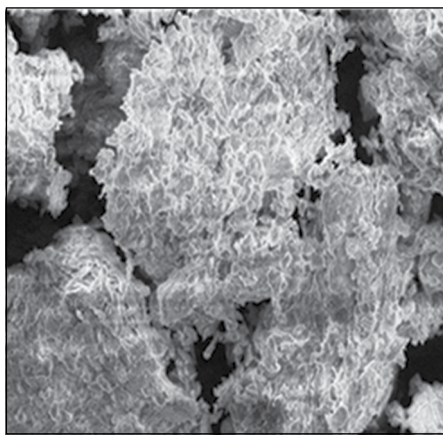


Figure 6 Microscopic view of primary quartz particles coated with illite within residual Malmesbury shale (Asante 2015)

the collapsible reworked residual granite (see Table 4).

The SEM results provided useful insights into the behaviour of collapsible soils by allowing examination of the soil microstructure. The particle morphology and mineralogy of the reworked residual granite and residual Malmesbury shale were examined and proved valuable in interpretation of the collapse potential test results. On a microscale level, the residual shale (non-collapsible) comprises rounded and sub-rounded quartz grains (larger primary mineral) coated with a thin, plate-like and flaky clay mineral, illite. These coated particles are surrounded by irregularly shaped secondary clay mineral, kaolinite, forming an interlocked structure (see typical SEM image in Figure 6). The secondary clay minerals have a preferred orientation parallel to the lamination (small-scale sequence of fine layers) which impedes the formation of a collapsible fabric. At first glance, the observed void ratios (between 0.67 and 1.45) may be misleading in predicting collapse,

Table 4 Volumetric change in pore volume during collapse of reworked residual granite and residual Malmesbury shale (Asante 2015)

| Material type | Diameter (μm) | Class limit | Subclass | Average volume (undisturbed sample) (mm^3) | Average volume (after collapse) (mm^3) |
|---------------------------|----------------------------|-------------|-----------|---|---|
| Reworked residual granite | > 5 000 | Macropores | Coarse | 2 408.32 | 2.44 |
| | 2 000 – 5 000 | | Medium | 0.25 | 0.44 |
| | 1 000 – 2 000 | | Fine | 0.15 | 0.17 |
| | 75 – 1 000 | | Very fine | 0.12 | 0.11 |
| Residual Malmesbury shale | > 5 000 | Macropores | Coarse | 9.96 | 2.50 |
| | 2 000 – 5 000 | | Medium | 0.18 | 0.24 |
| | 1 000 – 2 000 | | Fine | 0.12 | 0.13 |
| | 75 – 1 000 | | Very fine | 0.00 | 0.12 |

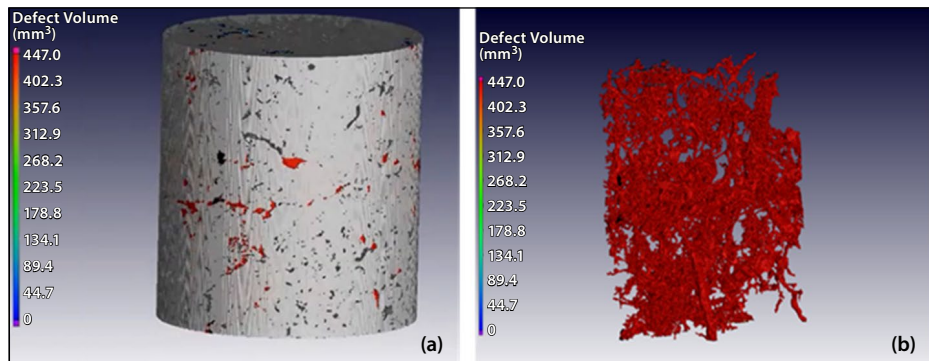


Figure 7 (a) Three-dimensional image of reworked residual granite showing void sizes, and (b) interconnected coarse voids (Asante 2015)

but these pores are unconnected (unlike the connected pores of the granitic soils), thus not lending themselves to the formation of a collapsible fabric.

The rounded and sub-rounded primary quartz minerals making up the framework of the silty sand reworked residual granite are surrounded by a fine matrix of partially leached and eroded feldspar, quartz and kaolinite and smectite clays. A porous, honeycomb-like structure is the result, leading to collapse settlement within the reworked residual granites, as observed in the collapse potential tests. A three-dimensional image of reworked residual granite from Stellenbosch, in which the network of connected coarse pores is evident, is shown in Figure 7. The soil pores, visible on the exterior surface of an undisturbed sample is shown in 7(a), whereas the connected void system is shown in 7(b). In cases where the void ratio of collapsible soils is low and potentially misleading to the engineer, examination of the soil microstructure could reveal the potential for collapse to occur. In this regard, the particle shape and orientation, and mineral composition and arrangement (no preferred orientation or

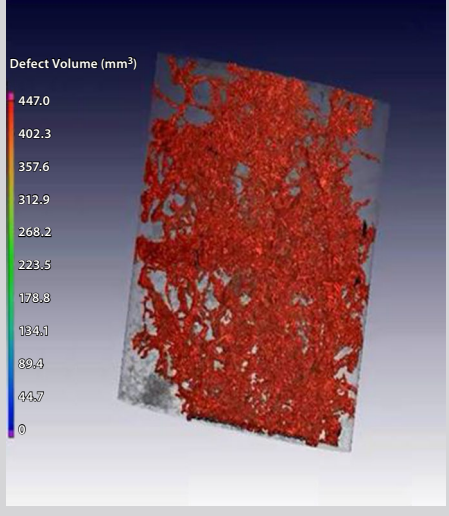
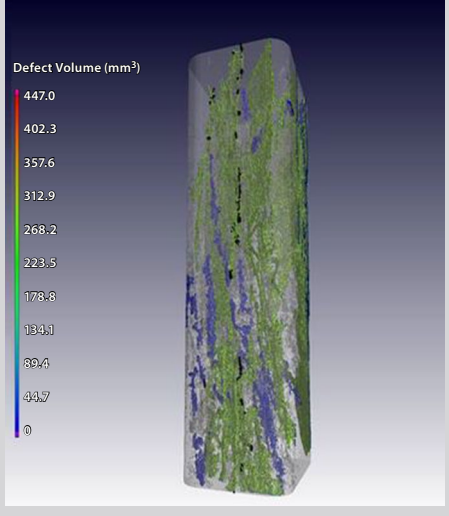
lamination, forming connected pores) will prove valuable in predicting collapse.

The difference within the microstructure of the residual shale and reworked residual granite is evident when studying the images produced by SEM. The particle morphology and mineralogy of the two soil types are inherently different, leading to the formation of contrasting soil fabrics, and subsequently collapse behaviour.

CONCLUSIONS

The Cape granite soils have in the past often been overlooked by engineers and engineering geologists as a problem soil with regard to its collapse potential. The identification of collapsible Cape granite soils on the outskirts of Stellenbosch during a geotechnical investigation for farm storage structures, first drew attention to the subject. The studies carried out by post-graduate researchers from Stellenbosch University confirmed the presence of collapsible soils at the majority of sampling locations underlain by reworked residual and residual granite in the Stellenbosch, Paarl and Darling areas.

Table 5 Summary of experimental findings for typical reworked residual granite and residual Malmesbury shale samples

| Property | Reworked residual granite | Residual Malmesbury shale |
|---|--|---|
| Collapse potential (%) | 9.73 (collapsible) | 0.42 (not collapsible) |
| Clay content (%) | 1 | 52 |
| Void ratio | 0.98 | 1.3 |
| Change in average volume of coarse macropores before and after collapse (mm^3) | 380 to 2.11 | 9.96 to 2.50 |
| 3D pore distribution | Porous structure formed by leaching of feldspar, quartz and clays producing an interconnected void system comprising coarse macropores (in red)  | Interlocked structure of coated quartz grains and laminated secondary clay minerals forming an unconnected void system comprising medium, fine and very fine macropores (in green and blue)  |

The collapse potential of a soil is governed by its microstructure, that is, the porosity, particle and pore size distribution, particle morphology and mineralogy. Collapsible residual granite soils often do not possess typical characteristics associated with collapse such as high porosity and low clay content; however, non-destructive methods such as CT-scanning and SEM can effectively be used to aid in identifying potentially collapsible soils by examining their microstructure. A summary of the experimental findings for typical samples of reworked residual granite and residual Malmesbury shale is given in Table 5, from which it is evident that microstructure analysis through CT-scanning and SEM can be useful in the identification of collapsible soils.

The image processing techniques employed by the researchers, resulted in the following additional conclusions:

- Collapse settlement occurs within the macropores of soils with a collapsible grain structure.
- For collapse settlement to occur, the voids must be interconnected.

- After collapse of the soil structure, new, but smaller voids are formed.
- CT-scanning (with the appropriate image analysis technique) can be used effectively to determine the distribution of particle sizes in soils.

RECOMMENDATIONS

Further research on the topic is suggested, including an assessment of the practicality of the use of scanning electron microscopy and CT-scanning in the identification of collapsible soils.

REFERENCES

- Asante, S 2015. *Alternate methods to determine the microstructure of potentially collapsible soils*. MEng Dissertation. University of Stellenbosch.
- ASTM 2011. *ASTM D2435, 2011. Standard Test Methods for One-Dimensional Consolidation Properties of Soils Using Incremental Loading*. West Conshohocken, PA: ASTM International.
- Brewer, R 1964. *Fabric and Mineral Analysis of Soils*. New York: Wiley.
- Brink, A B A 1981. *Engineering Geology of Southern Africa*, Vol 2. Pretoria: Building Publications.
- Gildenhuys, N 2010. *The occurrence and extent of collapse settlement in residual granite in the Stellenbosch area*. MEng Dissertation. University of Stellenbosch.
- Jennings, J E & Knight, K A 1975. A guide to construction on or with materials exhibiting additional settlement due to collapse of grain structure. *Proceedings, 6th Regional Conference for Africa on Soil Mechanics and Foundations Engineering*, Durban, South Africa.
- Muteb, C K 2013. *Geotechnical investigation for properties of collapsible soils: A case study conducted at Darling and Paarl area*. MEng Dissertation. University of Stellenbosch.
- Remley, P A & Bradford, J M 1989. Relationship of soil crust morphology to inter-rill erosion parameters. *Journal of the Soil Science Society of America*, 53: 1215–1221.
- Schwartz, K 1985. Problem soils in South Africa – State of the art: collapsible soils. *The Civil Engineer in South Africa*, 27(7).
- TMH1 (Technical Methods for Highways) 1986. *Standard Methods of Testing Road Construction Materials: Methods A1(a), A1(b), A5 and A6*. Pretoria: Department of Transport.

Guidelines for the preparation of papers and technical notes

Authors should comply with the following guidelines when preparing papers for publication in the journal

The *Journal of the South African Institution of Civil Engineering* is published **quarterly in March, June, September and December**. Articles submitted for publication are reviewed by a panel of referees under the guidance of the SAICE Journal Editorial Panel. The journal publishes research papers covering all the disciplines of civil engineering (structural, geotechnical, railway, coastal/marine, water, construction, environmental, municipal, transportation) and associated topics that are relevant to the civil engineering profession, and that preferably have particular relevance to civil engineering in southern Africa and the African continent.

When preparing articles for publication, authors should please take note of the following and comply with the guidelines as set out:

CLASSIFICATION OF ARTICLES CONSIDERED FOR PUBLICATION

- **Technical papers** are well-researched, in-depth, fully referenced technical articles not exceeding 6 000 words in length (excluding tables, illustrations and the list of references). Related papers that deal with 'softer sciences' (e.g. education, social upliftment, etc) are accepted if they are of a technical nature and of particular interest to the civil engineering profession. The latter type of paper will be subject not only to peer-review by civil engineers, but also to review by non-engineering specialists in the field covered by the paper.
- **Technical notes** are short, fully referenced technical articles that do not exceed 2 000 words. A typical technical note will have limited scope often dealing with a single technical issue of particular importance to civil engineering.
- **Review papers** are considered for publication as either technical papers or technical notes on condition that they are the original work of the author and will assist the reader with the understanding, interpreting or applying of the subject under review. A review paper must contain criteria by which the work under review was evaluated, and contribute by synthesising the information and drawing new conclusions from the dissemination of the previously published work.
- **Discussion** on published articles is welcomed up to six months after publication. The length of discussion contributions is limited to 1 500 words. Where appropriate, discussion contributions will be subject to the normal reviewing process and will be forwarded to the authors of the original article for reply.

POLICY REGARDING LANGUAGE AND ORIGINALITY OF SUBMITTED ARTICLES

- **Language:** Manuscripts should preferably be presented in English, as the journal is distributed internationally. Articles submitted in any of the other official South African languages should be accompanied by an expanded abstract in English.
- **Original work:** Papers and technical notes must be original contributions. Authors must affirm that submitted material has not been published previously, is not under consideration for publication elsewhere and will not be submitted elsewhere while under consideration by the SAICE Journal Editorial Panel. It is the responsibility of the authors to ensure that publication of any paper in the journal will not constitute a breach of any agreement or the transgression of any law. The corresponding author should confirm that all co-authors have read and approved the manuscript and accept these conditions. Authors are responsible for obtaining

permission to publish experimental data and other information that may be confidential or sensitive. Authors are also responsible for obtaining permission from copyright owners when reproducing material that had been published elsewhere. Proof of such permission must be supplied.

SUBMISSION PROCEDURES AND REQUIRED FORMAT

- **Online submission:** Manuscripts must be uploaded as PDF files (<http://journal.saice.org.za>). Individual file sizes may not exceed 10 MB. Should you experience problems uploading your paper, please contact the editor (verelene@saice.org.za).
- **Format:** Manuscripts should be prepared in MS Word and presented in double line spacing, single column layout with 25 mm wide margins. Line numbers must be applied to the whole document. All pages should bear the authors' names and be numbered at the bottom of the page. With the exception of tables and figures (see below) the document should be typed in Times New Roman 12 pt font. Contributions should be accompanied by an abstract of not more than 200 words.
- **First page:** The first page of the manuscript should include the title of the paper, the number of words of the main text (i.e. excluding figures, tables and the list of references), the initials and surnames of the authors, professional status (if applicable), SAICE affiliation (Member, Fellow, Visitor, etc), telephone numbers (landline and mobile), and e-mail and postal addresses. The name of the corresponding author should be underlined. Five keywords should be suggested.

- **Figures, tables, photos and illustrations:** These should preferably be submitted in colour, as the journal is a full-colour publication.
 - Their positions should be clearly marked in the text as follows: [Insert Figure 1].
 - Figures, tables, photos, illustrations and equations should be numbered consecutively and should appear in the text directly after they have been referred to for the first time.
 - Illustrations must be accompanied by appropriate captions. Captions for tables should appear *above* the table. All other captions should appear *below* the illustration (figures, graphs, photos).
 - Only those figures and photographs essential to the understanding of the text should be included. All illustrations should be referred to in the text.
 - Figures should be produced using computer graphics. Hand-drafted figures will not be accepted. Lettering on figures should be equivalent to a Times New Roman 9 pt font or slightly larger (up to 12 pt) if desired. Lettering smaller than 9 pt is not acceptable.
 - Tables should be typed in Times New Roman 9 pt font. They should not duplicate information already given in the text, nor contain material that would be better presented graphically. Tabular matter should be as simple as possible, with brief column headings and a minimum number of columns.

- **Mathematical expressions and presentation of symbols:**
 - Equations should be presented in a clear form which can easily be read by non-mathematicians. Each equation should appear on a separate line and should be numbered consecutively.
 - Symbols should preferably reflect those used in *Microsoft Word Equation Editor* or *Mathtype*,

or should be typed using the Times New Roman symbol set.

- Variables in equations (x , y , z , etc, as well as lower case Greek letters) should be presented in italics. Numbers (digits), upper case Greek letters, symbols of metric measurement units (m for metres, s for seconds, etc) and mathematical/trigonometrical functions (such as sin, cos and tan) are not written in italics, but in upright type (Roman). Variables and symbols used in the body of the text should match the format used in the equations, i.e. upright or italics, whichever is applicable.
- Metric measurement abbreviations/units should conform to international usage – the SI system of units should be used.
- Decimal commas may be used, but decimal points are preferred.
- Symbols should preferably be defined in the text, but if this is not feasible, a list of notations may be provided for inclusion at the end of the paper.
- **Headings:** Sections and paragraphs should not be numbered. The following hierarchy of headings should be followed:

HEADING OF MAIN SECTION

Heading of subsection

Heading of sub-subsection

- **References:** References should follow the Harvard system. The format of text citations should be as follows: "Jones (1999) discovered that ..." or "recent results (Brown & Carter 1985; Green *et al* 1999) indicated that ..."

References cited in the text should be listed in alphabetical order at the end of the paper. References by the same author should be in chronological order. The following are examples of a journal article, a book and a conference paper:

- Donald, A W 1954. Pore pressure coefficients. *Géotechnique*, 4(4):143–147.
- Terzaghi, K 1943. *Practical soil mechanics*. New York: Wiley.
- Smith, A W, Black, C & White, A 1999. Factors affecting the strength of soils. *Proceedings*, ASCE Conference on Shear Strength of Soils, Colorado, pp 503–532.

Papers published previously in the *Journal of the South African Institution of Civil Engineering* should be cited if applicable.

- **Footnotes, trade names, acronyms, abbreviations:** These should be avoided. If acronyms are used, they should be defined when they first appear in the text. Do not use full stops after abbreviations or acronyms.

- **Return of amended papers:** Papers requiring amendments will be accepted up to six months after the referee reports had been sent to authors, after which the paper will be withdrawn from the system.

FINAL ARTICLE

- **Copyright:** On acceptance of the paper or technical note, copyright must be transferred by the author/s to the South African Institution of Civil Engineering on the form that will be provided by the Institution.
- **Photos of authors:** The final corrected version of the paper should be accompanied by recent, high-resolution head and shoulders colour photographs and a profile not exceeding 100 words for each of the authors.
- **Proofs:** First proofs of papers will be sent to authors in PDF format for verification before publication. No major re-writes will be allowed, only essential minor corrections.

